Theoretical Investigation of Magnetic Properties of 3d and 4f Compounds

Zur Erlangung des akademischen Grades einer

DOKTORIN DER NATURWISSENSCHAFTEN

(Dr. rer. nat)

von der KIT-Fakultät für Chemie und Biowissenschaften

des Karlsruher Instituts für Technologie (KIT)

genehmigte

DISSERTATION

von

M.Sc. Twinkle Yadav

1.Referentin: Apl. Prof. Dr. Karin Fink

2 Referentin: Prof. Dr. Annie K. Powell

Tag der mündlichen Prüfung: 23.07.2021

Table of Contents

Acknowledgement

The research work presented in the thesis has been conducted at the Institute of Nanotechnology and Institute of Physical chemistry at Karlsruhe Institute of Technology, Germany under the supervision of Apl. Prof. Dr Karin Fink. I am beyond grateful for her support scientifically and morally during entire course of my thesis work, which really helped me to understand and learn so many new things and led to the work presented in the thesis. My sincere thanks to her for her continuous support over the entire period of my thesis. I would also like to thank Prof. Dr. Annie K. Powell for being my co- referee and Prof. Dr. Marcus Elstner and Prof. Dr. J. -D Grunwaldt for being my examiner.

I am also thankful to the SFB TRR88 '3MET' for the funding. I am also grateful to all my group members and colleagues for their help and support.

In the last, I would like to express my gratitude to my family and friends especially my sisters Sanchita and Vanshikha for believing in me and keep encouraging me.

1 Introduction

Worldwide, scientists have been giving attention to magnetism since long time. Magnetic materials are highly appealing because of their applications in vast area of scientific and technological fields, such as in biomedicine, drug delivery, imaging, environmental remediation processes, robotics, engineering, miniaturized devices, electronics, spintronics and data storage.[1] Development of new materials and techniques increase the growth in the fields of spintronics, electronics, and data storage. The capability of storing data in hard drives is increased tremendously in the last three decades. From oldest generation hard disk with a capability of recording up to 2 Kbits to present day's storing devices with a capability of more than 1 Tbits.[2] To enhance the potential of data storage, scientists have been working on new materials. In the recent years, research in the area of multifunctional nano-sized and nano-structured molecular materials has gained tremendous amount of attention. This multi-functionality can be achieved through a molecular approach by combining different molecular units responsible for particular properties or properties in the same compound.[3] The control of these properties at a molecular level results in the application of these materials in nano devices.[4] Interaction among electrons and localized magnetic moments in these materials lead to various potential technological applications, specifically in electronic devices. Such materials also exhibit peculiar magnetic field induced transitions and switchable conductivity by changing the magnetic field, temperature, magnetic order or spin state.[5–7]

Miniaturization of electronic devices and data storage led to the idea to use single molecules to store data or perform logical operations. In 1990, the study of a $[Mn_{12}(CH_3COO)_{16}(H_2O)_4O_{12}]$ $2CH_3COOH.2H_2O$ complex - usually known as $Mn_{12}OAc$ - exhibited interesting magnetic properties such as slow magnetic relaxation, strong magnetic anisotropy and can retain magnetizations long even in the absence of an applied field and at low temperature.[8,9] It led to large numbers of studies in the field of molecular magnetism and complexes which exhibited similar properties and are considered as Single molecule magnets (SMMs). SMMs exhibit magnetic memory arising purely from the molecule itself, hence making it potentially useful in a wide range of advanced technologies. This was an important achievement in the field of molecular magnetism. SMMs are metal-organic compounds containing one or a few paramagnetic centers. However, for SMM in order to be successful, it depends on the magnetic blocking temperature T_B. Blocking temperature is the temperature at which the relaxation time (t) is equal to the experimental measuring time of the technique used (τ_m).[10]

A magnetic nanoparticle exhibit superparamagnetic behavior above blocking temperature. Below this T_B , it exhibits the magnetic properties similar to the bulk material. A suitable T_B can be achieved in the presence of a high spin ground state and a large magnetoanisotropy.[11]

Transition metals like V(III), Mn(II/III/IV), Fe(II), Fe(III), Co(II/III), Ni(II) and Cu(II) have been used in SMMs.[11] Complexes containing Mn(III) in high spin are the most explored SMMs because of its large easy axis anisotropy. SMMs with 3d-metal ions often contain two or more spin centers. Hence, the coupling of the individual spin centers to a total spin by the exchange coupling *J* plays a crucial role in the design of SMMs. Strong *J* implies an energetically isolated ground state. The exchange coupling is often mediated by diamagnetic ligands.[11,12] Therefore, the combination of appropriate ligands with 3d metals can result in interesting magnetic properties. However, in the last decade, the focus of SMMs research shifted towards lanthanide (*f*) ions because of their ability to show large anisotropies.

Ab initio methods are generally used to study ligand environment in order to fabricate molecular devices capable of storing information.[13] Quantum chemical calculations can be used as an alternative to costly experimental hit and trials. High level ab initio calculations have reportedly been used for interpretation and design of SMMs. The development of pseudospin Hamiltonian and execution of this Hamiltonian gives the useful quantities such as crystal field splitting and the g-factors. Furthermore, comparison of theoretical results is done with experimental finding. However, now a days, interpretation of the obtained data can also be used as a predictive tool.[13–15]

In this present work, 3d and 4f complexes are studied by quantum chemical methods to understand their magnetic behavior. The project has been carried out within the collaborative research center SFB TRR88 "Cooperative Effects in Homo- and Heteronuclear Complexes (3MET)" in collaboration with the groups of Prof. van Wüllen and Prof. Krüger from TU Kaiserslautern as well as Prof. Powell from Karlsruhe Institute of Technology. For the theoretical description, methods are needed that can take the open shell character of the molecules, several electronic states and spin orbit coupling into account. In this work, ab initio calculations have been performed to understand the magnetic behavior of the transition metal and lanthanide based systems. The investigations were focused on 3d/4f systems with different ligand fields and geometries in this work.

This thesis is organized as follows. In chapter 2, the general background of magnetic properties is described. This includes the classification of different magnetic materials based on their macroscopic

properties as well as the microscopic properties of spin centers in molecules. In chapter 3, the electronic structure of SMMs is explained in detail and the role of transition and lanthanide metal ions are explained. In chapter 4, the used quantum chemical methods are presented. The applications are divided into two groups. Chapter 5 is devoted to calculations on transition metal ions more specifically Ni^{2+} and Co^{2+}. In case of Ni^{2+}, three different Ni^{2+} complexes with increasing complexity starting with a mononuclear compound with just one Ni^{2+} center in distorted octahedral surrounding with $S_{Ni}=1$. In the second, one of the ligands is reduced forming a second spin center $S_L=1/2$. The third is a binuclear Ni complex where the metal centers are connected by the ligand with $S_L=1/2$. For Co^{2+}, first three different Co^{2+} complexes with $S_{Co} = 3/2$ in different ligand fields varying from tetrahedral, distorted octahedral to almost perfect octahedral surrounding were studied. In a further example, a Co^{2+} spin center is studied with and without an additional electron on the ligand.

In chapter 6, calculations on lanthanide metal ions (Ln = Gd, Dy, Er, Ho, Tb) are presented. Two similar Ln3 complexes with change in the ligand substitution were studied. Firstly, each Ln(III) center was studied individually by replacing the other two centers with diamagnetic Y(III) to explore the properties of the individual spin centers. To deduce, further information on the interaction of the spin centers, two magnetic centers were studied together. Also, two different Gd(III) complexes were studied.

Summary and outlook are given in chapter 7.

2 Background

In the present scenario, interest in magnetic materials like SMMs or SIMs is increasing day by day. Development and understanding of new materials on a miniature scale is at the root of progress in many areas of materials science. In this chapter, basic concepts should be cleared.

2.1 **Origin of Magnetism**

The Ancient Greeks and Chinese had the knowledge about strange and rare stones (known as lodestone which is naturally magnetized piece of the mineral magnetite) with the power to attract iron. Iron magnets were considered only source of magnetism at that time. Then in 1750 Michell in England and in 1785 Coulomb in France discovered law of interaction between magnetic poles but it was still not related to the electric current flow. Later in 1820, during a presentation of the flow of an electric current in a wire, Hans Christian Oersted, a Danish scientist, observed that current in the wire resulted a nearby compass needle to move.[16](Figure 2.1)

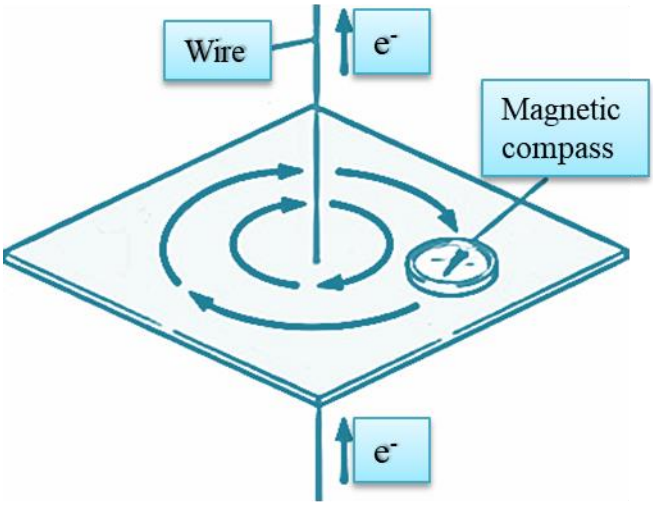

Figure 2.1 presence of magnetic field around the current carrying wire shown by a magnetic compass

After reading Oersted's observation about the effect of an electrical current on a compass needle, a French physicist, Andre-Marie Ampere concluded that electrical charge in motion is responsible for a magnetic field which was a very interesting conclusion because until then it was considered that permanent magnets and earth are only source for magnetic fields and electrical charge in motion was not involve in these cases This resulted in a introduction of molecular magnet. After this study, concept of

magnetic moment was explained through Ampere's circuital law which states that the line integral of the magnetic field along a closed path is equal to μ_o time the total current.

$$\oint B.dl = \mu_O I \qquad 2.1$$

During the same period when Ampere's law was discovered, Jean-Baptise Biot and Felix Savart, two French physicists worked on an equation (known as Biot-Savart law) for calculating the magnetic field generated by a constant electric current which shows a relation between the magnitude, direction and length of the electric current to the magnetic field[17]. The resulted equation is (2.2):

$$dB = \frac{\mu_o \mu_r}{4\pi} \times \frac{Idlsin\theta}{r^2} \qquad 2.2$$

Where I is current, r is a distance and θ is the angle between distance and direction of the current. Biot-Savart law is comparable with Ampere's circuital law.

2.2 **Classification of magnetic materials**

Magnetic material can be classified depending on different ordering of magnetic moments as shown in Figure 2.2

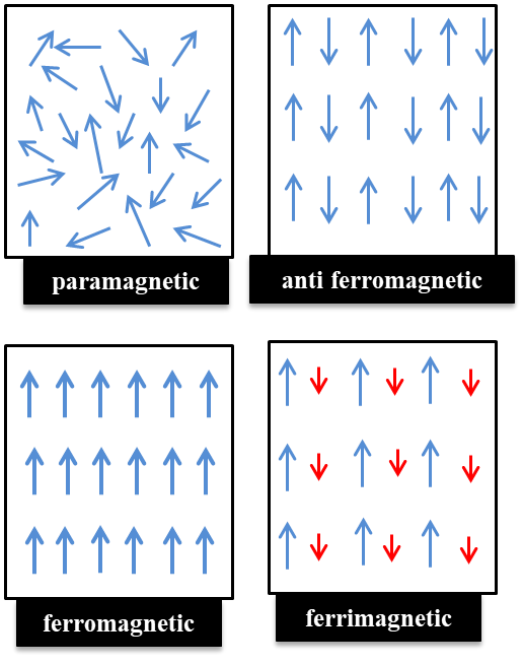

Figure 2.2: Different magnetic materials: paramagnetic, ferromagnetic and anti ferromagnetic

2.2.1 diamagnetism

In the absence of applied magnetic field, diamagnetic materials have no magnetic moment because of the completely filled electrons in the orbital which results in the cancelation of the magnetic moment. When subjected to an external magnetic field, the materials have small susceptibility and magnetization. In case of diamagnetic materials, susceptibility is temperature independent.[19]

2.2.2 paramagnetism

In case of paramagnetic material**,** atoms or ions have unpaired electrons. In this case, magnetic moment of atoms show random arrangements when there is no applied field resulting in zero magnetic moment. However, If it is put through an external magnetic field, magnetic moment of each atom align itself in the direction of the applied field producing positive magnetization According to the Curie law, it becomes difficult to arrange the atomic magnetic moment in an order as temperature increases and hence the susceptibility decreases.[19,20]

2.2.3 ferromagnetism

Ferromagnetic materials have unpaired electron spins which lined up parallel with each other in a region known as domain. As ferromagnetic materials display this long-range ordering phenomenon, magnetic moment of individual atom does not cancel out. When placed in a external magnetic field, it exhibits strong magnetization but special thing about ferromagnetic substance is if external magnetic field is removed, material still remains magnetic. The magnetic susceptibility is relatively very high in ferromagnets but in this case, materials are generally measured in terms of saturation magnetization i.e magnetization if all domains are aligned. Transition elements like Fe, Co and Ni shows ferromagnetic behavior. As temperature increases ferromagnetic material behaves as paramagnetic and that transition temperature is the Curie temperature (T_c).

2.2.4 anti-ferromagnetism

Antiferromagnetic material possesses the atomic magnetic moments arranged in a usual pattern like ferromagnetic substance but pointing in opposite direction. Therefore, the magnetic moment Cancel out each other and results in net magnetic moments equals to zero. Behavior of this material is similar to paramagnetic material and this transition temperature is Neel temperature. Some examples of anti-ferromagnets are Cr and MnO.

2.2.5 ferrimagnetic

The ferrimagnetic materials are similar to anti-ferromagnetics, in this case also the magnetic moments are aligned anti-parallel like anti-ferromagnetics but the magnitudes of magnetic moments are different here. The classical examples of ferrimagnets are the salts of transition metals known as ferrites. Ferrite has AB_2O_4 formula where A is divalent metal cation (Fe^{2+}, Co^{2+}) and B is trivalent metal cation (Fe^{3+}).

2.3 Basic principle of magnetic materials

Magnetic field in other words is a force on moving charge which is consistent with the Lorentz force law. Origins of magnetic field can be

i. Electric current
ii. moving charges
iii. magnetic moment

H is a free magnetic field, when applied to a material, behavior of the material is known as its magnetic induction, *B*, which in other words is the number of lines of force passing through a unit area of material[21]. Dependence of B and H on each other can be explained by using the equation:

$$B = \mu_0(H + M) \qquad 2.3$$

Here, M is the magnetization. It gives the information about the property of a material and shows how dipole moments of the molecule interact with each other and μ_0 is the permeability. The SI unit for M and H is $^{A}/_{m}$ and for μ_0 is Weber/(Am). Therefore, unit of B is weber/m^2 or tesla (T). Earth's field is in microtesla (μT), conductor carrying 5 A is in millitesla and the largest field produced in a laboratory till now is 45 T.

Magnetic flux or flux density,Φ, i.e the product of the magnetic field and the area. Usually, magnetic flux varies depending if it's outside the material or inside the material. This difference between the internal and external flux allows a classification of magnetic materials.

2.3.1 Susceptibility and Permeability

When a magnetic field is applied to a magnetic material, its response can be represented as susceptibility and permeability.

Magnetic susceptibility is a measure of the magnitude to which a material is magnetized in the presence of a given applied magnetic field.[22] Relation between Magnetization and magnetic field is given by

$$\chi = \frac{\boldsymbol{M}}{\boldsymbol{H}} \qquad 2.4$$

Magnetic permeability is a quantity which accounts for relative increase or decrease in the magnetic field in a material with respect to applied magnetic field in which the material is placed. Relation between magnetic flux and magnetic field is

$$\mu = \frac{\boldsymbol{B}}{\boldsymbol{H}} \qquad 2.5$$

In terms of magnetic flux, diamagnetic material repel lines and paramagnetic or antiferromagnetic have flux less inside than outside whereas ferromagnetic material has magnetic flux inside higher than outside and Permeability changes with the level of applied magnetic field and it is highly structure sensitive, therefore, it depends on purity, heat treatment, deformation[22] etc.

Respective values of susceptibility and permeability helps in classification of magnetic material by [22]:

- Empty spave; $\chi = 0$ and $\mu = 1$ because no matter is there to magnetize
- Diamagnetic; $\chi < 1$ and μ is slightly less than 1
- Paramagnetic and anti-ferromagnetic; $\chi < 1$ and μ slightly greater than 1
- Ferromagnetic and ferromagnetic; $\chi << 1$ and $\mu << 1$

Relation between M or B versus H is used to plot graphs known as magnetization curve as shown in figure 2.3. *M-H* curves show for diamagnetic material, a negative slope which implies susceptibility and permeability is negative. For para- and anti-ferromagnetics, the slope is positive, means susceptibility and permeability is positive. In case of ferro- and ferrimagnets susceptibility and permeability are large and positive and are functions of the applied field.

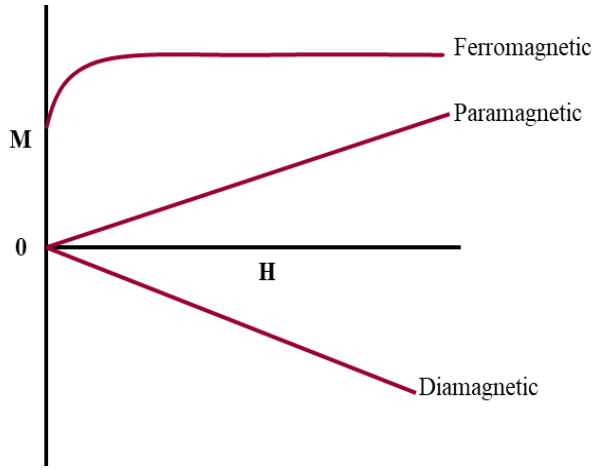

Figure 2.3: M-H curves for ferromagnetic; paramagnetic; and diamagnetic material

2.3.2 Curie Law

In a paramagnetic material, magnetization is directly proportional to an appltied magnetic field. As the temperature increases, it will become harder to remain in order for atomic magnetic moments or electron spin. The relation is reveresed i.e the susceptibility is inversely proportional to the absolute temperature. This relationship is defined as the curie law.

$$\chi = \frac{C}{T} \qquad 2.6$$

In ferromagnetic, anit-ferromagnetis and ferrimagnetic case, it is noted that electron spins are aligned in an ordered even in the absence of magnetic field. This is known as spontaneous magnetization.[24] As the temeprature increases, spontaneous magnetization vanishes. For more general cases, Curie-Weiss law is considered in which interaction between neighbouring magnetic moments (θ) taken into account by:

$$\chi = \frac{C}{T - \theta} \qquad 2.7$$

When θ is positive it means at low temperature material is ferromagnetic. As the critical temperature increases, magnetic order fades and the material exhibits paramagnetic behavior. But if θ is negative below transition temperature, material remains as anti-ferromagnetic. This transition temperature is known as Curie temperature (T_c) in ferromagnetism and Neel temperature (T_N) for antiferromagnets as shown in figure 2.4

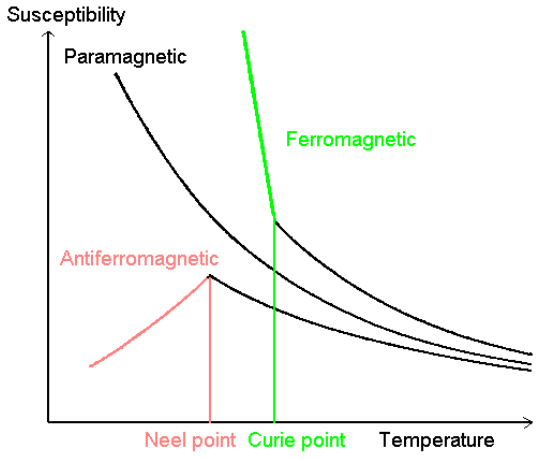

Figure 2.4: -Difference in magnetic susceptibility with temperature for diamagnetic, paramagnetic, ferromagnetic and Anti-ferromagnetic (Source: Wikipedia)

2.4 **Properties of Magnetic Material**

2.4.1 Hysteresis

Materials like ferromagnets display a long-range ordering phenomenon in which atomic magnetic moments are arranged parallel with each other in a domain. Inside the domain, it is extremely magnetized. The bulk sample is considered demagnetized because domains in the sample are arranged randomly with each other Thus when an external magnetic field is applied results in a lineup of the magnetic domains resulting increase in the magnetic flux density within the material so that if the external applied magnetic field is removed sample remains magnetized and do not return to zero. To make magnetization zero, a magnetic field is applied in opposite direction and it makes a loop known as hysteresis loop as shown in Figure 2.5. The absence of retrace ability of the magnetization is the property known as hysteresis and magnetic domains in the material are related to it.[14] commonly, this behavior can be seen in ferromagnetic materials

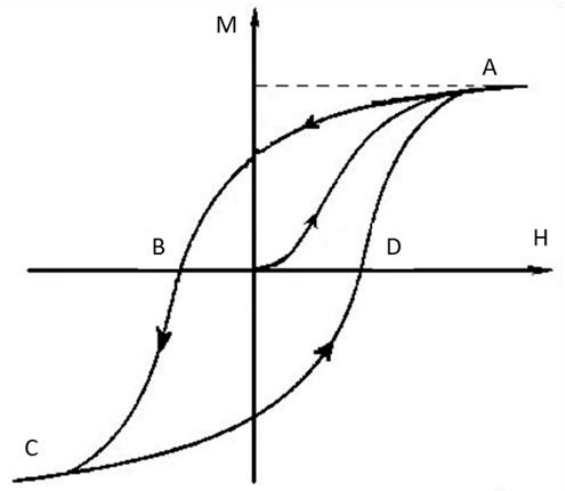

Figure 2.5: Hysteresis loop for a ferromagnetic material, M is magnetization, H is applied field (Source: Wikipedia)

- (a) Non-linear magnetization curve starts at zero and when all the magnetic domains are aligned in the direction of a field. It attains the saturation level .means maximum magnetization at a maximum temperature (i.e Curie temperature) it can reach. If the magnetic field is removed, material still shows magnetization.
- (B) Here magnetic field, H, equals to zero, but material is still partially magnetized as partial magnetic domain arrangement occurred.
- (C) Saturation level is attained in the opposite direction of the applied magnetic field.

- (D) Magnetic field in opposite direction is applied to demagnetize the material.

2.4.2 Coercivity

If the applied magnetic field is applied in reverse direction in hysteresis loop to reverse the magnetization curve, magnetic induction reduces to zero which is equals to coercivity (H_c). The opposite field needed to decrease zero is known as intrinsic coercivity (H_{ci}).

2.4.3 Anisotropy

Magnetic anisotropy follows where magnetic susceptibility fails to fulfill curie law. Magnetic anisotropy is the directional dependence of the magnetic moment in material and various factors are responsible for its origination[26]: Crystalline structure of the material is responsible for magnetocrstalline anisotropy. It is an intrinsic property of the material and depends on the direction of the material's magnetization. Magnetocrystalline anisotropy is generated by the atomic structure and bonding in the magnetic material. This anisotropy process also gives rise to energy due to lattice distortion in order to minimize its total free energy. Magnetic system when get deformed because of magnetization is known as magnetostriction.

2.5 3d/4f ions as magnetic centers

3d and 4f ion usually are the origin of magnetic properties and behave as magnetic centers because of their localized unpaired electrons. Hence magnetic properties are described by the electronic states of these centers. Origin of magnetism can be understood with quantum mechanics of electronic angular momentum; it has two sources- orbital motion and spin. For magnetism of electron, two basic approaches are taken, wave mechanics, because of Schrödinger and matrix mechanics, because of Heisenberg.

In wave mechanics, fundamental Schrödinger equation is:

$$H\psi = E\psi \qquad 2.8$$

H is Hamiltonian operator in the Schrödinger equation. It represents the sum of the kinetic and potential energy.

But cartesian coordinates (x,y,z) are not suitable for many problems like in the case of an atom, where the nucleus serve as a natural center. Therefore in case of atomic systems, orbitals can be chosen as

product of a radial and spherical harmonics which can be classified by quantum numbers it is appropriate to take into account the relation between Laguerre polynomials and spherical harmonics

$$\psi_{nlm}(r,\theta,\phi) = R_n(r)Y_{lm}(\theta,\phi\,) \qquad 2.9$$

2.5.1 Slater Determinant

Accuracy in computational calculations becomes more challenging with the increase in number of electrons. Therefore, it is important to introduce many electron wave functions. The complete wave function of an electron is product of both spatial part and spin part which is called spin orbital[27]. According to the orbital approximation, an *N*-electron atom contains *N* occupied spin orbitals. According to Pauli exclusion principle (explained in section 2.5.3 in detail), no two spin orbitals in this case must be identical. So to represent it mathematically[28], it can be written as

$$\psi(1,2,\dots,N) = \frac{1}{\sqrt{N!}}\begin{vmatrix} \varphi_1(1) & \varphi_2(1) & \cdots & \varphi_N(1) \\ \varphi_1(2) & \varphi_2(2) & \cdots & \varphi_N(2) \\ \vdots & \vdots & \ddots & \vdots \\ \varphi_N(N) & \varphi_N(N) & \cdots & \varphi_N\,(N) \end{vmatrix} \qquad 2.10$$

This expression is called as slater determinant. Rows are number of electrons and columns are orbitals and N! is for normalization.

The Hamiltonian for system with N electrons can be written as:

$$H = \sum_{i=1}^{N}\left\{-\frac{1}{2}\nabla_i^2 - \frac{Z}{r_i}\right\} + \sum_{i<j}^{N}\frac{1}{r_{ij}} \qquad 2.11$$

The energy of the state represented by slater determinant is given by:

$$E = \sum_a I_a + \frac{1}{2}\sum_{a,b}(J_{ab} - K_{ab}) \qquad 2.12$$

where the sums run over all occupied orbitals. First term represents one –electron part, J_{ab} is for coulomb interactions and K_{ab} is for exchange integrals, a and b are spin orbitals and factor ½ corrects for the double counting of pairs.

Solution of this Schrödinger equation results in the set of mathematical equation called wave functions. These wave functions (ψ) are also separated into radial function, *R*, it depends on the distance of the nucleus *r* from the electron and the angular function, *Y*, it depends on θ and φ. The radial parts of the wave function are defined by the quantum numbers *n* and *l* and angular parts of the wave function are defined by *l* and m_l.

2.5.2 Quantum Numbers

So what do quantum numbers represent? Quantum numbers give information about the allowed solutions to the Schrödinger equation. The principal and angular quantum numbers are represented by n and l and the magnetic quantum number is given by m_l. Many other properties of the electron can be determined by these quantum numbers [29].

- Principle Quantum Number (n):

  ..Energy of the electron level is described by the principle quantum number. An electron with an n value defines the nth electron shell. Even though, this value n is not itself responsible for any magnetic properties still it decides value of the l and m_l quantum numbers which influence magnetic properties.

- The Orbital quantum number (l)

  Principle quantum number (n) decides value of l. So $l = n$-1. It decides the magnitude of the orbital angular momentum of the electron and for an individual electron, the magnitude of the orbital angular momentum is related to the angular momentum quantum number (equation 2.13)

$$|L| = \sqrt{l(l+1)}\,\hbar \qquad 2.13$$

  Labels for the atomic orbitals i.e s, p, d and f are decided by the given values of l. For s orbitals, $l = 0$, for p orbitals $l = 1$ and so on. Radial distribution of the wave function is also predicted by the value of l. Subshells of the orbitals are also determined by l for example for $n = 1$, $l = 0$ and s has one orbital.

- The magnetic quantum number, m_l

  Magnetic quantum number ranges from $-l$ to $+l$. When $l = 1$, m_l have values from -1, 0, +1 which tells that p orbitals exist in three orientations when an external magnetic field is applied. $m_l\hbar$ gives the direction of field along the angular momentum.

- The spin quantum number, s

  Spin quantum number has the value $\frac{1}{2}$ for each electron and the magnitude of spin angular momentum can be calculated using spin quantum number as shown below in equation 2.14:

$$|S| = \sqrt{s(s+1)}\,\hbar \qquad 2.14$$

  Like magnetic quantum number m_l, there is m_s with allowed values of $-\frac{1}{2}$ and $+\frac{1}{2}$ only.

Ordering of atomic orbitals is energetically favored. Energy of the electron depends on *n* and *l*. Therefore electrons with lower angular momentum have lower energy because smaller *l* attracts more towards the nucleus due to shielding effect as compared to higher *l* values.

2.5.3 Pauli Exclusion Principle

In early 20th century, Wolfgang Pauli submitted a paper in which he concluded that in an atom there cannot be two or more equivalent electrons, for which in strong fields the values of all four quantum number coincide. This principle was used for further study of many particle systems in quantum mechanics by Heisenberg [30] and Dirac.[31] In these studies of Pauli exclusion principle as to occupy the same quantum state for two electron is prohibited, antisymmetric many electron wave functions were constructed and it proved that for these functions two particles in the same state is not possible[32].

2.5.4 Hund's Rules

In 1925 Freidrich Hund established rules from a combination of an experimental studies and quantum mechanics. After his observation, he stated few rules which commonly known as Hund's rule [33]:

1. In the many electron system, multiple states arise from same configuration but the state with maximum total spin is the ground state indicating that the
2. States of same configurations possessing same total spin, the ground state is one with highest angular momentum quantum number *L*.
3. If the shell is less than half filled then the state with lowest value of *J* is the ground state whereas if the shell is more than half filled then the ground state is with highest value of *J*.

2.5.5 Spin-orbit coupling

As mentioned in the section 1.5.1, an electron carries both spin angular momentum and orbital angular momentum. Orbital angular momentum of an electron results in magnetic moment with a related magnetic field but it's not an only source of magnetic moment in an electron. Spin of an electron also responsible for a magnetic moment. In the magnetic field, orbital motion interacts with electron's magnetic moment. This interaction is known as spin-orbit coupling. Extent of spin-orbit coupling is measured by assuming the orbiting motion of the nucleus around the electron specified by the nuclear charge and the nuclear number, Z (2.15). Usually, Hamiltonian for spin-orbit coupling is given by

$$\mathcal{H} = \lambda \boldsymbol{L}.\boldsymbol{S} \qquad 2.15$$

With the *l* and *s* quantum number of each electron, total angular momentum is calculated. However, the way of calculation for total angular momentum varies with the magnitude of orbit-orbit, spin-spin and

spin-spin couplings. For many electron systems, two different methods for estimating total angular momentum are possible [33]:

Aside from the attraction between the nucleus and electrons, other two major factors which contributed to the atomic system's energy:

1) Inter-electronic repulsion, that results in the energy separation between the terms of the given configuration.
2) Spin-orbit interaction gives rise to the energy gaps between the components of the term.

Russell-Saunders coupling or in general terms also known as *LS* coupling is preferred for light atom in which spin-orbit interaction is weak, the electronic repulsion dominates over spin-orbit interaction. Hence, to calculate the total angular momentum, first orbital angular momentum and spin angular momentum from each individual electron are calculated to obtain the total orbital momentum and total spin momentum (equation 2.16) and then the total angular momentum is obtained by combing total orbital momentum and total spin momentum (equation 2.17)

$$\begin{cases} L = |l_1 - l_2|, |l_1 - l_2| + 1, \ldots., l_1 + l_2 \\ S = |s_1 - s_2|, |s_1 - s_2| + 1, \ldots., s_1 + s_2 \end{cases} \qquad 2.16$$

$$J = L + S, L + S - 1, \ldots\ldots, |L - S| \qquad 2.17$$

2.5.6 The Anomalous Zeeman effect

The Dutch physicist Pieter Zeeman observed that when an atom is placed in an external magnetic field, the atomic energy levels split which results in spectrum change. This phenomenon is known as Zeeman effect [34] (as shown in figure 2.8).

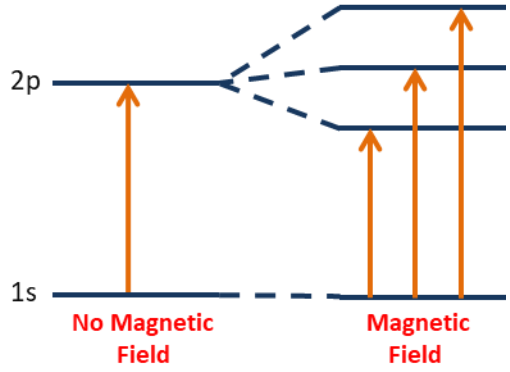

Figure 2.6: Splitting of energies in presence of magnetic field

When there is no spin angular momentum, it is known as normal Zeeman effect. But for more complex arrangement of lines in the spectrum which is a result of spin-orbit coupling is given by the anomalous Zeeman effect, this is much more common. Zeeman Hamiltonian is given by

$$\mathcal{H} = g_e \mu_B . S . B \qquad 2.18$$

Here, g_e is a constant and value for it is 2.00. This g is known as landè g-factor[37] which van be calculated by using *L*, *S* and *J* as given in equation 2.19

$$g = 1 + \frac{J(J+1) + S(S+1) - L(L+1)}{2J(J+1)} \qquad 2.19$$

Scientists have been working on the development of new materials such as single molecule magnets. Single molecule magnets (SMM) are much in attention because of their advantages of the molecular scale with the properties of bulk materials. However, for SMM in order to be successful depends on the magnetic blocking temperature $T_{B,}$ because value of Tb depends on rate magnetic field. SMM based on 3d and 4f elements attracted more attention in few years because of their promising advancement in molecular magnetism. In next chapter, it is described in detail.

3 Single Molecule Magnets

Single molecule magnets possess the classical macroscale properties of a magnet to the quantum properties of a nanoscale quantity[1]. It is described as the molecule which can maintain its magnetization even if an external magnetic field is removed [38,39]. It has benefits of the molecular scale with the properties of bulk magnetic material and is desirable for high-density information storage and for quantum computing, furthermore because of its molecular nature it leads to interesting quantum effects. SMMs can be possible in different shapes and sizes and give permission for selective substitutions of the ligands that changes the coupling to the environment and achievable exchange of the magnetic ions due to which magnetic properties show considerable change without altering the structure or coupling[1,40,41]

The first SMM was discovered in 1996, after studying a transitional metal compound with dodecametallic manganesesacetate ($Mn_{12}OAc$) synthesized by Prof. Tadeusz Lis[42] in 1980.

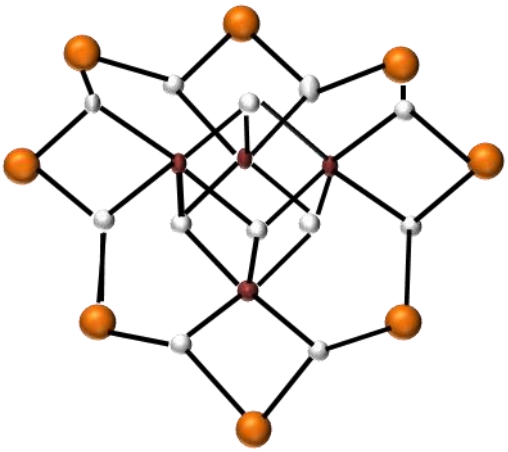

Figure 3.1: Molecular structure of $Mn_{12}OAc$ and chemical structure of its core. Orange spheres are Mn^{3+}(S =2), Red spheres are Mn^{4+} (S = 3/2) and white spheres are oxygen atoms

In Figure 3.1, it can be seen that there are twelve Mn atoms in this molecular structure, four Mn(IV) ions are in inner ring like tetrahedron and eight Mn(III) ions are in outer ring forming octagon with sixteen acetate groups covering the magnetic core from nearby molecules. Magnetic properties of $Mn_{12}OAc$ was shown by using high-field electron paramagnetic resonance (EPR) and measurements with a superconducting quantum interference device (SQUID) magnetometer suggesting that the ground state of the given molecule is S = 10. The antiferromagnetic coupling between the Mn(III) ions with spin of S

= 2 and the Mn(IV) ions with spin of S = 3/2 results in the large ground state spin S = 10. The low lying electronic states are usually described by the spin of the ground state taking zero field splitting of the different Ms levels by spin orbit coupling into account which is a precondition for a potential energy barrier for magnetization reversal.[43,44] The zero field splitting parameter D in this case is around -0.5 cm^{-1} and the sign of the D indicates the energy barrier as shown in Figure 3.2. If D is negative that means it is easy axis type anisotropy.

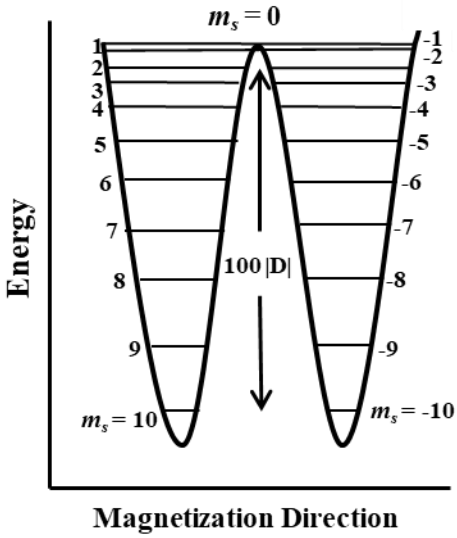

Figure 3.2: Plot of the potential energy versus the magnetization direction for a SMM with a ground state spin of S = 10.

Large energy barrier contribute in the magnetization of SMM in one direction. For $Mn_{12}OAc$ molecule barrier is between E (ms = 0) – E (ms = ±10) = 100D = 70 K. When magnetic field is applied at 2 K in order to magnetize the above mentioned molecule it was observed that after removing the magnetic field, even after two months, magnetization is about 40 % of the saturation.[45,46] After few studies, magnetic hysteresis loops for $Mn_{12}OAc$ was calculated and likelihood of magnetic data storage at the molecule was observed by looking at the hysteresis loop [8].

After the observations of interesting properties in molecule $Mn_{12}OAc$ leads to new beginnings in development of molecular nano-materials. Large numbers of molecular complexes were synthesized as SMMs based on d-block and f-block ions.[47–49] due to their large spin ground states. SMMs are interesting because of their magnetic bi-stable nature i.e energy barrier between reversal of a spin form

$+M_s$ to $-M_s$, represented in the form of double well potential energy shown in figure 3.3 in which each well means the lowest energy $\pm M_s$ and it is usually given by:

$$\boldsymbol{U_{eff}} = S^2|D| \qquad 3.1$$

$$\boldsymbol{U_{eff}} = \left(S^2 - \frac{1}{4}\right)|D| \qquad 3.2$$

Where *S* is the ground state spin of the system, equation (3.1) is for integer and equation (3.2) is for non-integer spins respectively, *D* is the ZFS parameter. *D* is positive if smallest M_s state is lower in energy than the larger M_s state but *D* is negative when it is vice versa. When *U* i.e. energy barrier of a system is greater than the thermal energy, system remains magnetized even after removing an applied magnetic field because the system cannot rearrange its magnetic moment, hence it remain in a potential energy minimum. This is also responsible for a magnetic hysteresis at low temperatures.[50,51]

If the ground state spin of the complex is S > ½, then it leads to zero field splitting (ZFS) which can be expressed by Hamiltonian given below:[52]

$$\hat{H} = D\left[\hat{S}_z^2 - \frac{1}{3}S(S+1)\right] + E(\hat{S}_x^2 - \hat{S}_y^2) \qquad 3.3$$

Where *S* is the total spin, *D* and *E* are the zero field splitting (ZFS) parameters; *E* is the rhombic ZFS parameter and *D* is the axial ZFS parameter; expressed as;

$$D = \frac{3}{2}D_{zz} \qquad 3.4$$

$$E = \frac{1}{2}(D_{xx} - D_{yy}) \qquad 3.5$$

D_{xx}, D_{yy} and D_{zz} (in equation 3.4 and 3.5) are principle values of the **D** tensor.

The Spin-Hamiltonian to describe the coupling of the two spins centers can be given as [53,54]

$$H_{SH} = -2J\vec{S}_1.\vec{S}_2 \qquad 3.6$$

The Hamiltonian has a spin states which are related to spin quantum number S in order of a range of $|S_1 + S_2|$ to $|S_1 - S_2|$. Energy between two states are calculated as

$$\Delta E(S) = E(S) - E(S-1) = -2JS \qquad 3.7$$

3.1 Transition metals

Researchers are very curious, when it comes to d-block systems because inspite of having several disadvantage like,

i. Magnetic moments are smaller
ii. Spin-orbit coupling constant is not very high
iii. Ligand field coupling is stronger than the spin orbit coupling which extinguish first order orbital contribution.

this makes it less suitable for having high $\boldsymbol{U_{eff}}$ and/or hign blocking temperature (T_B), if it is compared with their equivalent lanthanides. However, as more knowledge in the study of 3d single-molecule or single-ions in a ligand filed is gained, new ideas that give permission to couple the anisotropy of ions to create a poly-nuclear system can begin. In last decades, large number of studies have been done on first row transition elements like Mn(II), Fe(II), Co(II), Ni(I)(II) and Cr(II)[11,12,51].

Anisotropic zero field splitting parameter *D* and *E* play role in lifting the degeneracy of the M_S levels related to a given *S*. There are two possible ways that contribute in the ZFS and consequently to the magnetic anisotropy:

i. First order spin-orbit coupling which explains the mixing of spin and orbital angular momentum in the ground state of a molecule
ii. Second order spin-orbit coupling which means mixing of excited states with the ground state.

To measure the splitting of states after spin-orbit coupling, spin-orbit coupling parameter (λ) is used which can be given as:[49–51]

$$\lambda = \frac{\zeta}{2S} \qquad 3.8$$

Where ζ spin-orbit coupling constant and S is the total spin of the system

In 3d ions, splitting of the orbitals depend on;

- Geometry of the system
- Valence state of the metal ion present in the system

- Nature of ligands
- Size of d orbitals

Orbitals in d-subshell pointing directly at the ligand experience more repulsion i.e. less stable and higher in energy.[55,56]

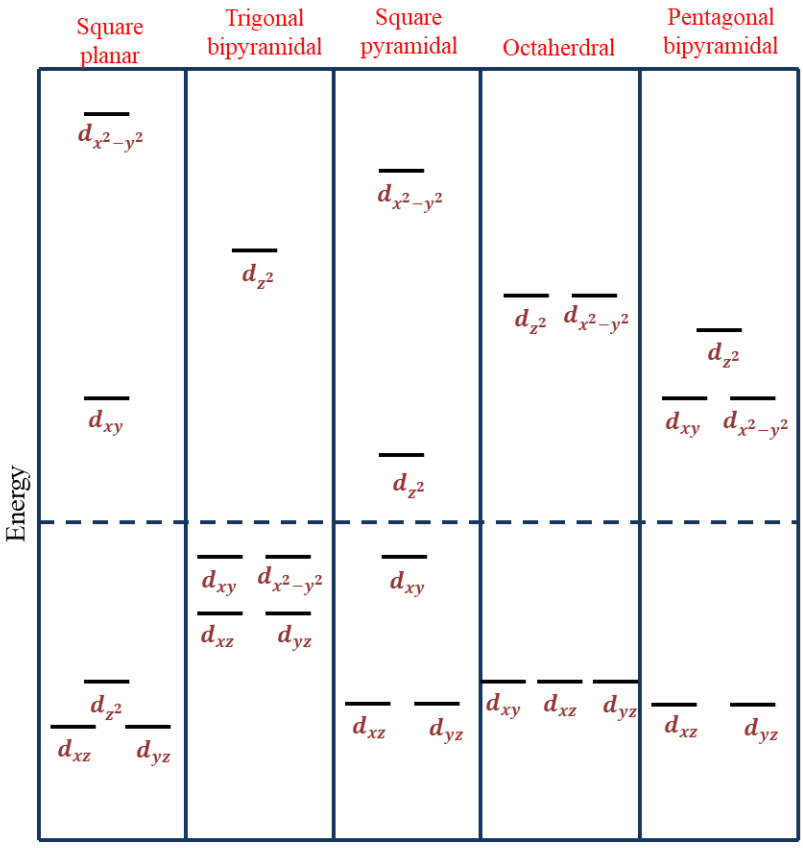

Figure 3.3 Crystal field splitting in some common geometries

Ni(II) in an octahedral ligand field is considered here as an example for second order spin orbit coupling, Ni^{2+} has d^8 configuration which has ^3F as ground term state which splits into three states $^3A_{2g}$, $^3T_{1g}$ and $^3T_{2g}$ in octahedral field (shown in Figure 3.5(b)). As geometry of a molecule cannot be always be in accurately symmetric whether it is octahedral or tetrahedral. Thus, in distorted octahedral field, triplet ground state is no longer degenerate which result in mixing of $^3T_{1g}$ and $^3T_{2g}$ states with ground A term. This lifting of degeneracy of states is responsible for anisotropy, which is important for knowing the properties of SMM.

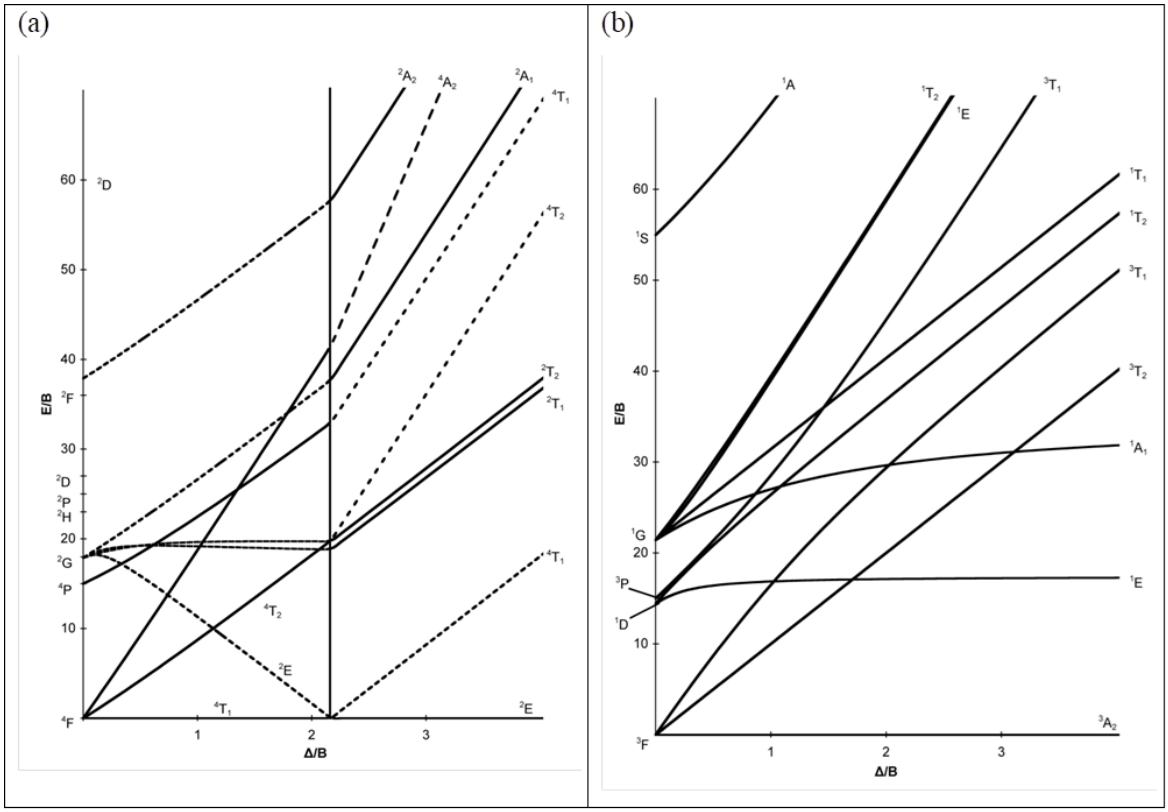

Figure 3.4 Tanabe –Sugano diagram for (a) d^7 system; (b) d8 system and (c) orgel diagram(Source: Wikipedia)

In Figure 3,5(a), Co^{2+} is taken here as an example, In case of Co^{2+} ground state term is ^4F which in octahedral field splits into $^4T_{1g}$, $^4T_{2g}$ and ^4A_g.. $^4T_{1g}$ is ground state term, with $^4T_{2g}$ and ^4A_g as first and second excited states.

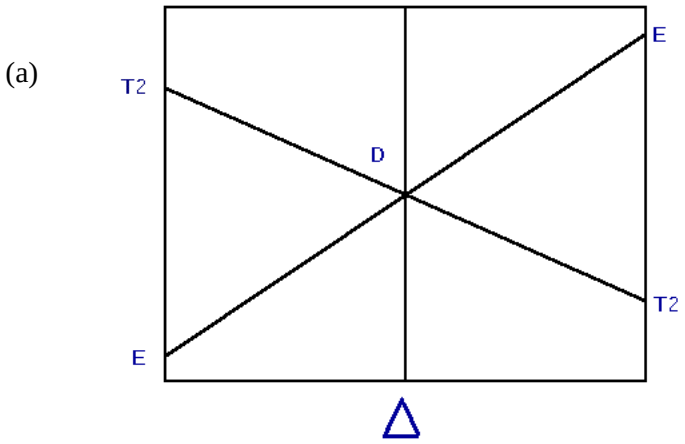

(b)

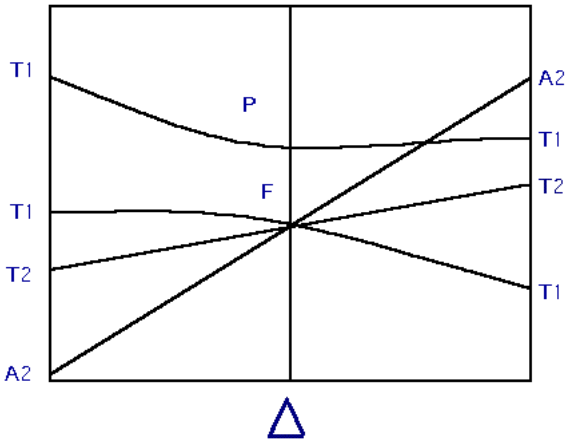

Figure 3.5: Orgel diagram for d^n configuration for tetrahedral and octahedral (Source: Wikipedia)

However as explained in orgel diagram in Figure 3.6 ground state term is different for different coordination number and geometry.[58] This illustrates that by changing the coordination number which in turn changes the geometry of a system; it can lead to huge changes in the magnitude of magnetic anisotropy of d-block metal ions, which is a governing property of magnetic behavior of SMM.

3.2 Lanthanide Metal

In case of lanthanides, orbital angular momentum plays an important role for the calculations of magnetic properties. Rare-earth ions do not behave like transition metal ions, in case of d electrons f transition metal crystal field splitting is stronger than spin orbit coupling as mentioned in above section, however, when it comes to 4f metal ions spin orbit coupling is stronger than crystal field effects.[59]

Electron-electron interaction, Ligand-field, spin-orbit coupling, exchange interaction and magnetic field are responsible for splitting of the electronic states of a magnetic system. Behavior of electrons present in d orbitals and f orbitals in the presence of different effect interactions[60] can be observed as

- 4f has H_{ex} smaller than H_{LF} and $H_{so.}$
- H_{mag} and H_{ex} has comparable energy

General electronic configurations of 4f atoms is $[Xe]4f^n6s$, with n increasing from 0 to 14, however, there are few exceptions like La, Ce, Gd, Lu with the electronic configuration of $[Xe]4f^n5d^16s^2$. In lanthanides, trivalent state is most stable that means loss of 5d and 6s electrons.

Information from unpaired 4f electrons are used to get ground multiplet $^{2S+1}L_J$, where *S* is total spin, *L* is total orbital angular momentum and *J* is total angular momentum.[62] Spin-orbit coupling results in the splitting of the multiplet term with same *L* and *S*. If subshells are more than half filled then $J = L+S$ is lowest in energy and if it is less than half-filled then $J = L-S$ is lowest in energy. Energies of the term $^{2S+1}L_J$ is given by

$$E = \left(\frac{\lambda}{2}\right)[J(J+1) - L(L+1) - S(S+1)] \qquad 3.9$$

Here λ is the spin-orbit coupling as mentioned in equation 3.8. Each *J* has *2J+1* degeneracy states which can further split in various other interactions as shown below.[63,64]

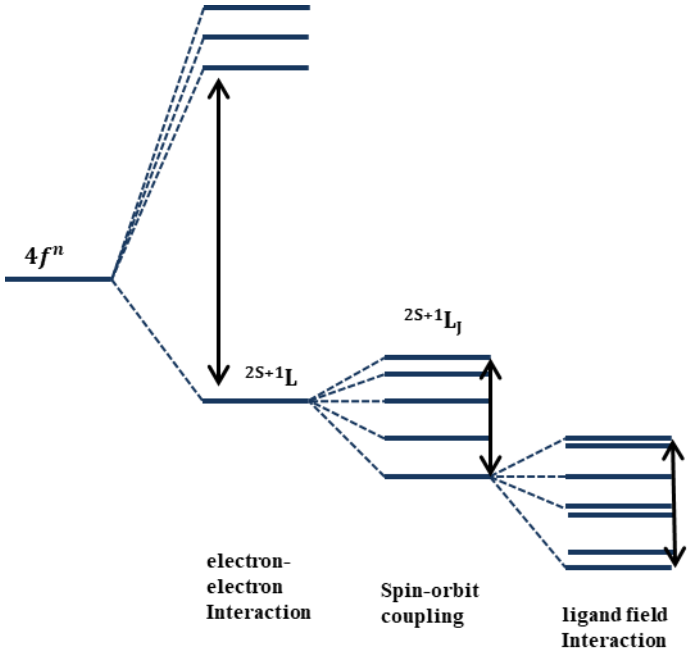

Figure 3.6 Energy scale of the 4f ions

If magnetic field is applied, *2J+1* level split into further M_J energy levels which is $-J \leq M_J \leq +J$.[56,59,60,63,64] The Zeeman Effect can be defined by using spin Hamiltonian as

$$H = \mu_B . g_J . J . B \qquad 3.10$$

Where g_J is Landé factor which can be obtained by *L*, *S* and *J*;

$$g_J = 1 + \frac{J(J+1) + S(S+1) - L(L+1)}{2J(J+1)} \qquad 3.11$$

Curie law is followed by lanthanide free ions for calculating the magnetic susceptibility;

$$\chi^M = \frac{N_A g_J^2 \mu_B^2}{3kT} J(J+1) \qquad 3.12$$

Here χ^M is the molar susceptibility and N_A is the Avogadro number.

Table 3.1- Term symbols, landè factor, and magnetic susceptibility for 4f ions

Ion	$4f^n$	$^{2S+1}L_J$	g_J	$\chi_M T$
Ce^{3+}	1	$^2F_{5/2}$	6/7	0.80
Pr^{3+}	2	$^3H_4$	4/5	1.60
Nd^{3+}	3	$^4I_{9/2}$	8/11	1.64
Pm^{3+}	4	$^5I_4$	3/5	0.90
Sm^{3+}	5	$^6H_{5/2}$	2/7	0.09
Eu^{3+}	6	$^7F_0$	5	0.00
Gd^{3+}	7	$^8S_{7/2}$	2	7.88
Tb^{3+}	8	$^7F_6$	3/2	11.82
Dy^{3+}	9	$^6H_{15/2}$	4/3	14.17
Ho^{3+}	10	$^5I_8$	5/4	14.07
Er^{3+}	11	$^4I_{15/2}$	6/5	11.48
Tm^{3+}	12	$^3H_6$	7/6	7.15
Yb^{3+}	13	$^2F_{7/2}$	8/7	2.57

In the present work, complexes with 3d and 4f ions are calculated and their magnetic properties are studied. Zero field splitting parameters, g-factors and magnetic susceptibilities calculated to see if or how the given complexes fit for SMMs.

4 Quantum Calculations

The Schrödinger equation is the most elementary equation in non-relativistic quantum mechanics and it can be described as time- independent and time-dependent. Time-independent Schrödinger equation is:

$$\hat{H}\Psi(\mathrm{x},\mathrm{R}) = E\Psi(\mathrm{x},\mathrm{R}) \qquad 4.1$$

x and R are space and spin coordinates of N electrons and spatial coordinates of M nuclei described by wave function Ψ. *E* is the total energy of the system and $\hat{H}$ is Hamilton operator which includes the kinetic energy of electron and nuclei, potential energy of electron-nucleus interactions, electron-electron interaction and nucleus interaction(given in equ. 4.2)

$$\hat{H} = -\frac{1}{2}\sum_{i=1}^{N}\nabla_i^2 - \frac{1}{2}\sum_{a=1}^{M}\frac{1}{M_a}\nabla_a^2 - \sum_{i=1}^{N}\sum_{a=1}^{M}\frac{Z_a}{r_{ia}} + \sum_{i=1}^{N}\sum_{j>i}^{N}\frac{1}{r_{ij}} + \sum_{a=1}^{M}\sum_{b>a}^{M}\frac{Z_a Z_b}{R_{ab}} \qquad 4.2$$

In above equation, *a* and *b* goes over all M nuclei, i and j goes over all N electrons.

However, as the size of the system increases solving Schrödinger equation becomes effortful. Hence, for many-electron system approximate wave function is required. The variational method is an alternative solution for this issue. According to the variational theorem, energy calculated with any reference wave function Φ is always greater or equal to the ground state energy E_0

$$\frac{\langle\Phi|\hat{H}|\Phi\rangle}{\langle\Phi|\Phi\rangle} \geq E_0 \qquad 4.3$$

Such reference wave function is usually constructed as CI wave function which is expressed as a linear expansion

$$\Psi_k = \sum_{I=1}^{N} c_{kI}\Phi_I \qquad 4.4$$

Where c_k is expansion coefficients and Φ_I is basis functions. With the CI methods expansion coefficients are determined by variational method. The Hartree-Fock method is one of the variational methods with a function comprising of a Slater determinant. Hartree-Fock equation can be derived by minimizing the energy with respect to spin-orbitals

$$\hat{F}\phi_i = \epsilon_i \phi_i \qquad 4.5$$

Where $\hat{F}$ is Fock operator which is an effective one-electron operator given as a

$$\hat{F} = \hat{h} + \hat{J} - \hat{K} \qquad 4.6$$

$\hat{h}$ accounts for the kinetic energy of an electron and potential energy of the electron interacting with the nucleus, $\hat{J}$ is the Coulomb operator describing Coulomb interaction of an electron with the other electrons and $\hat{K}$ is exchange operator which is difficult to explain and does not have a simple classical explanation. It arises from the antisymmetry requirement of the wavefunction. The Hartree-Fock equations can be solved by the linear combination of N atomic orbitals (LCAO)[65] to form MOs:

$$\phi_i = \sum_{\mu=1}^{N} c_{\mu i}\, \chi_\mu \qquad 4.7$$

Where $c_{\mu i}$ are the expansion coefficients and χ_μ are the atomic orbitals. However, the Hartree Fock method has limitations. In HF theory the movement of electrons is correlated with the electron exchange only which inhibits two electrons with parallel spins to be in the same point in space. The possibility of finding electron *i* at some point is not effected by movement of another electron *j* if they have opposite spin. Also in the case where more than one electronic configuration is crucial for the understanding of certain near degenerate electronic states then HF method has shortcomings.

4.1 Complete Active Space Self Consistent Field

As discussed above single reference approach is not valid where an orbital near-degeneracy problem appears. In multi reference method wave functions, single excitations are required from inactive to virtual, inactive to active and active to virtual orbitals complying with Brillouin's theorem.[66] Complete active space self-consistent field (CASSCF) wave function consist of CI expansion of active orbital subspace including core-virtual, active –virtual and core –active excitations.[67] In this method, all

determinants which are derived from the set of active orbitals are treated as a reference function. Active space CAS(N,M), which represents N electrons in M orbitals, is given by total spin and a fixed set of orbits as linear combination of slater determinants which includes all possible states represented by N electrons in M orbitals.

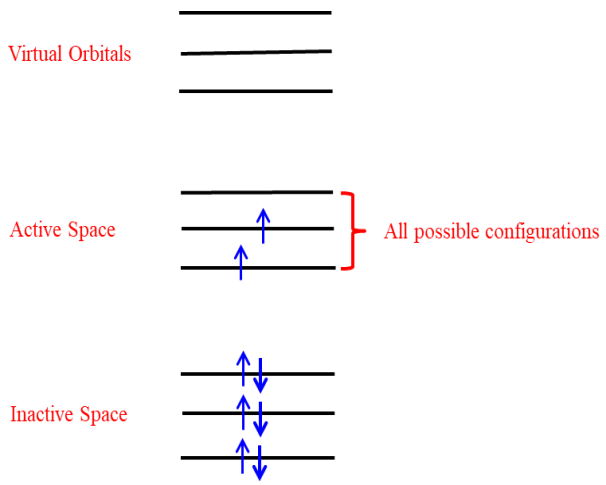

Figure 4.1: CASSCF orbitals, where inactive orbitals are doubly occupied and full CI calculations are carried out in active space

Configuration state function (CSF) or sum of slater determinants is taken as a wave function (ψ_0) for multi reference method. Single excited wave function can be modified under Brillouin condition:[67]

$$\psi_{pq} = \frac{1}{\sqrt{|\gamma_{pp} - \gamma_{qq}|}} \hat{E}_{pq}\psi_0 \qquad 4.8$$

Where $\hat{E}_{pq}$ is a spin averaged excitation operator, γ_{pp} is the occupation number of the orbital, ψ_{pq} is single excited function.

Two operators can be used to show the excitations as expressed in equation 3.4 and 3.5. Here indices *p,q,r,s* represents general molecular orbital, indices *i,j,k,l* represents core MO and indices *t,u,v,w* as active molecular orbitals

$$F_{pq}^{core} = h_{pq} + \sum_{i} \{2(pq|ii) - (pi|qi))\} \qquad 4.9$$

$$G_{pq}^{act} = \sum_{tu} \gamma_{tu} \left\{(pq|tu) - \frac{1}{2}(pt|qu)\right\} \qquad 4.10$$

CASSCF method includes complete CI calculation in the active space, density matrices calculations, operators F^{core}, G^{act} and J running over the active orbitals

Magnetic properties of the metal complexes are calculated and interpreted with sufficient accuracy by using certain existing programs. Zero field splitting parameters, are anisotropy parameters g-factors and magnetic susceptibilities calculated using the SCF; CASSCF and SOCI programs. The further development and implementation was done by T Bodenstein[68] by taking the methods for calculating magnetic properties of the Bochum program package for the *ab initio* calculation of open-shell electronic structures which was originally developed in the working group of V.Stammeler (Bochum). Versions from Bochum, Karlsruhe and Tübingen (in collaboration with R.F. Fink) of individual programs put together.

4.2 CAS-SO-CI approach

Low-lying spin states of a spin system is described by using method of configuration interaction (CI), wave function for all possible spin configuration is generated within the set of active orbitals and the many-electron Hamiltonian is diagonalized with in the full space of all these possible spin configurations. These calculations result in the energies of the low –lying spin states and from there by using equation 3.7 exchange coupling constant *J* can be calculated. However, this method often resulted in not so accurate numerical values and also it was computationally costly to get more accurate values.

In CAS-CI approach, molecular orbitals are divided in to three subspaces: inactive space, active space and virtual space just like CASSCF method The single set of orthogonal molecular orbitals obtained by a state-averaged CASSCF calculation is further used by CAS-CI calculations, where a full CI in the active space is done and it gives explanation of all electronic states that belong to the active space. However, in CAS-CI, LS state covalent state is stronger than the ionic state; therefore, orbitals produced by state averaged CASSCF method have good description of covalent states than the ionic i.e charge transfer states. Hence, energy for the charge transfer is not accurate by covalent orbitals which led to underestimation of values of *J*. Modified CAS-CI (MCAS-CI) approach[54] corrects the charge transfer state in the wave function by taking relaxation energy (R) for the charge transfer state. This method is not computationally costly and do not involve complicated calculations of matrix elements.

Implementation for the calculation of spin-orbit coupled CAS-CI method is done by T.Bodenstein[68] for spin-orbit calculations. It includes algorithm based on the determinant-based full CI approach by

Knowles and Handy[69] and the SOCI method by Sjøvoll, Gropen and Olsen.[70] The implemented Hamiltonian includes:

$$\hat{H} = \hat{H}_0 + \hat{H}_{so} + \hat{H}_{ZM} + \hat{H}_{MCASCI} \qquad 4.11$$

Where $\hat{H}_0$ is the electronic Born-Oppenheimer Hamiltonian, $\hat{H}_{SO}$is spin-orbit operators, $\hat{H}_{ZM}$ is Zeeman operator and $\hat{H}_{MCASCI}$ operator.

Davidson diagonalization[71] (59) method is used for the diagonalization of the CI matrix, as for the large active space, the memory requirement of an $\boldsymbol{N} \times \boldsymbol{N}$ matrix makes difficult for direct diagonalization. In the implemented program[68] used for these calculations, Diagonal elements and relaxation energies ca be calculated directly. Matrix vector products can be calculated independently of each other. According to the implemented Block-Davidson algorithm, it acts as an iterative subspace in which eigenvector c^k, the kth eigenvector of the Hamiltonian, is converted in a linear vector:[68,72]

$$c^k = \sum_i^B a_i^k \, b_i \qquad 4.12$$

Where b_i is the basis and the a_i^k are expansion coefficients

As mentioned in reference 46, if a basis does not contain any part of a vector, algorithm may not converge but by starting with the appropriate basis, this problem can be fixed.

4.1.1 Spin orbit operators:

If relativistic contribution is considered for many-particle states, the starting point for the derivation of relativistic Hamiltonian generally is the relativistic equations of motion. Relativistic corrections can be made. In the present program[68], calculation of the energy differences in systems is done in which the non-scalar spin orbit effects dominate which includes spin orbit coupling and spin dipolar interaction[73]. For a good approximation of quasi-relativistic description, this associated Hamiltonian operator can be used:

$$\hat{H}^{DCB} = \sum_i \hat{H}^{Dirac}(i) + \frac{1}{2}\sum_{ij} \hat{H}^{coulomb}(i,j) + \hat{H}^{Breit}(i,j) \qquad 4.13$$

$$\hat{H}^{Breit}(i,j) = \hat{H}^{Retardation}(i,j) + \hat{H}^{Gaunt}(i,j) \qquad 4.14$$

Where $\hat{H}^{Coulomb}(i,j) = \frac{1}{r_{ij}}$ explains the instantaneous Coulomb interactions, $\hat{H}^{Breit}(i,j)$is the relativistic corrections to the two-particle interactions. The $\hat{H}^{Retardation}(i,j)$ corrects the electrostatic interaction and $\hat{H}^{Gaunt}(i,j)$ term is for magnetic interaction between two electrin current.

Equation 4.13 results as the beginning for many approximations. The Zeeman interaction of the spin magnetic moment of an electron induces the magnetic field in the presence of an electric field **E**

$$\hat{H}_{so}^{(1)}(i) = \frac{e}{2m_e c^2}\hat{s}_i^T(E \times \hat{p}_i) \qquad 4.15$$

Equation 4.15 takes different form because of the electric field resulted by the atomic nuclei K, where the angular momentum operator of the electron *i* with respect to the nucleus *K* with the distance of r_{iK}.

$$\hat{H}_{so}^{(1)}(i) = \sum_K \frac{Z_K e^2}{8\pi\epsilon_0 m_e^2 c^2}\frac{\hat{s}_i^T(\hat{r}_{iK} \times \hat{p}_i)}{r_{iK}^3} \qquad 4.16$$

However, for multi electron systems, fields generated by the other electrons are also taken into account and the resulting effective interactions results in three spin orbit operators:

$$\hat{H}_{SO}^{(1)} = \frac{\alpha^2}{2}\sum_{iK}\frac{Z_K \hat{s}_i^T \hat{l}_{iK}}{r_{iK}^3}, \qquad 4.17$$

$$\hat{H}_{SsO}^{(2)} = -\frac{\alpha^2}{2}\sum_{ij}\frac{\hat{s}_i^T \hat{l}_{ij}}{r_{ij}^3}, \qquad 4.18$$

$$\hat{H}_{SoO}^{(2)} = -\frac{\alpha^2}{2}\sum_{ij}\frac{\hat{s}_i^T \hat{l}_{ij}}{r_{ij}^3}, \qquad 4.19$$

Above mentioned spin-orbit operators explains one electron interaction and two electron interaction. Equation 4.18 explains the interaction of the spins of electron's own movement in the presence of other electrons and equation 4.19 gives the interaction of spin of one electron with the orbitals movement of the other electron. The two-electron term have a different sign and hence compensate parts of single-particle terms 4.17 which physically corresponds to the observed shielding.

Spin Hamiltonian after taking spin operator into account results in:

$$\hat{H}_{SO} = \hat{H}_{SO}^{(1)} + \hat{H}_{SsO}^{(2)} + \hat{H}_{SoO}^{(2)} \qquad 4.20$$

For excitation $i \longrightarrow j$, two Slater determinant consisting spin orbit operator takes a form of:

$$\widehat{H}_{ij}^{SO} = \langle i|\widehat{\mathcal{H}}^{SO}(1)|j\rangle + \frac{1}{2}\sum_{k} n_k \{\langle ik|\widehat{\mathcal{H}}^{SO}(1,2)|jk\rangle - \langle ik|\widehat{\mathcal{H}}^{SO}(1,2)|kj\rangle - \langle ki|\widehat{\mathcal{H}}^{SO}(1,2)|jk\rangle\} \quad 4.21$$

$\mathcal{H}^{SO}(1)$ and $\mathcal{H}^{SO}(1,2)$ are spin orbit operators as discussed above and n_k is the occupation number. By adding the fix occupation number factor in equation 4.21 mean-field approach can be introduced by taking the average over the two-electron contribution of the valence shell or in case of CASSCF calculations average over the two electron contribution over active space.[73]

$$\widehat{H}_{pq}^{SOMF} = \langle p|\widehat{\mathcal{H}}_{SO}^{(1)}|q\rangle + \frac{1}{2}\sum_{fix(r)} n_r \left\{\langle pr|\widehat{\mathcal{H}}_{SO}^{(2)}|qr\rangle - \langle pr|\widehat{\mathcal{H}}_{SO}^{(2)}|rq\rangle - \langle rp|\widehat{\mathcal{H}}_{SO}^{(2)}|qr\rangle\right\} \quad 4.22$$

In the present program, $\widehat{H}^{SOMF}$ operator also considers different shielding effects in atomic shells that cannot be generated by a single scaling factor. The two-electron term works efficiently for lanthanide systems also.

4.2 Zero Field Splitting Parameters

The Zero field splitting parameters (D; and E) considered as a fitting parameters for experimentally determined electron paramagnetic resonance (EPR). The main source of ZFS is interaction of the orbital angular momentum and spin angular momentum which results in lifting of the degenerate states with few cm^{-1}.

The components of the tensor including only angular momentum operator led to the magnetic parameters, which results in different spins and calculation of magnetization, magnetic susceptibility.[74]

Generally, effective Hamiltonian for calculating the zero field splitting (ZFS) in the absence of magnetic field is given as

$$\widehat{H}_S^{ZFS} = \hat{S}^T D \hat{S} \quad 4.23$$

Where $\hat{S}$ is the spin operator and **D** is 3 × 3 matrix

$$\mathbf{D} = \begin{pmatrix} D_{11} & D_{12} & D_{13} \\ D_{21} & D_{22} & D_{23} \\ D_{31} & D_{32} & D_{33} \end{pmatrix} \quad 4.24$$

As **D** is a traceless tensor i.e sum of diagonal elements is zero. First, analytical matrix of effective Hamiltonian is expressed non diagonal tensor with a complete D component and then diagonalization is performed to get the ZFS tensor components. Matrix elements $\langle S, M_s | H | S, M_S' \rangle$ are solved to get *D* tensor.

The ZFS Hamiltonian takes a form of

$$\hat{H}_S^{ZFS} = D\left(\hat{S}_z^2 - \frac{1}{3}\hat{\boldsymbol{S}}^2\right) + E\left(\hat{S}_x^2 - \hat{S}_y^2\right) \quad 4.25$$

Where *S* is the total spin and $\hat{S}^2 = \hat{S}_x^2 + \hat{S}_y^2 + \hat{S}_z^2$, D and E are zero field parameters.. D is axial parameter and E rhombic parameter. These two parameters play an important role for magnetic anisotropy. These two parameters are related to the diagonal elements of the tensor

$$D = \frac{1}{2}\left(-D_{xx} - D_{yy} + 2D_{zz}\right) = \frac{3}{2}D_{zz} \quad 4.26$$

$$E = \frac{D_{yy} - D_{xx}}{2} \quad 4.27$$

Relationship between D and E is given by

$$|\mathrm{D}| \geq 3E \geq 0 \quad 4.28$$

Matrix elements are calculated with $|S, M_S\rangle$ spin functions of the ground state and diagonalization is performed on the obtained matrix producing the energies of the sub-levels after spin-orbit coupling.[75,76] If *D* is positive that means system has easy plane magnetism however if *D* is negative that means system has easy axis magnetism which shows magnetic axis lies in *z* axis.

However, for a system with $S \geq 2$, the relative Hamiltonian can be expressed as Stevens operator;

$$\mathrm{H} = \sum_{k} \sum_{q=-k}^{k} B_k^q \, \hat{O}_k^q \qquad 4.29$$

Where B_k^q is crystal field parameter and $\hat{O}_k^q$ are operator equivalent, k is the rank and q is order which can be even, odd, positive and negative.

From last decades many researchers worked on extended Stevens operator, from conventional Stevens operator by Stevens in 1952 to Rudowicz (1985, 1987, 1988) to Hoffman (1990) to Ryabov(1999).[77]

Generalized algebraic for of ESOs can be represented in terms of angular momentum operators

$$O_k^q = \frac{\alpha}{2F_{k,q}} \sum_{m=0}^{k-q} a(k,q;m)\left[J_+^q + (-1)^{k-q-m} J_-^q\right] J_z^m \qquad 4.30$$

$$(q = 0,1,2 \ldots\ldots, k)$$

Where factor α = 1 for all *q* if k is an odd integer and α = 1 or ½ for even and odd *q* with even *k* and *F* is a coefficient with largest common factor for all *a(k, q; m)*.

In the program, the spin-orbit-coupled wave functions are projected onto this subspace. The SOCI wave functions then subjected to a Löwdin orthogonalization.[78] This has the advantage of to preserve the original character of the wave functions. Then, the numeric effective Hamilton operator constructed on the basis of the eigenfunctions of $\hat{S}_z$ in *S*.

4.3 Calculation of g-matrices

In the presence of external magnetic field, energy levels of a system split into respective sub levels. This can be describe by model Zeeman Hamiltonian

$$\hat{H}_{ZE} = \mathrm{g}.\mu_B.B.S \qquad 4.31$$

Where *S* is total spin, *B* is magnetic field and g is g-tensor which describes direction of the magnetic axis.

In the case of free atoms, ion or lanthanides where total angular momentum ***J*** dominates and energy levels of ***J*** is given as ***2J+1***.

According to Wigner-Eckart theorem, Zeeman Hamiltonian can be written as

$$\widehat{H}_{ZE} = g_J.\mu_B.B.J \qquad 4.32$$

Where g_J Landé formula as is mentioned in above sections. Landé factor can be derived by using equation 4.32 which can be also written as

$$\widehat{H}_{ZE} = \mu_B.B.(L + g_s S) \qquad 4.33$$

Assuming $g_s = 2$

$$g_J = 1 + \frac{J(J+1) + S(S+1) - L(L+1)}{2J(J+1)} \qquad 4.34$$

But in the above mentioned case few assumptions are made and should also keep in mind that with the consideration of uniform magnetic field, one should also consider the non-uniform field generated by nuclear magnetic field and electric quadrupole moments which is responsible for hyperfine structure and it is very sensitive to the atomic wave function.

Zeeman interaction can be put into three categories and gives the details about the properties of an ion embedded with ligand

4.3.1 In the presence of weak field

In the presence of weak field, spin orbit multiplets are closer resulting in the lift of degeneracy of J multiplets. In weak field; J is approximated as good quantum number. Example for this case is rare earth ions, as in rare earth *4f* ions are shielded by the by the *5s* and *5p* orbitals which pushes ligand ions away.

4.3.2 In the presence of Intermediate field

This case is suitable for many iron salts where first crystal field effect is considered and after that spin-orbit coupling affect is studied as a perturbation.

4.3.3 In the case of strong field

In the case of strong field, L and S considered as strong quantum number. It can be seen in transition ions where crystal field energy is stronger and the ground state energy splits into crystal field term. In this case crystal potential is changed by one-electron orbit and new configuration of minimum energy is

calculated and then electron-electron interaction was switched on. Usually, case of strong field is related to covalent bonding in which wave functions containing the explanation of localized terms of magnetic behavior of an ion are inadequate. But many properties can be studied by symmetry of the surroundings.

In the current program [68], g-factor is calculated by using two different approaches: (i) Sampling method (ii) ,Mapping method. In anisotropic materials, g predicts the shape of matrix. For a pseudospin S = ½, Zeeman splitting is given by

$$\Delta E_Z^{\tilde{S}=1/2} = \mu_B \sqrt{\sum_{ijk} B_i \, g_{ik} g_{ik} B_j} \qquad 4.35$$

4.3.4 Sampling Method

In this method, a grid is described around the magnetic system and a finite magnetic field with varying strength in the defined direction is applied. The electronic states energies in the presence of the magnetic field are calculated by using perturbation theory.[79] G-factor was considered constant dimensionless quantity with the value approximately ≅ 2.00232 but later it was established that spin-orbit interaction is the main reason for the deviation from the constant g-factor value of the free electron.[80,81] In the presence of magnetic field, behavior of electronic states is adapted to a linearly Zeeman expression

$$\left(-\frac{\Delta E}{\Delta B}\right) \sim g \mu_B \Delta M_S \qquad 4.35$$

The linear contribution to the g-factor can be determined for a given M_s value. Magnetic Induction is then projected onto a hemisphere. In the implemented project, an icosahedron is inscribed with surfaces labeled. as n-fold In this way $10n^2$ geodesic triangles are constructed in the hemisphere. Then the vector with the largest g-factor is identified as the main magnetic axis. After that coordinates on a circle which are orthogonal to first vector are scanned. Then the third axis is calculated by calculating the vector product of the first two.

4.3.5 Mapping Method

In the Zeeman splitting, given in equation 4.34 the products of the g-matrices can be combined as

$$\mathbf{G} = \mathbf{g}\mathbf{g}^{\mathrm{T}} \qquad 4.36$$

Where T indi

Figure 4.2: Mapping Method (Adapted from Reference 64)

The G converts like a Cartesian symmetrical tensor known as Abragam-Bleaney tensor. The g-factors correspond to the square roots of the eigen values of G, the main magnetic axes the eigen vectors. For calculation of G, the values generated by equation 4.31 and 4.33 in pseudospin base Zeeman splitting can be connected with each other.[68]

The elements of G can be calculated by comparing coefficients.[68,82] For $\tilde{S} = 1/2$ results in:

$$\Delta E = \mu_B \sqrt{2 \sum_{ij} B_i B_j \sum_{\varepsilon,\varepsilon'=+,-} \langle K_n^{\varepsilon} | \hat{L}_i + g_e \hat{S}_i | K_n^{\varepsilon} \rangle \langle K_n^{\varepsilon'} | \hat{L}_j + g_e \hat{S}_j | K_n^{\varepsilon'} \rangle} \qquad 4.37$$

Here, the sum $\sum_{\varepsilon,\varepsilon'}$ goes through over the two components of the nth Kramer doublet in the energy levels. Whereas for pseudospin $\tilde{S} = 1$, this expression changes a bit and the sum runs over three components of the pseudo triplets. Equation 4.34 gives the following for components

$$G_{ij}^{n,\tilde{S}=1/2} = 2 \sum_{\varepsilon,\varepsilon'=+,-} \langle K_n^{\varepsilon} | \hat{L}_i + g_e \hat{S}_i | K_n^{\varepsilon} \rangle \langle K_n^{\varepsilon'} | \hat{L}_j + g_e \hat{S}_j | K_n^{\varepsilon'} \rangle \qquad 4.38$$

As part of SOCI calculation, first the Zeeman matrices in the three spatial directions in CI basis constructed and then transformed into the spin-orbit coupled SOCI states. By using equation 3.35, the elements of the tensor G is calculated and through diagonalization of the g-factors and the main magnetic axes can be found out.

4.4 Magnetic Susceptibility

General equation $-\vec{\mu}.\vec{B}$ is used to determine the energy of the system in the magnetic field from the beginning. From this equation 4.35 can be derived. The ZFS is may not only the reason for the anisotropic behaviour, as well because of orbital degeneracy and spin-orbit coupling in direct manner.[83]

Response of the spin states to a field perturbation can be determined by studying the experimental magnetic properties. The magnetization (M) can be determined:

$$\boldsymbol{M}(B,T) = \frac{N_A}{Z(B,T)} \sum_{S,M_S} \mu_{S,M_S} \exp(-\frac{E_{S,M_S}(B)}{k_B T}) \qquad 4.39$$

Where N_A is the Avogadro number which after multiplying, and the denominator is the partition function:

$$\boldsymbol{Z}(B,T) = \sum_{S,M_S} \exp(-\frac{E_{S,M_S}(B)}{k_B T}) \qquad 4.40$$

Where k_B is the Boltzmann constant which is equal to $1.380 \times 10^{-23} \mathrm{J.K^{-1}}$ and energy expressed in $\mathrm{cm^{-1}}$, it is equal to $0.695\ \mathrm{cm^{-1}.K^{-1}}$

But if the system is behaving anisotropic then keeping in mind the state specific magnetic moments derived from equation 4.35 results in the magnetization as:

$$\boldsymbol{M}(B,T) = N_A k_B T \frac{d \ln(Z(B,T))}{dB} \qquad 4.41$$

Result of macroscopic sample depends on the temperature. The magnetic susceptibility is variation of the magnetization in the presence of different field

$$\boldsymbol{\chi}(B,T) = N_A k_B T \frac{d^2 \ln(Z(B,T))}{dB^2} \qquad 4.42$$

In general to determine the properties of a magnetic material, the simulation of experimental data was done by using the spin Hamiltonian operators and this experimental data is usually acquired from the measurement with SQUID magnetometers. Susceptibility curves are obtained by simulating magnetization (M) of a canonical ensembles (u, v $\in \{x, y, z\}$) :

$$\boldsymbol{\chi_{uv}} = \frac{\partial M_u}{\partial H_v} \qquad 4.43$$

$$\boldsymbol{\chi_{uv}} = N\frac{\partial}{\partial H_v}\frac{\sum_n\left(-\frac{\partial E_n}{\partial H_u}\right)exp\left(-\frac{E_n}{k_BT}\right)}{\sum_n \exp\left(-\frac{E_n}{k_BT}\right)} \qquad 4.44$$

Magnetization behaves approximated linearly $M \approx \chi H$ in small field. By taking the Boltzmann average over all the possible states, magnetic susceptibility can be calculated. Magnitude of the Zeeman splitting produced by the field in the experiments is generally very small, thus in equation 4.44 differential quantity $\left(\frac{\partial E_N}{\partial H_u}\right)$ can be substitute with a difference instead:[79]

$$\boldsymbol{\chi_{uv}} \approx \frac{N}{H_v}\frac{\sum_n\left(-\frac{\partial E_n}{\partial H_u}\right)exp\left(-\frac{E_n}{k_BT}\right)}{\sum_n \exp\left(-\frac{E_n}{k_BT}\right)} \qquad 4.45$$

$$\approx \frac{N}{H_v}\frac{\sum_n\left(-\frac{E_n(H_u)-E_n(0)}{H_u}\right)exp\left(-\frac{E_n}{k_BT}\right)}{\sum_n \exp\left(-\frac{E_n}{k_BT}\right)} \qquad 4.46$$

Susceptibility is determined by this approximation using weighted energy differences. With the help of the partition function in equation 4.47, equation 4.44 can additionally be expressed as equation 3.48:

$$\boldsymbol{Z} = \sum_n \exp\left(-\frac{E_n}{k_BT}\right) \qquad 4.47$$

$$\boldsymbol{\chi_{uv}} = Nk_BT\frac{\partial^2 \ln Z}{\partial H_v \partial H_u} \qquad 4.48$$

The differential part in equation 4.48 shown above can be determined numerically also;

$$\frac{\partial^2 Z(H)}{\partial H_u^2} = \frac{Z(H-hu)-2Z(H)+Z(H+hu)}{h^2}+O(h^2) \qquad 4.49$$

In the implemented program, in order to determine the magnetic susceptibilities energies of all interested states in a temperature range are needed. These energies are obtained by diagonalizing spin Hamiltonian operators. The program is using the Fortran program by V.Staemmler (Bochum). This program determines the eigenvalues of a Hamiltonian operator with the magnetic centers *i,j,…:*

$$\widehat{H}_S = \sum_{i=1}^{n}\sum_{j>i}^{n} J_{ij}\hat{S}_i^T\hat{S}_j + \sum_{i=1}^{n} D\,\hat{S}_{z,i}^2 + \mu_B \sum_{i=1}^{n} \hat{S}_{z,i} g_i H_z \qquad 4.50$$

To determine the magnetic properties of *n* number of centers, Dimension of the product of Zeeman states is given by

$$\hat{S}_{z,j} \otimes_{i=1}^{n} \left|i, S_i, M_{S,i}\right\rangle = M_{S,j} \otimes_{i=1}^{n} \left|i, S_i, M_{S,i}\right\rangle \qquad 4.51$$

$$Dim(S) = \prod_{i=1}^{n} (2S+1) \qquad 4.52$$

Equation 4.52 result in increase of number states and therefore, for huge Hilbert spaces Davidson-Liu algorithm as discussed in the above section is used to determine the lowest energy states. Additionally, Program was updated to add the part to calculate rhombic zero-field splitting parameter *E* along with the anisotropic g-factors which result in complex spin Hamiltonian operator:

$$\widehat{H}_S = \sum_{i=1}^{n}\sum_{j>i}^{n} J_{ij}\hat{S}_i^T\hat{S}_j + \sum_{i=1}^{n} D_i\left(\hat{S}_{z,i}^2 - \frac{1}{3}S_i(S_i+1) + \frac{E_i}{D_i}(\hat{S}_{+,i}^2 + \hat{S}_{-,i}^2)\right) + \mu_B \sum_{i=1}^{n} \hat{S}_i^T\, Diag(g_{x,i}, g_{y,i}, g_{z,i}) H \qquad 4.53$$

To stimulate the magnetic susceptibilities, equation 3.44 or equation 3.46 is used. In the present thesis, few 3d and 4f complexes are studied to investigate the respective magnetic properties of the complex. The implemented program present is used to calculate the eigen-states of a multi spin Hamiltonian operator described in equation 4.53 and to simulate the magnetic susceptibilities in order to compare it with the experimental data.

4.5 Calculation Scheme

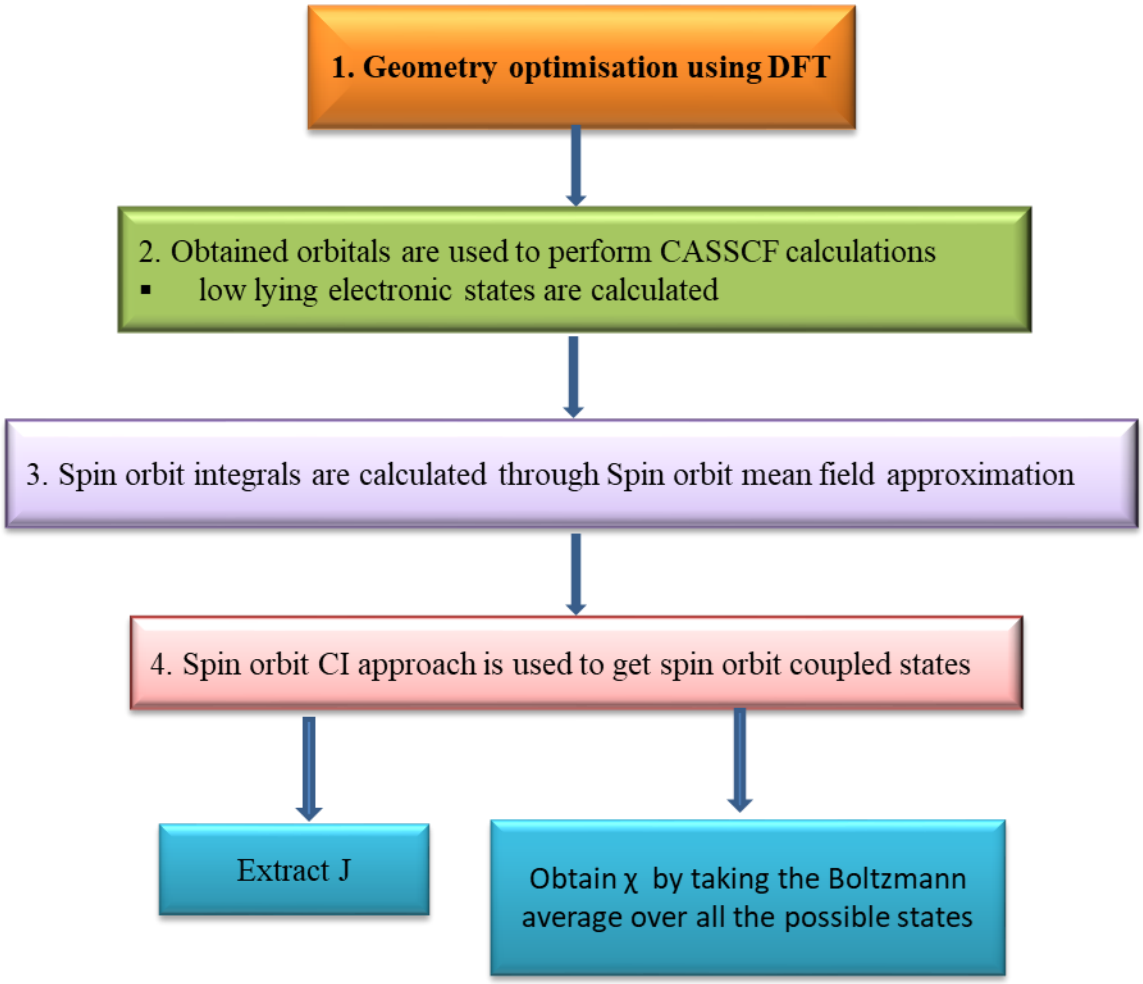
1. Geometry optimisation using DFT
2. Obtained orbitals are used to perform CASSCF calculations
low lying electronic states are calculated
3. Spin orbit integrals are calculated through Spin orbit mean field approximation
4. Spin orbit CI approach is used to get spin orbit coupled states
Extract J
Obtain χ by taking the Boltzmann average over all the possible states

5 Applications (I)-Transition Metals (3d^n)

In the present work, magnetic properties of transition metal (Ni and Co) complexes are calculated for different systems including mononuclear and polynuclear complexes by applying various theoretical methods. The aim is to search for SMMs. Criteria for this are ground states with large S values which can for example be achieved by strong ferromagnetic exchange [11]. Furthermore magnetic anisotropy is needed. For this purpose, understanding of zero field splitting is crucial. The zero field splitting parameters are not only important in the field of single molecule magnets but also for numerous applications in bioinorganic chemistry and catalysis. Though, being an important factor it is difficult to measure ZFS parameters experimentally as the magnitude of these factors are very small, hence it is calculated computationally [84]. Ni(II) and Co(II) transition metals are compelling choices for SMM, since these two 3d ions often exhibit considerable magnetic anisotropy and the probability is high that this can lead to high energy barriers[84–86]. Usually, the magnetic exchange-coupling between paramagnetic centers is studied with diamagnetic ligands. and magnetic exchange coupling can be interpreted by Goodenough-Kanamori rules.[87,88] However, exchange coupling becomes weak if the distance between the centers is increased. One approach to obtain stronger couplings is to put paramagnetic ligands as bridging ligands which results in direct exchange interactions giving strong magnetic coupling.[89,90,91] One of the first studies done with radical ligands is V(tetracynoethylene) which produced excellent spontaneous magnetization above room temperature. After that a series of paramagnetic ligands has been studied including nitroxide, nitronyl nitroxide[92], verdazyl and dithiadiazolyl radicals, and semiquinione[93]. Often, these paramagnetic ligands exhibited strong metal-radical exchange within the molecule. Below magneto-structural studies are shown to understand the behavior which is responsible for high or low anisotropies, ferromagnetic or antiferromagnetic spin-spin coupling. Therefore the electronic structures of Ni and Co complexes with radical ligands are investigated in the following sections.

5.1 Ni (II)

Ni (II) has a $3d^8$ configuration giving rise to 25 states including 10 triplets and 15 singlets. In the SOCI all 45 microstates belonging to this spin state have to be considered. In the free ion, this corresponds to F, P, D, G and S states among which ^3F is the ground state.

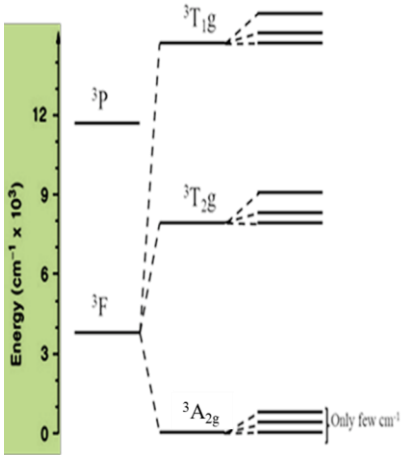

Figure 5 1 Scheme of LF splitting

As it is mentioned several times above that in case of transition metals, ligand field dominates spin orbit coupling, hence ^3F further splits in to its three components i.e single ^3A_2g, ^3T_2g and ^3T_1g (as shown in Figure 5.1).In this work we will present three case studies with Ni(II) ion (i) mononuclear complex (ii) radical complex and (ii) polynuclear complex. The complexes are synthesized in the group of Prof. H.-J Krüger (Technical university of Kaiserslautern). Calculations shown here are based on the density functional theory (DFT) using TURBOMOLE[94] package. Two basis sets def-SV(P) and def2-TZVP with the generalized gradient approximation (GGA) functional BP86 were used to perform each calculations. Firstly, for all Ni(II) complexes, only the positions of the hydrogen atoms were optimized using the X-ray structure. Then, these structures are taken to perform complete active space self-consistent field (CASSCF) calculations with the program of Meier and Staemmler[67] with code optimized by T .Bodenstein[68,128] for magnetic systems.

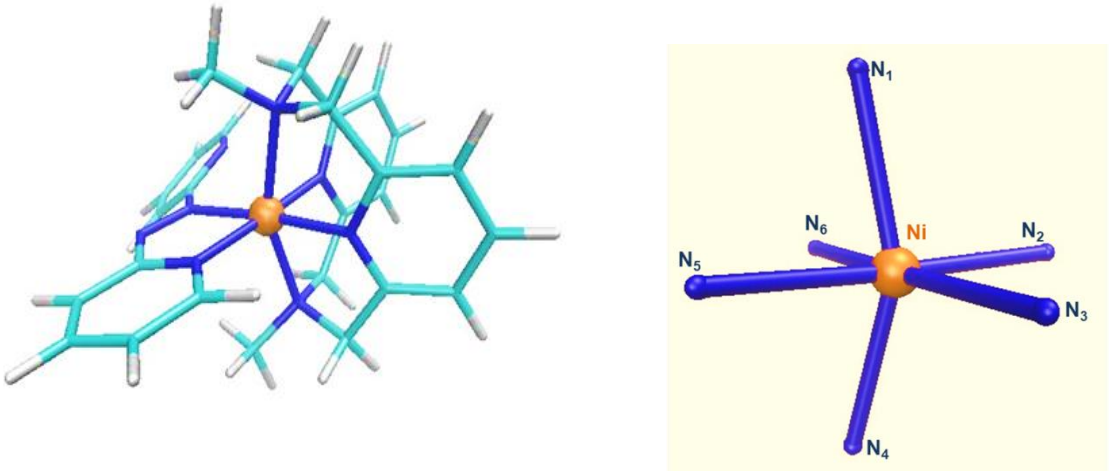

Figure 5.2: Ni-complex (1)

5.1.1 $[Ni(II)L]^{2+}$

For a given Ni(II)-ligand system, coordinates were divided in two sets, (I) in which carbon, nitrogen and Nickel atoms were fixed (X-ray) and (II) in which nothing was fixed (DFT). After optimization we found out that energy in case of def2-TZVP is lower than def-SV (P). Bond distances of Ni-N are slightly shorter in Case A than Case B. The optimized geometries show Ni-N bond lengths of 1.99, 2.01, 2.03, 2.09, 2.17 and 2.17 Å in case of X-ray whereas in case of DFT, bond lengths are 2.01, 2.03, 2.06, 2.09, 2.22 and 2.27 Å which is in agreement with reported values.[95,96] So the first goal is to find the correct set of reference orbitals to assign in active space which can be easily done by localizing the orbitals. Boys localization method is used in CASSCF, this method gives MOs as compact as possible. Active space considered here in CASSCF calculations is CAS (8, 5) i.e 8 valence electrons in 5 d orbitals. The orbitals were optimized for a state average over the ten triplet states belonging to the ^3F and ^3P states of free ion which means all 3d orbitals are considered as same weighted. The ground state orbitals are related to e_g orbitals. In the presence of quasi octahedral ligand field, the next excited state is 8000 cm^{-1} higher in energy than the ground state in case of X ray whereas in case of DFT, excited state is 7000 cm^{-1} higher in energy than the ground state. Zero field splitting of ground state is around 5 cm^{-1} in X.ray and around 9 cm^{-1} in case of DFT (as shown below in Table 5.1.1).Triplet is the ground state whereas the lowest singlet state which belongs to ^1D was found to be about 18343 cm^{-1} in Case of X-ray and 17800 cm^{-1} in case of DFT above the ground state.^1S is found to be above 70000 cm^{-1} from the ground state in both the cases so we can neglect it. For further calculation of magnetic properties, we will discuss about the X-ray structure as in this case interactions with the nearby molecules and counter ions can change the structure where as DFT calculations considered for an isolated gas phase molecules.

Table 5.1 1 : CASSCF and SOCI energies in cm^{-1} for the electronic states of $[Ni(II)L]^{2+}$

$[\mathbf{Ni(II)L}]^{\mathbf{2+}}$							
X ray				DFT			
CASSCF	SOCI	CASSCF	SOCI	CASSCF	SOCI	CASSCF	SOCI
0.00	0.0 5.2 8.1	16329	16307 16432 16702	0.0	0.00 8.9 11.9	15055	15083 15254 15426
8552	8347 8464 8627	16835	16941 17089 17159	7542	7234 7340 7644	15552	15795 15852 15876
8973	9061 9109 9233			7678	7784 7958 8086		
10753	10733 10822 10825			10303	10263 10364 10376		
15460	15069 15346 15484			13914	13588 13862 13945		

Magnetic susceptibilities were calculated using averaged partition sums [97]. by averaging over different field directions of the lowest triplet and D tensors were calculate by effective Hamiltonian theory [98,99]. The D-tensor and g-tensor are calculated by the SOCI calculations. It is observed that D is positive (as shown below in Table 5.1.2) implying that the m_s=0 component is lowest in energy [100]. The g tensors were calculated for triplet states by taking lowest three energies from SOCI calculations with pseudospin S = 1.0 for which g is rather isotropic in the order of 2.2 as given below in Table 5.1.2. The calculated magnetic susceptibility gradually increases to 1.29 cm^3K/mol (as shown below in Figure 5.1.1b). At low temperature it drops suddenly. In Figure 5.1.1a the energies of the lowest three states are shown with respect to the external magnetic field and it is observed that in case of magnetic applied in x and y direction, change in ground state and second excite state was relatively large while in case of z direction ground state doesn't show change in ground state. It can be interpreted that complex has easy axis in xy plane.

Table 5.1 2 : D-tensor and energies in cm^{-1} as well as the g-tensor and the magnetic main axes for the lowest triplet state of $[Ni(II)L]^{2+.}$

	Dxx	Dyy	Dzz	g1	g2	g3
	-0.74	-3.69	4.43	2.25	2.27	2.20
Axes of D-tensor				Magnetic main axes		
x	0.91	-0.40	0.06	-0.32	-0.05	0.94
y	0.40	0.91	0.05	0.94	-0.04	0.31
z	-0.08	-0.02	0.99	0.02	0.99	0.06
	E1	E2	E3	D	E	E/D
	0.00	5.18	8.13	6.65	1.47	0.22

(a)

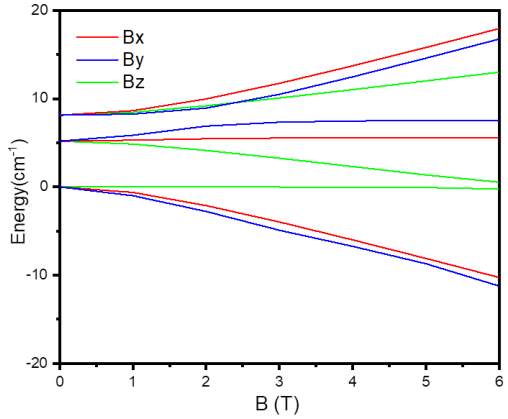

(b)

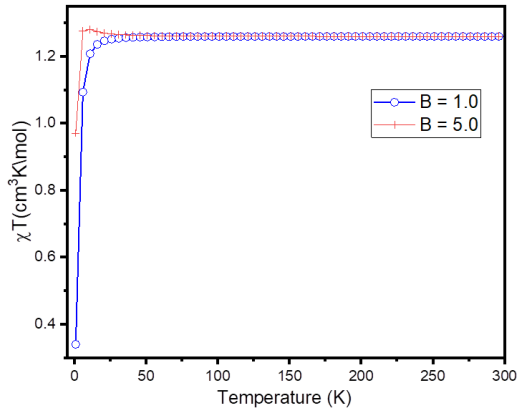

Figure 5.1 1: (a) Energies of the triplet ground state component of $[Ni(II)L]^{2+}$ (b) Magnetic Susceptibility of triplet ground state with Magnetic field B = 1.0 and 5.0 T $[Ni(II)L]^{2+}$

5.1.2 $[Ni(II)L^{-}]^{+}$

In this case study, in mononuclear Ni(II) complex , its azopyridine ligand is also hosting a radical electron thus making it a radical complex. Addition of electron resulted in 135 orbitals, 132 doubly occupied and 3 singly occupied orbitals. It is confirmed by visualizing natural molecular orbitals (NMOs). In the radical $[Ni(II)L^{-}]^{+}$system, the additional electron is present in the π-electron system of

the azopyridine ligand as shown in Figure 5.1.2 and this proposes second spin center in the system. The ligand orbital is orthogonal to the two singly occupied Ni orbitals in the ground state. In this case the coordinates were also divided in two sets (i) in which carbon, nitrogen and Nickel atoms were fixed (X-ray) and (ii) in which nothing was fixed (DFT) but we found out that both optimized structure have approximately equal energies. The optimized structure has shown no changes in the structure. It has same bond distances. Energy was found out to be lower in case of def2-TZVP basis set than def-SV (P). Active space considered here is CAS (9, 6) i.e 9 valence electrons in 6 orbitals. Addition of electron resulted in 90 spin free states including 20 quartets, 70 doublets. Quartet states are four-fold degenerate (i.e. ±3/2, ±1/2) and doublet states are doubly degenerate (i.e. ±1/2) which results in total 220 spin-orbit states. We found out that in that the two spin center couple ferromagneticlly resulting in quartet state as ground state which resulted in two Kramer's doublets with zero field splitting of around 8.7 cm^{-1} and next lowest doublet state was found about to be 353 cm^{-1} and after that next excited doublet state lies above 7000 cm^{-1} higher in energy. The g-tensors and zero field splitting parameters were analyzed by using quartet ground state with a pseudo spin of S = 3/2. The result of the wave function analysis gives a positive sign for D which is in agreement with the results obtained for the g-tensor. The g tensor for the ground state is almost isotropic in the order of 2.2 (as shown in Table.5.1.4)and same were also calculated for lowest three Kramer's doublets and it is observed that second Kramer's doublets is axial while third Kramer's doublets is slightly axial in the range of 2.3-2.5. The quartet ground state and next excited doublet state is taken into account in order to calculate magnetic susceptibilities with B = 1.0 and 5.0 T, and it is observed that χT increases to 2.24 cm^3K/mol at low temperature. At around 100 K, the doublet state starts to get populated which led to decrease in the χT at higher temperature.

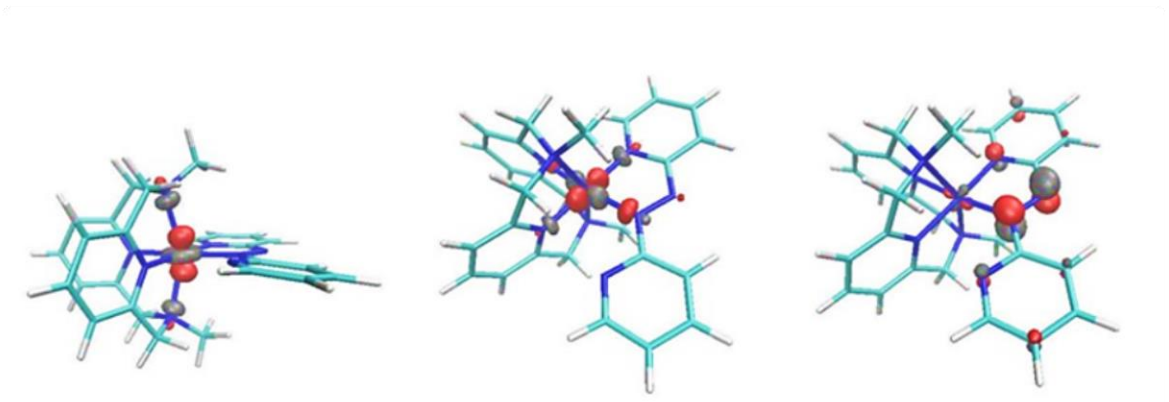

Figure 5.1 2: Singly occupied natural orbitals obtained for the quartet ground state obtained at DFT level for compound 2 (contour value: 0.09)

spin	X ray		DFT	
	CASSCF	SOCI	CASSCF	SOCI
3/2	0	0.0 8.7	0	0.0 8.7
1/2	352	353	352	353

Table 5.1 4: D-tensor in cm^{-1} and g-factor for the lowest electronic states of $[Ni(II)L^{-}]^{+}$. g-tensors are calculated for the pseudo spin S=3/2 as well as for individual Kramers dublets (KD) S=1/2. Energies, zero field splitting parameters and the exchange coupling constant are given in cm^{-1} .

S = 3/2	Dxx	Dyy	Dzz	g1	g2	g3			
	-1.10	-1.76	2.87	2.20	2.22	2.14			
Axes of D-tensor				Magnetic main axes					
x	-0.42	-0.90	0.04	-0.85	-0.51	-0.04			
y	0.89	-0.43	-0.08	-0.51	-0.85	0.06			
z	-0.09	0.005	0.99	0.03	-0.07	0.99			
	D	E	J						
	4.3	0.3	235						
KD	E1= 0.0			E2= 8.7			E3 = 353		
	g1	g2	g3	g1	g2	g3	g1	g2	g3
	3.88	4.90	2.09	0.52	0.48	6.37	2.39	2.47	2.28
x	-0.44	-0.89	-0.04	0.35	0.93	-0.04	-0.91	-0.39	-0.04
y	0.88	-0.45	0.08	-0.92	0.36	0.08	0.38	-0.91	0.06
z	-0.09	-0.004	0.99	0.09	0.01	0.99	-0.06	0.04	0.99

(a)

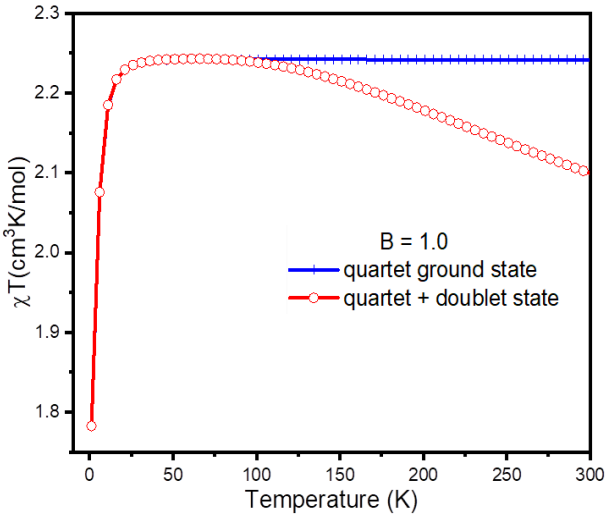

(b)

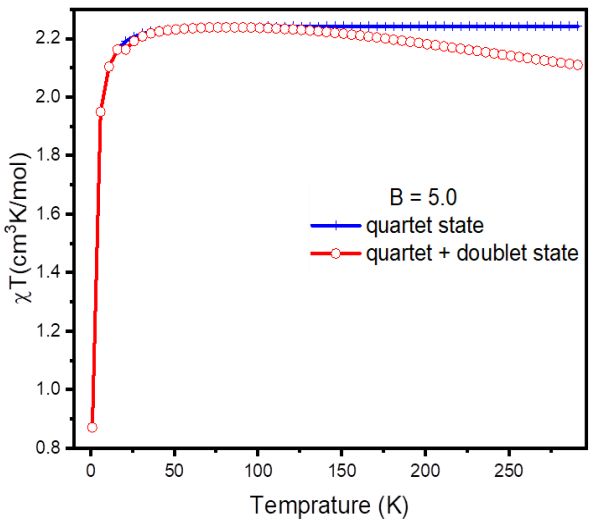

(c)

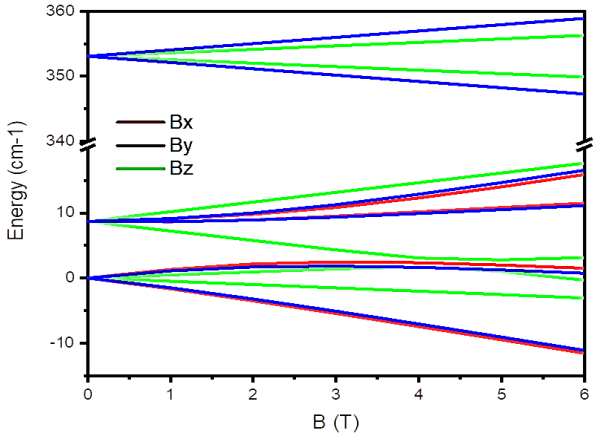

Figure 5.1 3: (a) and (b) Magnetic Susceptibility of quartet ground state with the next excited state with Magnetic field B = 1.0 and 5.0 T $[Ni(II)L^{-}]^{+}$ (c) Energies of the lowest three KDs of $[Ni(II)L^{-}]^{+}$

5.1.3 $[Ni(II)L^{-}Ni(II)]^{3+}$

In this case study, we studied magnetic properties of binuclear metal centers with an additional electron present on the ligand.

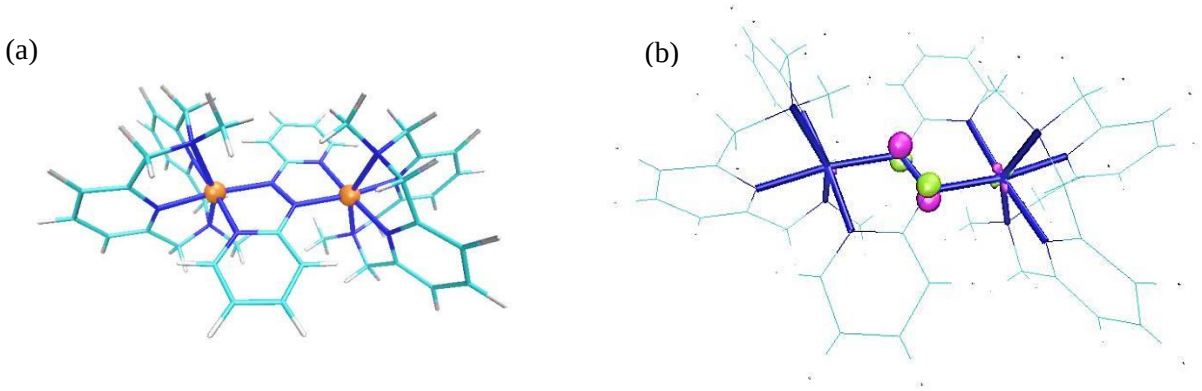

Figure 5.1 4: (a) Ni complex in with two Ni(II) center connecting with a bridge ligand (b) Additional electron present on the bridging ligand (contour value: 0.09)

The ligand orbital is orthogonal to both the Ni orbitals in the ground state i.e Ni_1 spin $S_1 = 1$, ligand spin $S_L = ½$ and Ni_2 spin $S_2 = 1$. Active space considered here is CAS (17, 11) i.e 17 valence electrons in 11 orbitals. We found out that in that the three spin center couple ferromagneticlly resulting in sextet state as ground state which resulted in three Kramer's doublets with zero field splitting of 6.0 cm^{-1} and next excited state is quartet state was found about to 90 cm^{-1} and after that next excited doublet state lies at 186 cm^{-1} higher in energy. The g-tensors and zero field splitting parameters were analyzed by using sextet ground state with a pseudo spin of S = 5/2. The result of the wave function analysis gives a for D tensor. The g tensor for the ground state is almost isotropic in the order of 2.2. The g tensors were also calculated for lowest three Kramer's doublet that belong to lowest sextet state and it is observed that first and three Kramer's doublet is highly axial while second Kramer's doublet is showing slightly anisotropic behavior in the range of 3.7-5.5. The sextet ground state and next excited quartet and doublet states are taken into account in order to calculate magnetic susceptibilities as energy gap between the ground states and excited states is not very significant, and it is observed that χT increases to 5.36 cm^3K/mol at low temperature (as shown in Figure 5.1.5(a) and (b)).

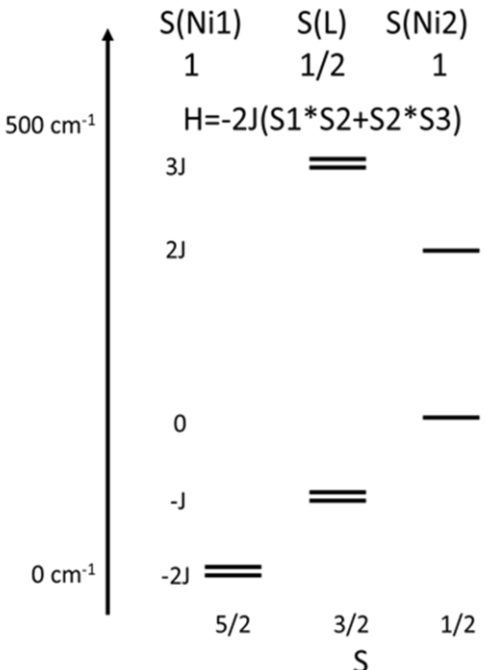

At around 30 K, as the higher excited states start to get populated, decrease in the χT at higher temperature is observed. The lowest three KD is used to plot the energies as function of an external magnetic field shown in 5.1.5(c).

Table 5.1 5 Spin-orbit states energies in cm^{-1} for the electronic states of $[Ni(II)LNi(II)]^{3+}$

State	KD	Spin-orbit states
Sextet	1	0.00
	2	6.00
	3	13.15
Quartet	5	90.30
	6	101.46
Doublet	8	186.25
Doublet	9	367.97
Quartet	10	453.00
	11	466.89

Table 5.1 6 D-tensor in cm^{-1} and g-factor for the lowest electronic states of $[Ni(II)L^{-}]^{+}$. g-tensors are calculated for the pseudo spin S=3/2 as well as for individual Kramers dublets (KD) S=1/2. Energies, zero field splitting parameters and the exchange coupling constant are given in cm^{-1}.

S = 5/2	Dxx	Dyy	Dzz	g1	g2	g3
	-0.26	-1.09	1.35	2.21	2.25	2.16
Axes of D-tensor				Magnetic main axes		
x	0.92	0.37	0.04	-0.17	-0.03	-0.98
y	-0.36	0.92	-0.05	-0.98	0.05	0.17
z	-0.05	0.03	0.99	0.04	-0.99	-0.04
	D	E				

	2.03	0.4							
KD	E1= 0.0			E2= 6.0			E3 = 13.15		
	g1	g2	g3	g1	g2	g3	g1	g2	g3
	2.24	1.28	10.23	4.11	3.71	5.51	0.28	0.23	10.74
x	-0.93	-0.04	-0.36	0.94	0.33	-0.04	0.91	-0.40	-0.04
y	0.36	0.05	-0.93	-0.33	0.94	0.05	-0.40	-0.91	0.05
z	-0.05	0.99	0.03	0.05	-0.03	0.99	0.06	0.03	0.99

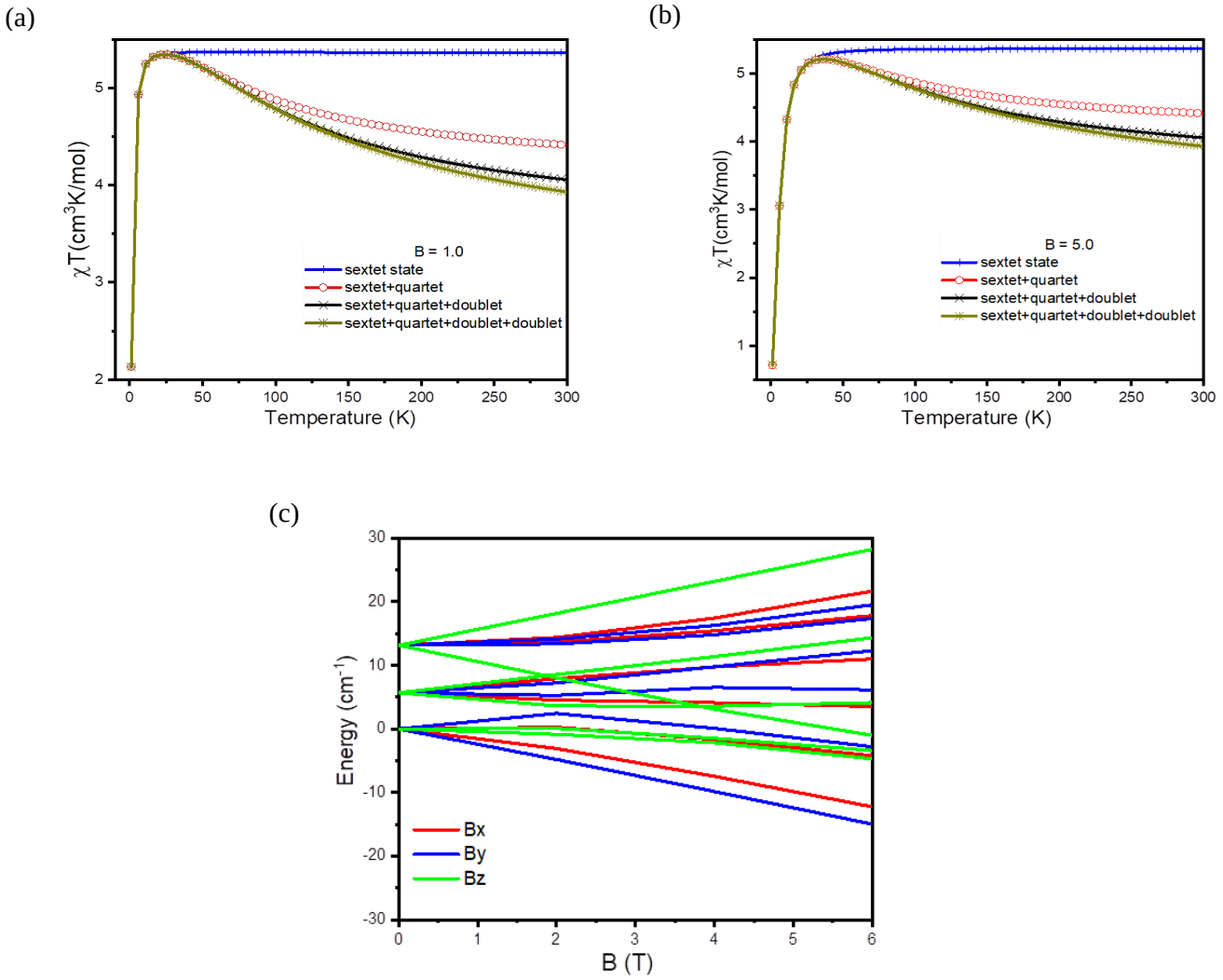

Figure 5.1 5: (a) and (b) Magnetic Susceptibility of ground state with the excited state with Magnetic field B = 1.0 and 5.0 T, (c) Energies of the lowest three KD that belong to ground state

5.2 Co (II)

Co (II) has $[Ar]4s^2 3d^7$ electronic configuration and in case of octahedral geometry i.e. six-fold coordination, there are two possibilities for this $3d^7$ (i) the high spin where total spin S = 3/2 as d-electron spins are arranged as shown in Figure 5.2.1 with three unpaired electrons; and (ii) the low spin where total spin S = ½ as number of unpaired electron is only one. Orientation of electrons is decided by the strength of the crystal field ligand. In case of tetrahedral geometry, HS orientation is preferred.[101]

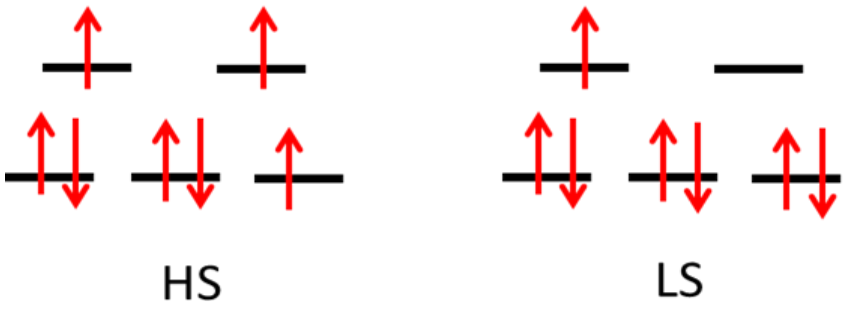

Figure 5.2 1: Scheme of d^7 electrons in HS (high spin) and LS (low spin)

In the calculation shown below, HS electronic configuration is considered that means total spin S = 3/2. Hence, this configuration results in 50 spin free state with ^4F as ground state and ^4P, ^2H, ^2G, ^2F, ^2P $2x^2D$ as higher excited states. After spin-orbit coupling, these 50 spin free states give rise to 120 spin orbit states. In the presented work here, Co (II) complexes are calculated with different ligand field to find out how surrounding of a metal center helps in tuning its magnetic properties. First three complexes were in the collaboration with Dr Guo Peng, Nanjing Tech University, China and the last complex is in collaboration with Prof. Dr. Annie Powell's group, KIT.

5.2.1 Co (II) with different ligand substitution

(a)

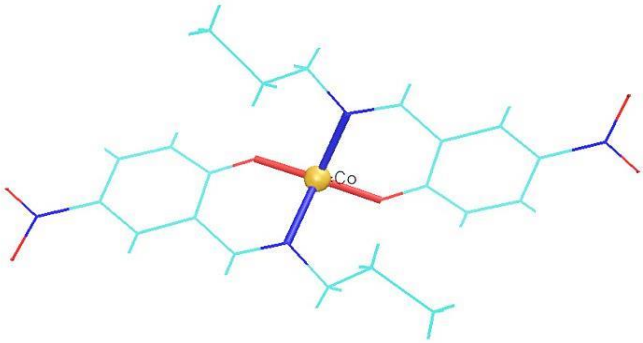

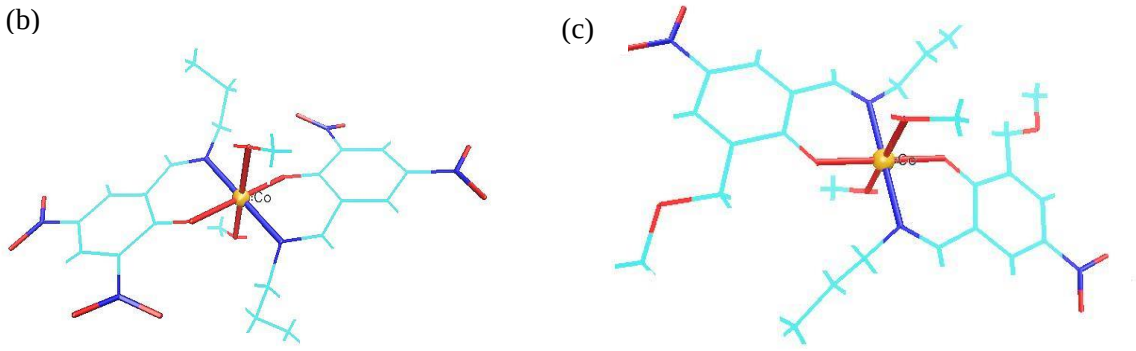

Figure 5.2 2: The structure of (a) [Co $(L_1)_2$]; where L_1 = 4-nitro-2-((E)-(propylimino) methyl) phenol; (b) [Co $(L_2)_2(CH_3OH)_2$] L_2 = 2,4-dinitro-6-((E)-(propylimino) methyl) phenol and (c) [Co $(L_3)_2(CH3OH)_2$] where L3 = 2-(methoxymethyl)-4-nitro-6-((E)-(propylimino)methyl)phenol);

In the case of structure a, Co(II) ion is in distorted tetrahedral geometry, attached with two same ligand in a asymmetrical manner and bond distance of Co-N and Co-O is in the range of 1.97-1.90 Å and bond distance of Co-O is shorter than Co-N which is in agreement with the previously reported value.[102] However, in case of structure b and structure c is in octahedearl geometry where the Co(II) ions are attached to two nitrogen atoms and four oxygen donors from two ligands and two methanol molecules. Structure 2 has distorted octahedron geometry while structure 3 is near to perfect octahedron. In both the structute (b) and (c), the ligands are similar except in structure (c), group $–NO_2$ is replaced CH_2OCH_3 group as can be seen in Figure 5.2.2. Equitoral bond distances of Co-N and Co-O for both structure (b) and (c) are longer than axial bond length it shows that both the structures are compressed. All calculations on structures **a-c** are done on the X-ray structures. The positions of the hydrogen atoms were reoptimized with density functional calculations using BP86 functional/def-SVP basis set with the Turbomole program package [94]. Based on these structures, the basis sets of Co, O and N were extended to def2-TZVP. State average CASSCF calculations were performed including all quartet states with 7 electrons in the five 3d orbitals were performed. Based on the CASSCF orbitals, SOCI (spin orbit configuration interaction) calculations were performed with a program developed in Karlsruhe and Kaiserslautern,[68] by taking a spin-orbit mean field approach for the 2-electron-spin-orbit integrals [103,104].g-tensors are obtained by the Abragam-Bleaney tensor which are described by Gerloch and McMeeking[105]. The magnetic susceptibilities are calculated by Boltzmann averaging from the derivatives of the energy with respect to the magnetic field.

Table 5.2 1: Energies of the 7 lowest quartet states and the lowest doublet state obtained in the CASSCF calculations. All energies are given in cm^{-1} relative to the lowest quartet state.

Quartet states (4F)	Complex 1	Complex 2	Complex 3
1	0	0	0
2	1941	544	127
3	3674	982	498
4	6110	5484	5793
5	7288	7701	7792
6	8650	8284	7991
7	10971	15044	15488
First doublet	15741	13310	12979

CASSCF caluclation were performed using CAS(7,5) as active space. According to CASSCF caluclations ,splitting of the ^4F states is shown in Table 4.1.7 and it is observed that in complex 1, the ground state is separted by 1941 cm^{-1}in energy from next state, however in case of complex 2 and 3. The energy gap between the ground state and the next state by 544 cm^{-1} and 127 cm^{-1}, respectively, which is relatively smaller than the complex 1 . The lowest doublet states are found at the energies of 15741 cm^{-1} for **1**, 13310 cm^{-1} for **2** and 12979 cm^{-1} for **3**, respectively. These lowest doublet states are at much higher energy than the lowest three quartet state which implies that doublet states do not interfere in the SOCI calculations. After SOCI calculations, ground quartet state of complex 1 is well separated from the next quartet state which lies at 2032 cm^{-1}. Ground quartet state split into two Kramer's doublets with zero field splitting of 76 cm^{-1}. In case of complex **2** and complex **3**, the ground quartet state with an energy difference of 187 cm^{-1} and 275 cm^{-1} respectively. The lowest three quartet states of the CASSCF calculations interact strongly in the SOCI calculation, leading to six KDs in the range of 1500 cm^{-1} as shown in Table 4.2.2. g-tensors for lowest quartet state was calculated by analyzing the wave function using pseudospin S = 3/2 which gives g_x = 2.27, g_y= 2.10, g_z = 2.60, D = -36.4 cm^{-1} and E = 6.3 cm^{-1}. The g-tensors were also calculated for individual KDs (as given in Table 5.2.3) which agree well with the sign of D implying of easy axis magnetic anisotropy in complex 1. The simulated magnetic susceptibility (χT) for complex 1 is 2.60cm^3K/mol. In case of complex 2 and 3, the g factors of the first

KD doublet show highly anisotropic behavior (as shown in Table 5.2.3). Magnetic susceptibility (χT) for **2** and **3** is 2.99 and 2.86 cm^3K/mol.

Table 5.2 2: Energies of the 7 lowest Kramers doublets obtained in the spin orbit CI calculations. All energies are given in cm^{-1} relative to the lowest Kramers doublet.

KDs	Complex 1	Complex 2	Complex 3
1	0	0	0
2	76	187	275
3	2032	698	486
4	2186	1029	916
5	3702	1340	1086
6	3845	1484	1205
7	6291	5806	6282

Table 5.2 3: The calculated g-tensors (S' = 1/2) of the lowest Kramers doublet for 1-3.

KD		Complex 1	Complex 2	Complex 3
1	g_x	1.261	2.423	2.886
	g_y	0.989	1.824	2.613
	g_z	7.574	7.821	7.305
2	g_x	3.291	2.493	2.434
	g_y	2.420	2.160	2.898
	g_z	5.196	5.175	0.175
3	g_x	-	2.642	1.089
	g_y	-	1.109	0.447
	g_z	-	5.611	1.983

(a)

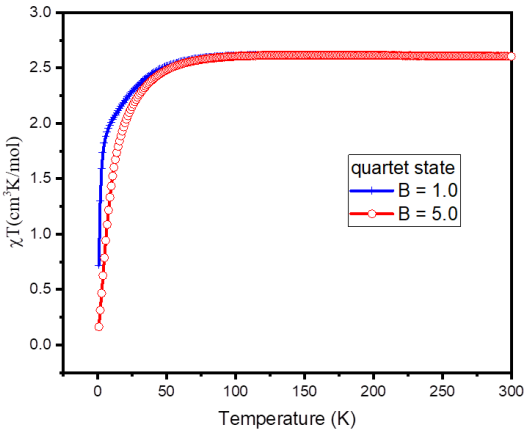

(b)

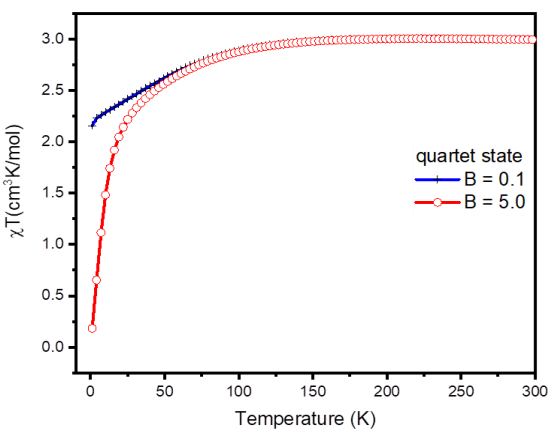

(c)

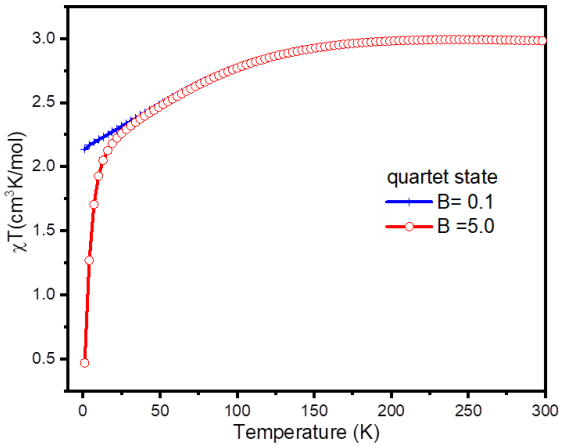

Figure 5.2 3: Magnetic Susceptibility of ground state with the excited state with Magnetic field B = 1.0 and 5.0 T (a) complex 1, (b) complex 2 and (c) complex 3

5.2.2 Co(II) radical complex

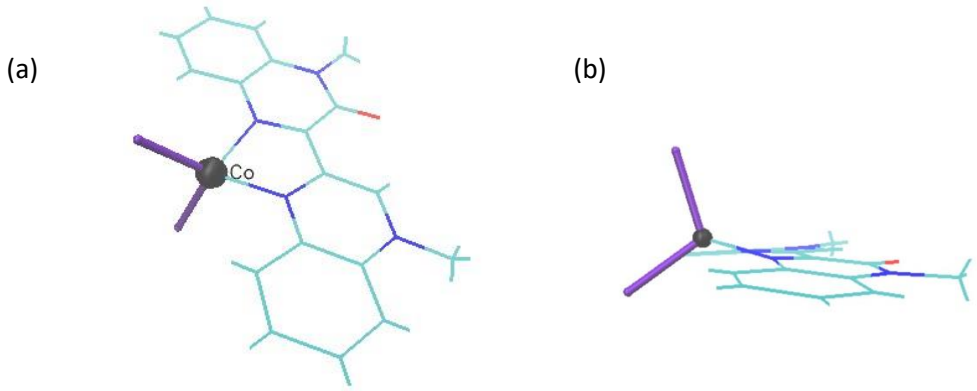

Figure 5.2 4: The structure of (a) [Co $(L)_2Cl_2$]; (a) top view (b) side view; (Violet – Cl; black – Co; blue – nitrogen; red - oxygen

In this case study we have a Co(II) complex in a distorted tetrahedron geometry where Co(II) ion is connected with two chloride and two nitrogen donor atoms from ligand. Co(II) is bit out of plane as can be seen in Figure 5.2.4. The bond lengths of Co-N and Co-Cl are in range of 1.99 Å an 2.22 Å repectively, the N1-Co-N2 and Cl1-Co-Cl2 bond angles are 80.77 and 108.88 respectively, which is in agreement with the previously reported values.[106,107]. The positions of the hydrogen atoms were reoptimized with density functional calculations with the TURBOMOLE program package [94]. Based on these structures, the basis sets of Co is extended to x2c-TZVPall while for O and N def-SV(P) is used with BP86 functional. Based on the CASSCF orbitals, SOCI (spin orbit configuration interaction) calculations were performed with a program developed in Karlsruhe and Kaiserslautern,[68] by taking a spin-orbit mean field approach for the 2-electron-spin-orbit integrals.[103,104] The g-tensors are obtained by the Abragam-Bleaney tensor which are described by Gerloch and McMeeking,[105] magnetic susceptibilities are calculated by Boltzmann averaging from the derivatives of the energy with respect to the magnetic field.

In this Co(II) system, additional electron is located on the π-electron system of the ligand which resulted in a second spin center in the complex. Active space in this case is considered to be CAS(8,6) i.e 8 electrons in 6 orbitals. Co(II) is d^7 i.e three orbitals singly occupied in ground state, so the Co spin is S_{co} = 3/2 and the additonal electron on the ligand resulted in spin S_L = ½. Two spin center couple anti-ferromagnetically because Co orbitals and ligand orbital is non orthogonal, resulting triplet as a ground state. State average CASSCF calculations were performed including ten triplet states with 8 electrons in the six orbitals were performed. In CASSCF calculations, triplet is the ground state and the next two

state is quintet and triplet state which is 1138 cm^{-1} and 2320 cm^{-1} higher in energies , repectively. After the CASSCF caluccation, SOCI caluclations were performed and the ground triplet state as expected splits further into its component with zero field splitting is 17 cm^{-1}. The next excited quinete state is quintet state is 2900 cm^{-1} higher in energy than the ground state. As energy gap between ground state and next state is nearly 3000 cm^{-1},implying second order spin orbit effect. From the energy it can also be interpreted that ground state is well isolated hence the magnetic parameters were calculated for ground state only. Wavefunction of ground state was studied using pseudo spin $S = 1$ to calulate the D , E and g-tensors. Calculated g tensors are $g_x = 2.19$, $g_y = 2.07$ and $g_z = 2.32$ which is nearly isotropic. The positive sign of D indicates $m_s = 0$ as lowest component in ground state. Contributuion of E in E/D = 0.26 is quite large. The Energies of the lowest three states of the SOCI calculation were calculated with respect to magnetic field shown in Figure.The calculated magnetic susceptibility χT increases to 1.21 cm^3Kmol^{-1}.

Table 5.2 4: Lowest spin-orbit energy levels. D-tensor and energies in cm^{-1} as well as the g-tensor and the magnetic axes for the lowest triplet state

Spin orbit state (cm^{-1})	Dxx	Dyy	Dzz		g1	g2	g3
0.000	-1.62	-14.59	16.22		2.19	2.07	2.32
17.84	0.51	-0.19	-0.83	x	0.50	0.84	0.16
30.81	0.61	-0.59	0.51	y	0.63	-0.49	0.59
2936.37	0.60	0.77	0.18	z	-0.58	0.19	0.78
2940.00				D		E	
2960.72				24.33		6.48	
2982.12							
2985.137							

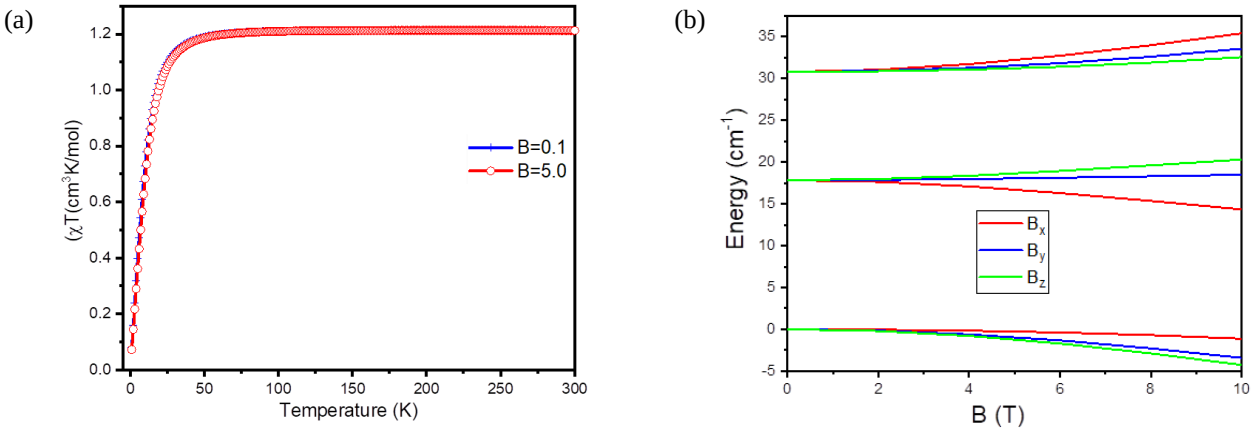

Figure 5.2 5: (a) calculated magnetic susceptibility with B = 0.1 and 5.0 T; (b) Energies of the components of the triplet state in a magnetic field (applied in each direction)

➢ Co complex without additional electron

In this case study, complex discuss above is only studied but there is no additional electron present on the ligand. Therefore, in this case we have active space 7 electrons in 3d orbitals (7,9). All the computational details are same as above mentioned. The orbitals here were optimized for a state average of seven quartet state belonging to lowest ground term only. The $3d^7$ configuration of Co(II) ion has 50 spin free states; 10 quartet state and 40 doublet state but spin-orbit coupling resulted in 120 states as explained above. In CASSCF calculation, we observed that next quartet state is 2336 cm^{-1} higher in energy than th e ground quartet state. The ground state in $[Co(II)L]Cl_2$ is quartet state which resulted in two Kramer's doublets with the zero field splitting of 36 cm^{-1}. Next state is doublet state which is 2286 cm^{-1} higher in energy (as shown in Table 5.2.5).

Table 5.2 5: Lowest spin-orbit energy levels; g-tensor and the magnetic axes for the ground state and lowest two Kramer's doublet along with zero field splitting parameter

KDs	Spin orbit state (cm^{-1})	g1		g2	g3
1	0.00		2.33	2.40	2.16
2	36.15	x	0.48	0.33	-0.80
		y	0.60	0.53	-0.59
3	2286.24	z	-0.62	0.77	0.05
4	2622.38	D = 18.01 E = 0.85			
5	2961.22	KD1			KD2
6	3304.50	E1 = 0.00			E2 = 36.14

	g1		g2	g3	g1	g2	g3
		4.38	5.04	2.15	0.33	0.30	6.48
	x	0.17	0.55	0.81	0.03	0.57	-0.81
	y	0.16	0.79	-0.57	0.13	0.80	0.57
	z	-0.97	0.23	0.04	0.99	-0.12	-0.04

The analysis of wave function shows positive sign for D. With spin of 3/2; g is isotropic in the order of 2.3cm^3K/mol. The g factor is also calculated for individual Kramer's doublets and second Kramer's doublets is axial. In the simulation of the magnetic susceptibility ground state quartet state is considered which increases upto 2.49cm^3K/mol (as shown in figure 5.2.6).

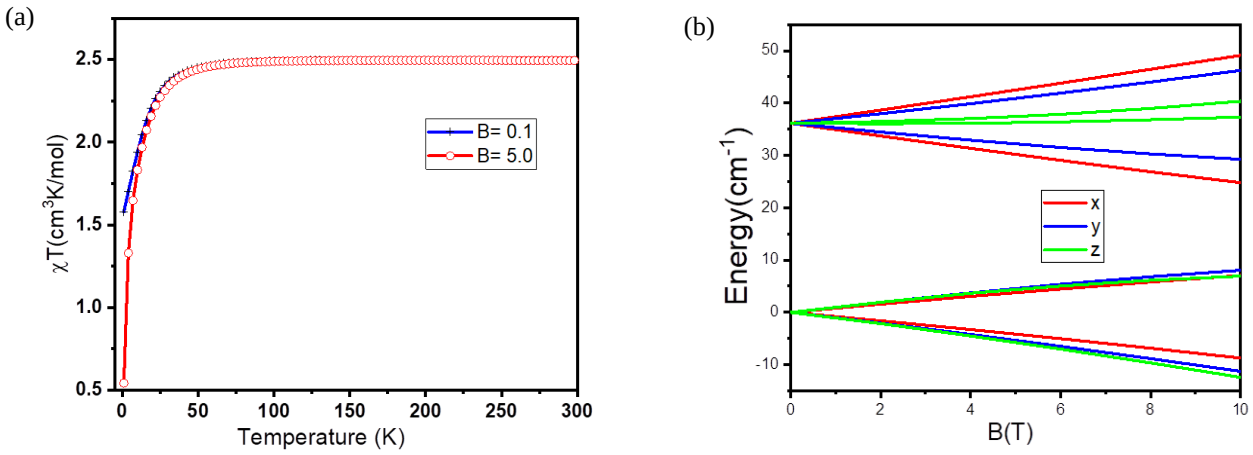

Figure 5.2 6: (a) calculated magnetic susceptibility with B = 0.1 and 5.0 T; (b) Energies of the components of the lowest two KD in a magnetic field (applied in each direction)

➢ Additional Electron

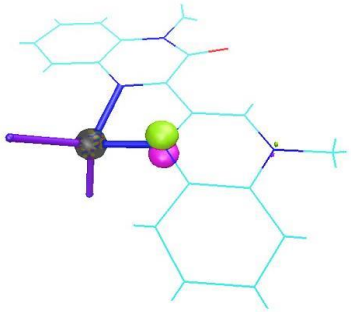

Figure 5.2 7: Additional electron present on the ligand [Co $(L)_2Cl_2$];

In this case, Co in the complex is replaced with diamagntic Zn(II) to make the complex one spin center and calculations were done on additional electron. For [Zn(II)L]Cl_2 , active space is one electron in one orbital (1,1).The ground state is doublet state and as there is only one doublet state that means SOC calculations result in one Kramer's doublets and as expected no zero field splitting (as shown in below in 5.2.6). With spin of ½ , g is isotropic in the order of 2.00. Magnetic susceptibility is calculated or the ground state which increases up to 0.37 cm^3K/mol.

Table 5.2 6 : Lowest spin-orbit energy levels; and g-tensors

Spin orbit state (cm^{-1})		g1	g2	g3
0.00 0.00		2.00	2.00	2.00
	x y z	0.00 0.00 1.00	1.00 0.00 0.00	0.00 1.00 0.00

5.3 Conclusion

In the end, for all systems, we performed spin orbit configuration interaction calculations (SOCI) based on orbitals from complete active space self-consistent field calculations. In the SOCI all Slater determinants in an active space of the 3d-orbitals and the singly occupied ligand orbital are considered to obtain the low lying electronic states, their zero-field splittings, g-tensors and magnetic susceptibilities. The Ni centers are coupled ferromagnetically to the ligand electron. In Ni(II)-radical system, the resulting S=3/2 ground state is split by 9 cm^{-1} into two Kramer's doublets. Ni(II) complex with bridging ligand complex has an S=5/2 ground state split into 3 Kramer's doublets. For section 5.2.1, three mononuclear Co(II) complexes complex 1 is in tetrahedral geometry, whereas complexes 2 and 3 is in distorted octahedral geometry. All the three mononuclear complexes have shown an easy axial anisotropy. However, section 5.2.2, Co center coupled anti-ferromagnetically to the radical electron present on the ligand, resulting triplet as a ground state and next higher state which is quintet lies 3000 cm^{-1} higher in energy.

6 Applications II- Lanthanide ($4f^n$)

In the presented work, we also investigated a few lanthanide complexes. Our aim was to study the magnetic properties of these lanthanide complexes to see if there is a potential to use these complexes in future as molecular magnetic materials. Lanthanide-based single molecule magnets are great center of attraction because of their high magnetic anisotropy and strong spin-orbit coupling, which possibly results in a ground state with large angular momentum[1,108,109] and because of that the interest in Ln(III) SMM increased over transition metal SMM. However, the presence of Lanthanide in a complex makes the theoretical description more difficult than for 3d metal ions because there is high contribution of orbital component.[110] In this thesis a detailed study of magnetic properties of different families of complexes with Ln(III)= Gd (III), Dy(III), Er(III) , Ho(III), Tb(III) is presented. First mononuclear lanthanide complexes studied and then polynuclear complexes.

While for 3d compound orbitals for the SOCI calculations were in general obtained by CASSCF, ROHF was used for the lanthanide complexes. In ROHF an average over selected slater determinants is used to calculate the energy and to optimize the orbitals. The energy is given in equation 6.1

$$E = \sum_{r} 2f_r h_{rr} + \sum_{r,s} f_r f_s (2a_{rs} J_{rs} - b_{rs} K_{rs}) \qquad 6.1$$

where the factors f_r are fractional occupation numbers. If f_r is equal to 0, this indicates a virtual orbital that does not take place in any slater determinant and if it is equal to 1, the orbital is doubly occupied in all slater determinants; a and b are Roothaan parameters which are obtained by taking the average over the high spin states of chosen *f*- elements. The appropriate a and b parameters were provided by Prof. C. van Wüllen, Technical University of Kaiserslautern. Here, with CASSCF calculations, ROHF calculations were also performed to study the validity of the method.

6.1 Mononuclear-Complex Ln_3-ethoxy complex

Two Lanthanide systems are studied here which were synthesized in Prof. Dr Annie Powell's group, Karlsruhe, and are based on molecules studied earlier.[110–112] Both systems have Ln(III) as a central main frame forming a triangle. The major difference in the two structures is different ligands. **Structure 1** (as

shown in Figure 6.1.2a) is $Ln_3(L)_3(\mu 3\text{-}OH)_2(H_2O)_4Cl_2$ and **structure 2** (as shown in Figure (6.1.2b)) is $Ln_3(L_3)(\mu 3\text{-}OH)_2(CH_3OH)(H_2O)_2Cl_3$ where L is 3-ethoxysalicylaldhehyde.

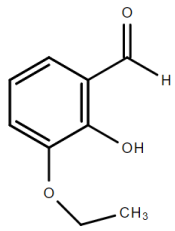

Figure 6.1 1: Structure of ethoxysalicylaldheyde

In **structure 1** and **structure 2**, the Ln ions are in +3 oxidation state and the Ln(1), Ln(2) and Ln(3) ions are connected to each other by two bridging hydroxyl oxygen atoms. Three ethoxy ligands are linked to each Ln(III) ion but in **structure 1** one Ln(III) center is linked with two water molecules and two Ln(III) centers are linked with water molecules and chloride ions. Whereas in **structure 2** one Ln(III) center is linked with a chloride ion and -MeOH and two Ln(III) centers are connected with water molecules and chloride ions. For both the complexes, each Ln center has a coordination number equal to eight and the coordination geometry can be explained as a distorted square anti-prism by the positions of the surrounding atoms. The bond angle and bond length for both complexes are given in Table 6.1.1 and Table 6.1.2 and they fall in the range of reported bond lengths and angles in the literature.[113–117]

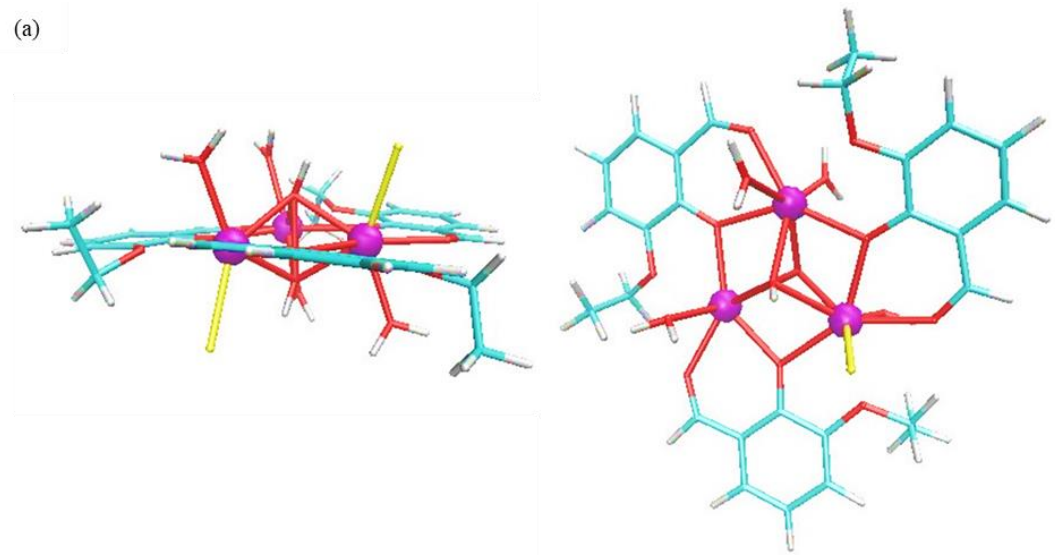

(b)

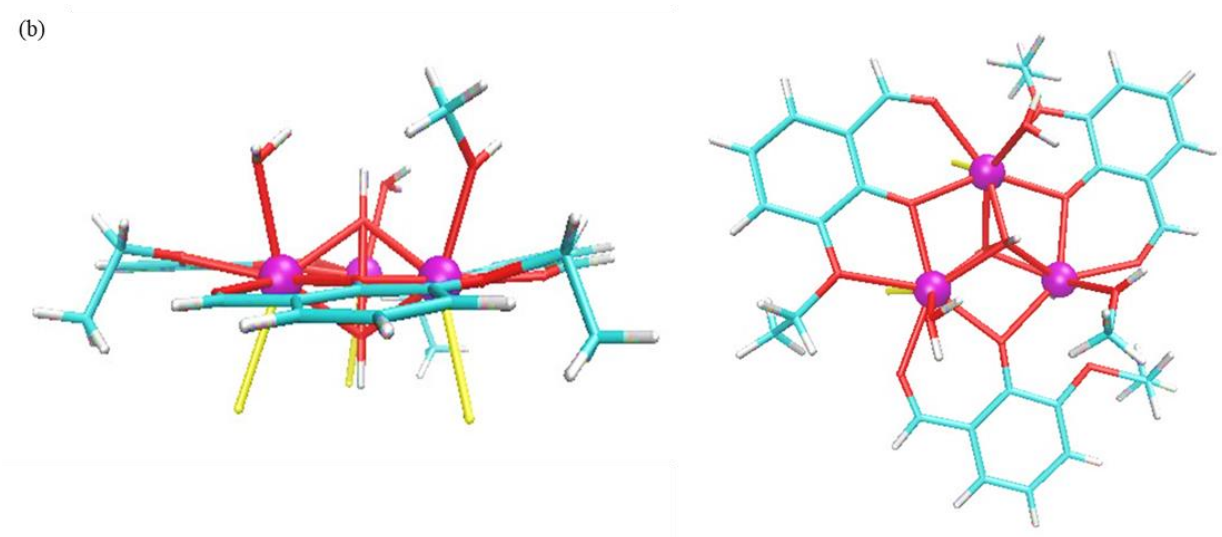

Figure 6.1 2:(a) structure 1, (b) structure 2

Table 6.1. 1: Ln-O bond distances (Å) for all Lanthanide ions (Ln = Gd,Tb, Dy, Ho, Er) for **structure 1** with repective surrounded oxygen atoms.

Center 1		Center 2		Center 3	
Ln(1)-O1	2.33	Ln(2)-O1	2.33	Ln(3)-O1	2.31
Ln(1)-O2	2.34	Ln(2)-O2	2.33	Ln(3)-O2	2.34
Ln(1)-O3	2.35	Ln(2)-O3	2.35	Ln(3)-O3	2.35
Ln(1)-O4	2.37	Ln(2)-O4	2.35	Ln(3)-O4	2.36
Ln(1)-O5	2.38	Ln(2)-O5	2.36	Ln(3)-O5	2.37
Ln(1)-O6	2.39	Ln(2)-O6	2.37	Ln(3)-O6	2.40
Ln(1)-O7	2.50	Ln(2)-O7	2.38	Ln(3)-O7	2.50
Ln(1)-Cl	2.68	Ln(2)-O8	2.50	Ln(3)-Cl	2.69
O1-Ln(1)-O2	140.0	O1 Ln(2)-O2	141.31	O1 Ln(3)-O2	140.42
O2-Ln(1)-O3	101.65	O2-Ln(2)-O3	105.98	O2-Ln(3)-O3	145.16
O3-Ln(1)-O4	71.91	O3-Ln(2)-O4	75.48	O3-Ln(3)-O4	72.44
O4-Ln(1)-O5	132.80	O4-Ln(2)-O5	139.43	O4-Ln(3)-O5	135.29

O5-Ln(1)-O6	60.65	O5-Ln(2)-O6	136.96	O5-Ln(3)-O6	60.63
O6-Ln(1)-O7	130.53	O6-Ln(2)-O7	76.97	O6-Ln(3)-O7	128.62
Cl-Ln(1)-O1	99.19	O7-Ln(2)-O8	132.88	Cl-Ln(3)-O	91.59
Cl-Ln(1)-O2	92.51			Cl-Ln(1)-O2	100.37
Cl-Ln(1)-O3	143.00			Cl-Ln(1)-O3	79.77
Cl-Ln(1)-O4	77.61			Cl-Ln(1)-O4	144.57
Cl-Ln(1)-O5	140.73			Cl-Ln(1)-O5	79.98
Cl-Ln(1)-O6	80.28			Cl-Ln(1)-O6	140.09
Cl-Ln(1)-O7	78.33			Cl-Ln(1)-O7	78.69

Table 6.1. 2: Ln-O bond distances (Å) for all Lanthanide ions (Ln = Gd,Tb, Dy, Ho, Er) for structure 2 with repective surrounded oxygen atoms.

Center 1		Center 2		Center 3	
Ln(1)-O1	2.33	Ln(2)-O1	2.30	Ln(3)-O1	2.31
Ln(1)-O2	2.33	Ln(2)-O2	2.34	Ln(3)-O2	2.32
Ln(1)-O3	2.35	Ln(2)-O3	2.35	Ln(3)-O3	2.34
Ln(1)-O4	2.35	Ln(2)-O4	2.35	Ln(3)-O4	2.35
Ln(1)-O5	2.35	Ln(2)-O5	2.36	Ln(3)-O5	2.38
Ln(1)-O6	2.36	Ln(2)-O6	2.37	Ln(3)-O6	2.39
Ln(1)-O7	2.50	Ln(2)-O7	2.49	Ln(3)-O7	2.48
Ln(1)-Cl	2.68	Ln(2)-Cl	2.69	Ln(3)-Cl	2.71
O1-Ln(1)-O2	98.85	O1-Ln(2)-O2	140.28	O1-Ln(3)-O2	140.90
O2-Ln(1)-O3	79.29	O2-Ln(2)-O3	72.02	O2-Ln(3)-O3	73.57

O3-Ln(1)-O4	73.12	O3-Ln(2)-O4	135.75	O3-Ln(3)-O4	131.06
O4-Ln(1)-O5	73.07	O4-Ln(2)-O5	76.39	O4-Ln(3)-O5	60.10
O5-Ln(1)-O6	135.70	O5-Ln(2)-O6	128.98	O5-Ln(3)-O6	77.54
O6-Ln(1)-O7	82.65	O6-Ln(2)-O7	129.95	O6-Ln(3)-O7	74.76
Cl-Ln(1)-O1	95.60	Cl-Ln(2)-O1	94.25	Cl-Ln(3)-O1	90.34
Cl-Ln(1)-O2	143.24	Cl-Ln(2)-O2	102.88	Cl-Ln(3)-O2	107.21
Cl-Ln(1)-O3	137.39	Cl-Ln(2)-O3	78.83	Cl-Ln(3)-O3	78.68
Cl-Ln(1)-O4	94.46	Cl-Ln(2)-O4	144.18	Cl-Ln(3)-O4	77.42
Cl-Ln(1)-O5	76.83	Cl-Ln(2)-O5	78.23	Cl-Ln(3)-O5	136.01
Cl-Ln(1)-O6	80.72	Cl-Ln(2)-O6	138.43	Cl-Ln(3)-O6	145.86
Cl-Ln(1)-O7	78.89	Cl-Ln(2)-O7	78.75	Cl-Ln(3)-O7	79.15

For the calculation of the magnetic properties of the individual Ln(III) canters, two Ln(III) ions are replaced with Y(III) ions to make a given complex mononuclear. In this way each center is studied individually. For all calculations, density functional theory (DFT) is used using the TURBOMOLE[94] package. The BP86 functional and the x2c-TZVPall basis set[118] for Ln, x2c-SV(P)all basis set for Y and def-SV(P) basis set for rest of the atoms were applied. The bond distances of Ln (= Dy, Ho, Er, Gd, Tb)-O agree with the reported literature.[117,119] The optimized systems were used in Complete Active Space SCF (CASSCF) calculations followed by spin-orbit coupling calculations. The fourth order Douglas-Kroll-Hess hamiltonian was included, where scalar relativistic contributions were taken into account. Spin orbit coupling is also calculated using ROHForbitals and all the calulations are compared.

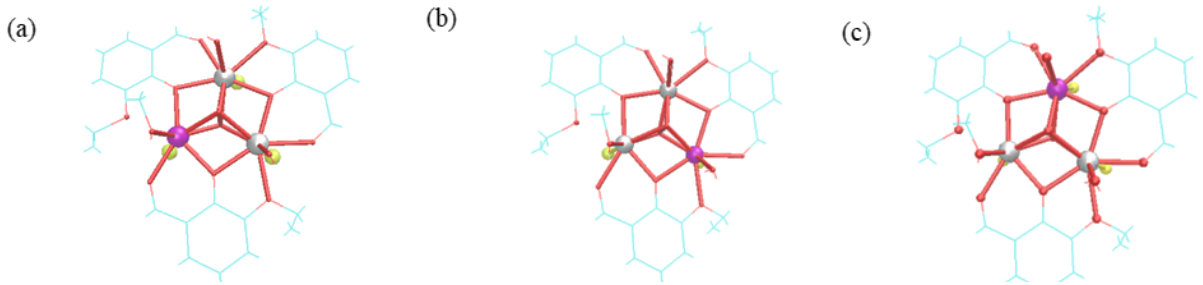

Figure 6.1. 3: Three different Ln(III) positions.(Color scheme : purple, Ln; white, Y; red, O; yellow, Cl, All carbons and hydrogens are in light Skelton)

6.1.1 Gd(III)

The properties exhibited by Gd(III) ions is different from the rest of the lanthanide ions, and the reason behind it is the spherically symmetric electronic structure of Gd(III).[120] This highly symmetric structure arises from the seven unpaired electron in seven 4*f* orbitals, making a high spin paramagnetic ion. Gd(III) is an undesirable choice for SMMs because of its magnetic isotropy or in other words absence of an intrinsic magnetic anisotropy. Therefore, SMM-behavior of Gd(III) complex can be induced by weak anisotropy caused by the Kramer' doublet obtained from the ground state. [121,122] Although it is not expected to be the right candidate for SMM studies, Gd(III) still proves itself useful to study many other magnetic properties like spin-glass properties[123] and due to its isotropic nature it can be used for the analysis of the magnetic exchange coupling. The knowledge of the magnetic coupling can be used to make better SMMs with anisotropic lanthanides [121]. The half-filled 4f orbitals give rise to a ground state with a total spin of S =7/2, however, possessing a half-filled shell results in zero total orbital angular momentum (L). Therefore, the total angular momentum (J) is dependent on the total spin momentum only which makes $J = S$. As the total orbital angular moment is zero in the case of Gd(III) ions, implying that the ground state is a pure S state, second order spin orbit coupling is observed because the first order effect diminished.[120] Considering all electronic configurations of $4f^7$ results in 1 octet, 48 sextets, 392 quartets and 782 doublets as spin free states. The ground state of the Gd(III) ion is a single octet state which belongs to ^8S and the next state is a sextet state after a large energy gap. The ground multiplet of the octet state i.e. $^8S_{7/2}$ splits in the ligand field into four Kramer's doublets and because of second order, the splitting of the octet ground state is minute[124], which helps in determine the interaction with the surrounding.[125]

6.1.1.1 Complex 1

In case of complex 1, the active space in the CASSCF calculations is taken as CAS(7,7), 7 electron in 7 orbitals. As the ground state is not spatial degenerate and all electrons are singly occupied in the S=7/2

state, the orbitals are calculated by taking the ground state. For spin free states for all the three centers, the next excited state lies at 41,000 cm^{-1} higher in energy, which is a huge gap and it ensured that the ground state is well isolated and there is no mixing from higher states and therefore for the further spin orbit calculations only the eight lowest states corresponding to the ground state are included. In case of Gd, as $L = 0$ there is only spin coupling calculations, it is observed that ground state ^8S splits in four Kramer's doublets which exhibits a very small energy difference within the range of 1 cm^{-1} which is in agreement with the reported values.[124,125] In case of ROHF method, the same behavior is observed for the splitting, which it is in the range of 0.70 cm^{-1}.

Table 6.1. 3: Energies (cm^{-1}) of the lowest Four Kramer's doublet of Gd(III) complexes obtained after Spin-Orbit coupling.

Structure 1(Spin orbit states)						
	center a		center b		center c	
	CASSCF	ROHF	CASSCF	ROHF	CASSCF	ROHF
KD1	0.00	0.00	0.00	0.00	0.00	0.00
KD2	0.27	0.16	0.23	0.33	0.38	0.26
KD3	0.51	0.33	0.55	0.54	0.63	0.43
KD4	0.89	0.60	1.04	0.77	0.85	0.59

The g-tensor including all eight states is calculated and it is found highly isotropic in order of 1.99 which agrees well with the expected value. In case of Gd(III), with respect to the accuracy, the calculations yield D and E equal to zero. Furthermore, because of the small energy gaps between the four lowest Kramer's doublets, the g-factors for individual Kramer's doublets are meaningless in case of Gd(III).

The simulated magnetic susceptibility (χT) at B= 0.1 T is 7.84 cm^3K/mol which remains constant at room temperature but suddenly decreases at low temperature which is consistent with the previously reported data.[126] The energies of the 4 KDs with respect to magnetic field show that at high magnetic

field splitting of KDs is around 30 cm^{-1} while zero field splitting is under 1 cm^{-1} as shown in Figure 6.1.5

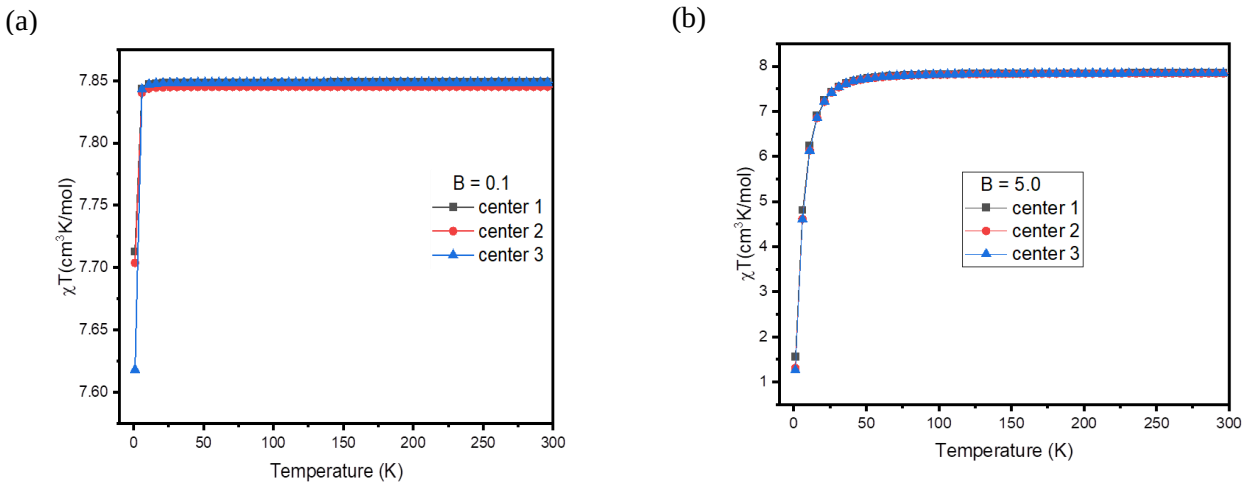

Figure 6.1 4:(a) Magnetic susceptibility of three Gd centers in a magnetic field B =0.1 T(b) Magnetic Susceptibility of three centers in Magnetic field B = 5.0 T in case of structure 1

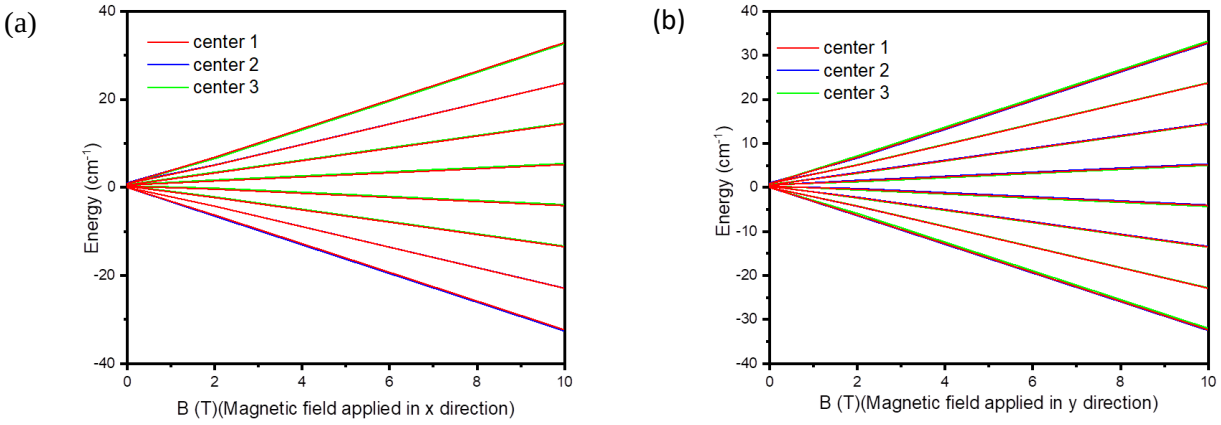

(c)

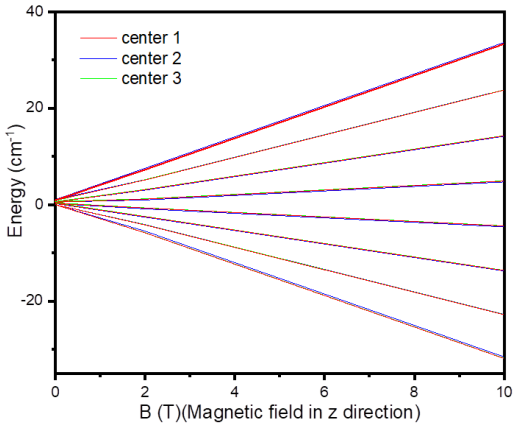

Figure 6.1 5: Zeeman plot of structure 1 of Gd(III) including Kramer's doublet (a) magnetic field in x-direction (b) magnetic field in y-direction and (c) magnetic field in z-direction

6.1.1.2 Complex 2

For complex 2, active is same as before CAS(7,7). For spin free states for all the three center, next excited state lies approximately around 41,000 cm^{-1} higher in energy same as complex 1. No orbital contribution dictates no spin orbit coupling, hence after spin coupling calculations, it is observed that ground state ^{8}S splits in four Kramer's doublets which exhibits very small energy difference within the range of 1 cm^{-1}. In case of ROHF method however, for center 1 and 3 splitting is observed in the range of 0.50 cm^{-1} while in case of center 2, splitting increased to 3 cm^{-1}.

Table 6.1.4: Energies (cm^{-1}) of the lowest four Kramer's doublets of Gd(III) complexes obtained after Spin-Orbit coupling.

Structure 2(Spin orbit states)						
	center a		center b		center c	
	CASSCF	ROHF	CASSCF	ROHF	CASSCF	ROHF
KD1	0.00	0.00	0.00	0.00	0.00	0.00
KD2	0.18	0.18	0.27	0.51	0.11	0.11
KD3	0.29	0.29	0.45	1.40	0.24	0.24

KD4	0.39	0.40	0.70	2.73	0.43	0.44

g-tensors including all eight states is calculated and it is found highly isotropic in order of 1.99 and g-tensors calculated for individual Kramer's doublets, KD 1 and 4 have shown a highly anisotropic behavior for each center same as complex 1 as shown in Table 6.1.5. The simulated magnetic susceptibility (χT) at B= 0.1 T is 7.84 cm^3K/mol (as seen in Figure 6.1.6) which remains constant at room temperature but suddenly decreases at low temperature which is consistent with the complex 1. The energies of 4 KD s with respect to magnetic field shows that at high magnetic field splitting of four KDs is around 30 cm^{-1} while splitting at zero field is under 1 cm^{-1} as shown in Figure 6.1.7

Table 6.1. 5: Main g-tensor values for individual Kramer's doublets

		KD1	KD2	KD3	KD4	ZFS parameter
Center 1	x	0.005	1.01	5.75	1.21	D = -0.03
	y	0.004	0.83	6.07	0.67	E = 0.005
	z	13.91	9.63	4.36	13.23	
Center 2	x	0.14	3.20	4.31	0.31	D = -0.04
	y	0.11	2.39	3.09	0.21	E = 0.01
	z	13.79	8.69	8.02	13.72	
Center 3	x	1.11	5.29	1.51	0.05	D = 0.03
	y	0.62	4.21	1.27	0.04	E = 0.006
	z	13.30	6.55	9.49	13.89	

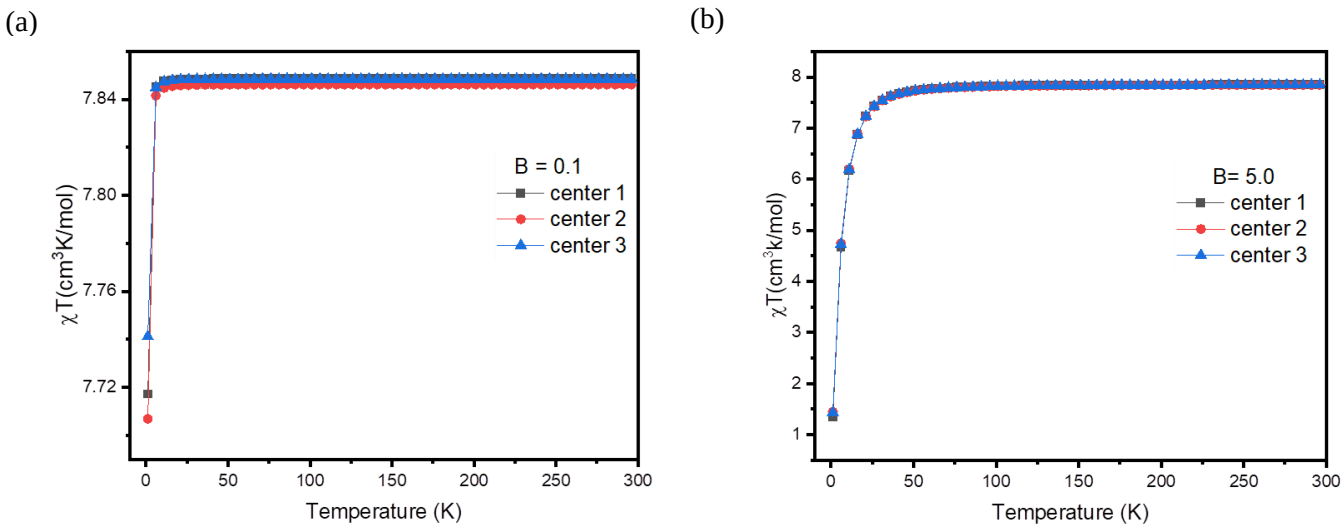

Figure 6.1 6: (a) Magnetic susceptibility of three Gd centers in Magnetic field B =0.1 T(b) Magnetic Susceptibility of three centers in Magnetic field B = 5.0 T in case of structure 2

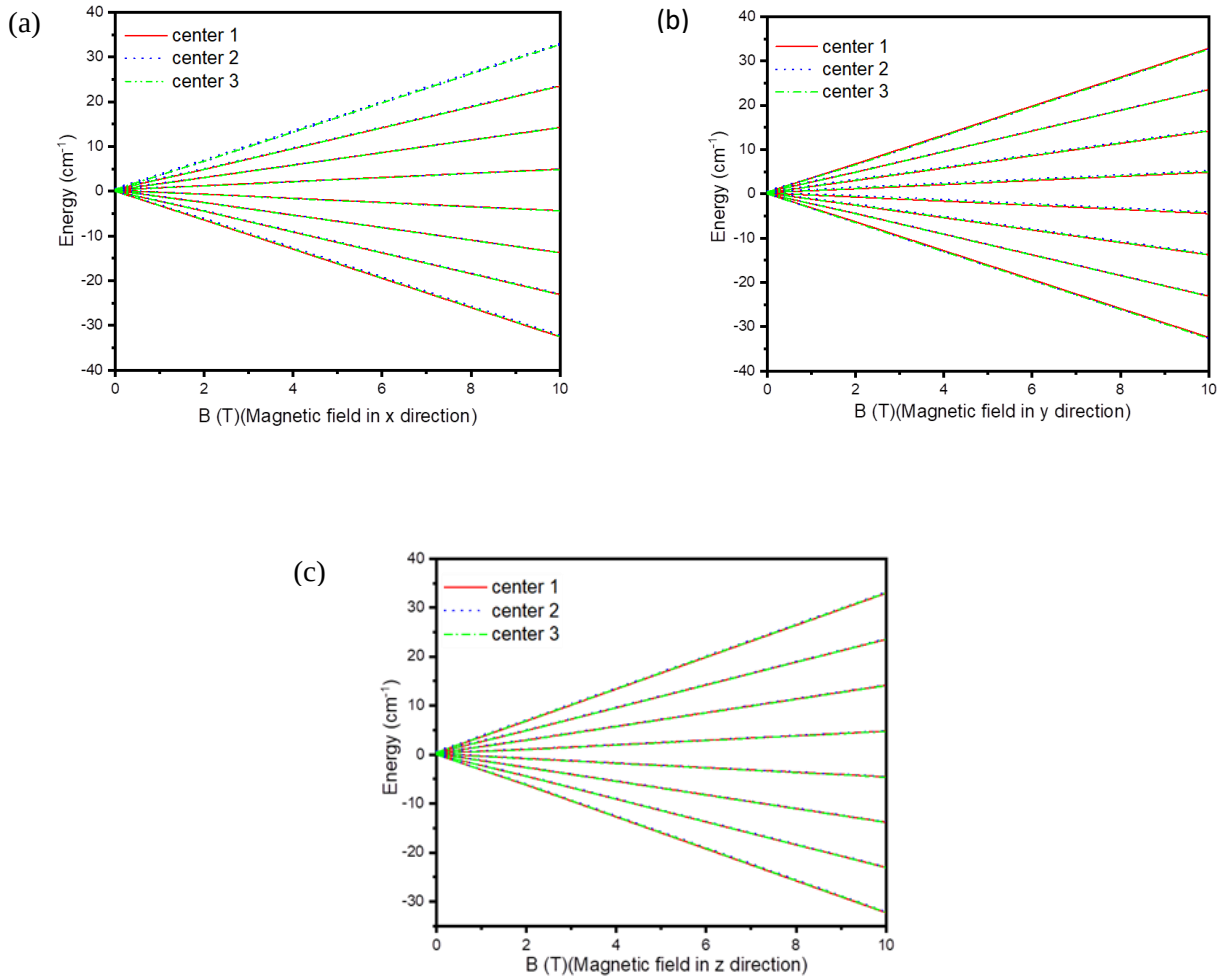

Figure 6.1 7: Zeeman plot of structure 2 of Gd(III) with (a) magnetic field in x-direction (b) magnetic field in y-direction and (c) magnetic field in z-direction

6.1.2 Dy(III)

Dy(III) has [Xe]$4f^9$ configuration that means 9 electrons in 7 orbitals which results in total spin of S = $\frac{5}{2}$ and total orbital momentum L = 5. Total angular momentum *J* can be calculated by using $|L + S| \ldots . |L - S|$ which led to $J = \frac{15}{2}, \frac{13}{2}, \frac{11}{2}, \frac{9}{2}, \frac{7}{2}, \frac{5}{2}$. Dy(III) ion contains 735 states without spin orbit coupling which includes 21 sextets, 224 quadruplets and 490 doublets. According to $^{2S+1}L_J$, the ground state term for Dy(III) ion is $^6H_{15/2}$. As we discussed above sections that in case of lanthanides spin-orbit coupling dominates ligand field interaction, hence, the energy levels split in terms of *J*.

6.1.2.1 Complex 1

In structure 1, two Dy(III) centers are linked with water molecule and chloride ion along with the ligand and on one Dy(III) center, chloride ion is replaced by water molecule. On each Dy^{3+} center, CASSCF calculation and ROHF calculations were performed. As predicted, ground state is $^6H_{15/2}$ and spin-orbit coupling resulted in eight Kramer's doublets which belongs to the ground $M_J = \pm 15/2$ for each Dy center and the next excited term for each center in case of both CASSCF and ROHF calculations is around 3600 cm^{-1}. However, in case of zero-field splitting energy, CASSCF energies are larger than in case of ROHF calculations with a difference of approx. 150 cm^{-1} (as given in Table 6.1.6)

Table 6.1. 6: Energies (cm^{-1}) of the lowest eight Kramer's doublet of Dy(III) complexes obtained after spin-orbit coupling for structure 1

Structure 1(Spin orbit states)						
	center a		center b		center c	
	CASSCF	ROHF	CASSCF	ROHF	CASSCF	ROHF
KD1	0.00	0.00	0.00	0.00	0.00	0.00
KD2	236.31	111.81	313.36	161.28	255.69	125.92
KD3	306.76	146.82	493.89	252.33	312.17	171.98
KD4	404.50	198.29	559.56	305.93	415.17	214.23
KD5	491.80	252.19	628.89	342.71	544.65	272.06
KD6	630.19	303.36	701.00	371.53	640.25	316.673

KD7	691.67	353.82	749.05	389.88	713.40	364.82
KD8	839.94	417.01	989.23	519.67	849.65	410.73

Using the Aniso program, g-tensors for each Kramer's doublets were calculated by taking pseudospin S = ½ for individual dysprosium centers and their main values are given in the Table 6.1.8 below. In each case it can be easily seen that first two Kramer's doublets is highly anisotropic and also the Kramer's doublets seven and eight are anisotropic. If, for all three Dy centers, the direction of anisotropic g-tensor is projected and the magnetic axes are in opposite direction from each other which means the complex possesses a toroidal magnetic moment (as can be seen in Figure 6.1.8). In eight Kramer's doublets, first (lowest) Kramer's doublets is highly axial but as it goes through KDs which belong to higher excited states its axialty decreases up to the KD 4 and then again start to increase forming mirror symmetry.[127] Zero field splitting parameters i.e. D and E parameter is approximately in the range of $E/D \leq |1/3|$, and each center calculation predicts that for Dy(I) center rhombic parameter E is slightly bigger but for Dy(2) and Dy(3) centers, contribution from rhombic zero field parameter is small. Magnetic susceptibility is calculated for B = 0.1 T and 5.0 T for the lowest $^{6}H_{15/2}$ states for each center and it is observed that in all three centers it sharply increases at low temperature 11 K which slowly reaches up to 13.64 $cm^{3}Kmol^{-1}$ at 300 K, which is in agreement with the reported values.[128] However when magnetic field increased to 5.0 T, for Dy(1) magnetic susceptibility increases at 36 K then increases to 13.59 $cm^{3}Kmol^{-1}$ at 300 K, for Dy(2), magnetic susceptibility increases at 50 K then goes to 13.59 $cm^{3}Kmol^{-1}$ at 300 K and for Dy(3) magnetic susceptibility increases at low 7 K then slowly reaches to 13.59 $cm^{3}Kmol^{-1}$. It can be observed from the energy differences in the Zeeman plot shown below in Figure 6.1.10 (c), (d), (e) that easy axis lies in x and y plane which supports toroidal magnetic moment.

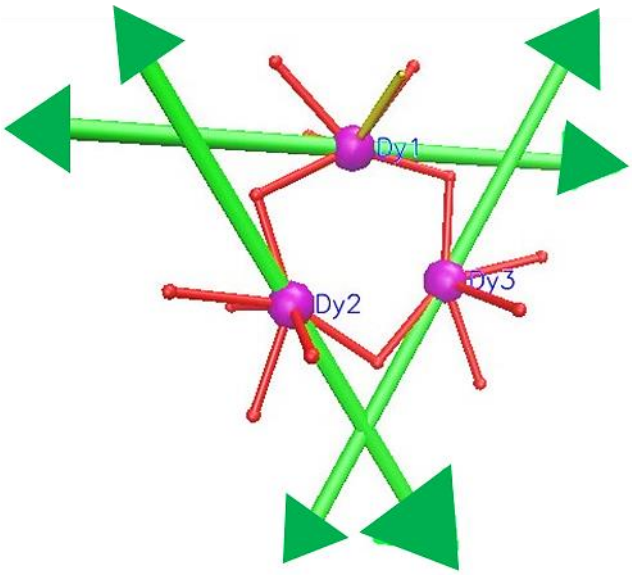

Figure 6.1 8: Toroidal magnetic moment of $Dy_3(L)_3$ (μ_3-OH)$_2(H_2O)_4Cl_2$ (structure 1)

Table 6.1 7 Main g-tensor values for individual Kramer's doublets and D & E parameters for structure 1

		KD1	KD2	KD3	KD4	KD5	KD6	KD7	KD8	ZFS parameter
Center 1	x	0.10	4.72	5.42	4.69	3.91	1.11	1.54	0.04	D = 7.45
	y	0.06	2.07	9.98	1.01	3.03	0.27	0.28	0.002	E = 2.20
	z	19.47	14.29	0.71	11.92	14.14	16.24	18.32	19.33	
Center 2	x	0.005	0.15	3.17	6.64	2.68	3.51	9.51	0.007	D = -10.42
	y	0.002	0.13	2.09	10.60	2.38	2.93	11.22	0.002	E = 1.76
	z	19.58	16.30	11.99	1.67	11.67	5.02	1.11	19.78	
Center 3	x	0.04	2.79	5.69	5.45	4.18	3.02	0.33	0.09	D = -8.29
	y	0.02	1.51	2.10	0.34	0.455	1.60	0.05	0.04	E = 0.66
	z	19.56	15.08	11.13	10.87	12.87	15.10	18.68	19.11	

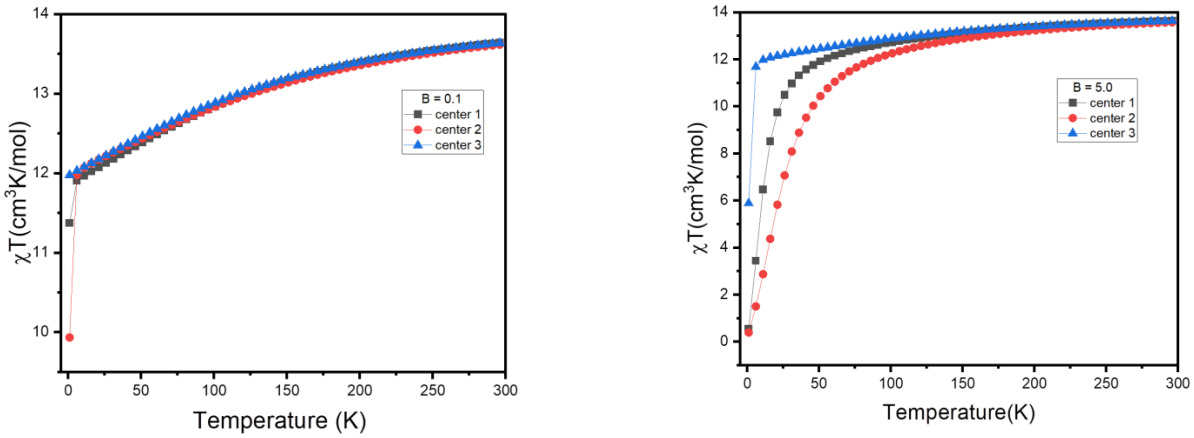

Figure 6.1 9: Magnetic susceptibility of three Dy centers in Magnetic field B =0.1 T(b) Magnetic Susceptibility of three centers in Magnetic field B = 5.0 T in case of **structure 1**

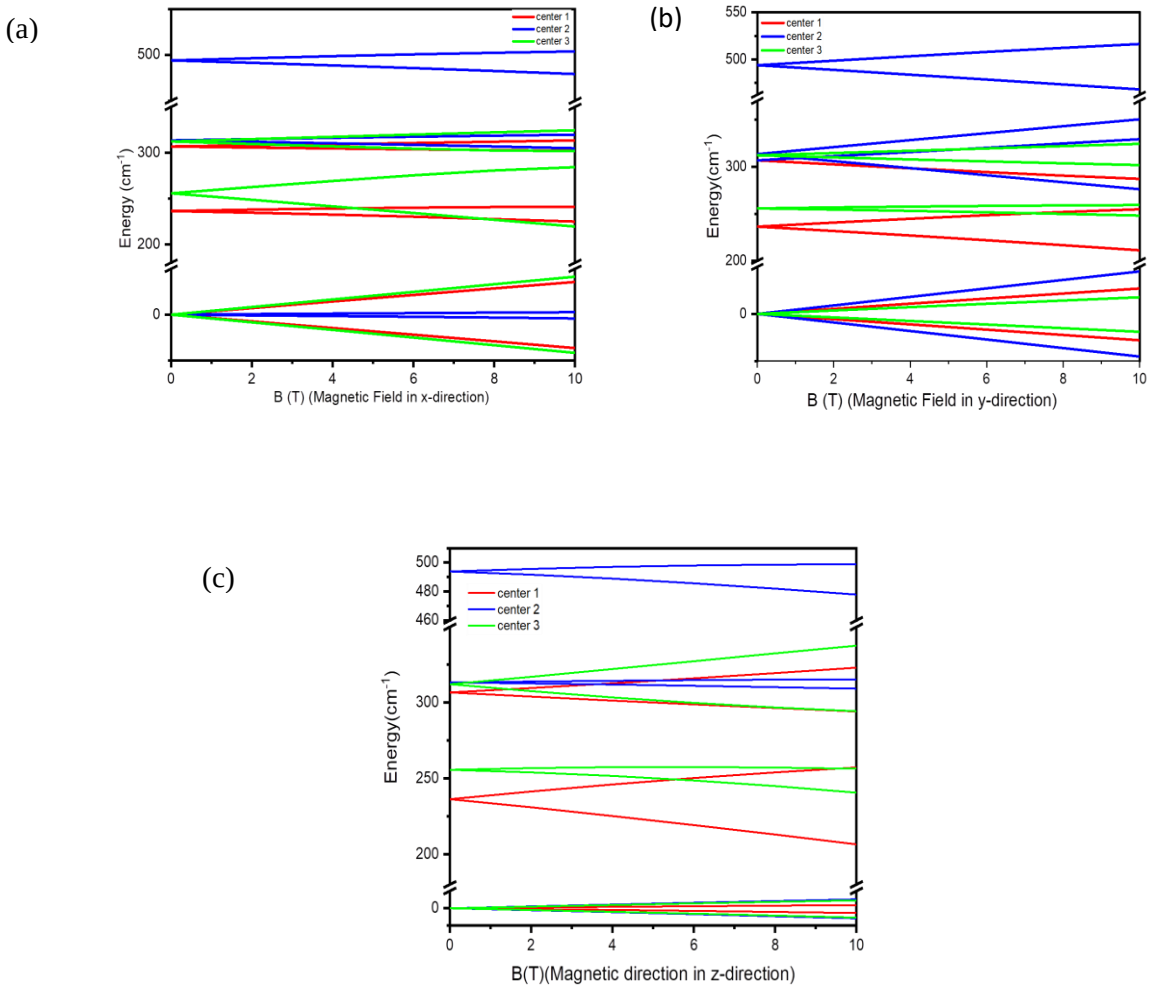

Figure 6.1 10: Zeeman plot of structure 1 including three lowest Kramer's doublets (a) magnetic field in x-direction (b) magnetic field in y-direction and (c) magnetic field in z-direction

6.1.2.2 Complex 2

In case of structure 2, all Dy(III) ions are linked with water molecules and chloride ions along with the ligand. On each Dy^{3+} center, CASSCF calculation and ROHF calculations were performed. As found earlier, the ground state is $^6H_{15/2}$ and spin-orbit coupling resulted in eight Kramer's doublets which belongs to the $M_J = \pm 15/2$ ground state for each Dy center and the next excited term for each center in case of both CASSCF and ROHF calculations is around 3600 cm^{-1}. However, in case of the zero-field splitting energy, in case of center 1(i.e. Dy center 1) CASSCF energies are smaller than in case of ROHF calculations with a difference of approx. 300 cm^{-1} (as given in Table 6.1.8) whereas as in case of other two Dy centers it is like observed in case of structure 1, CASSCF energies are larger than ROHF energies by 130 cm^{-1}.

Table 6.1 8 Energies (cm^{-1}) of the lowest eight Kramer's doublets of Dy(III) complexes obtained after Spin-Orbit coupling for **structure 2**

Structure 2(Spin orbit states)						
	center a		center b		center c	
	CASSCF	ROHF	CASSCF	ROHF	CASSCF	ROHF
KD1	0.00	0.00	0.00	0.00	0.00	0.00
KD2	100.98	411.98	225.53	104.07	253.84	126.20
KD3	147.30	615.15	302.91	139.40	358.24	178.54
KD4	217.38	726.80	368.88	180.20	403.33	197.46
KD5	338.55	957.55	512.65	234.77	506.26	236.20
KD6	448.72	1000.23	629.85	295.52	560.35	261.47
KD7	643.48	1430.73	688.31	325.296	655.56	309.27
KD8	747.24	1658.73	790.41	355.96	883.13	421.75

g-tensor for eight lowest Kramer's doublets is calculated and it can be seen in Table 6.1.10 that all the eight Kramer's doublets for all the three centers are found to be highly anisotropic which is very typical

for Dysprosium. The g-tensor components from main magnetic axes of lowest Kramer's doublets are taken to plot the magnetic direction and it can be seen that structure 2 also exhibits toroidal magnetic moment. The rhombicity ratio λ = E/D for Dy(I) is 0.16 and for Dy(II) is 0.13 whereas for Dy(III), E is a bit large which makes λ is equal to 0.32.[129,130] Magnetic susceptibility is calculated for magnetic field B = 0.1 T, including all the lowest sixteen states, in all three centers (Dy(I), Dy(II), Dy(III)) it increases up to 13.61 cm^3K/mol at 300K as shown in Figure 6.1.12(a), for magnetic field B = 5.0 T for center 1, center 2 and center 3 resulted in the rapid increase of magnetic susceptibility at 10K, 11K, 50K respectively and eventually attained a value of 13.63 cm^3K/mol at 300K. The Zeeman plot is plotted using lowest three states (ground state and two excited states) by considering B = 2.0T. 4.0 T, 6.0 T, 8.0 T & 10 T in x, -y & -z direction. By considering the energy differences in all centers, it can be seen that splitting is larger in x & -y direction than in –z direction implying easy axis in xy plane.

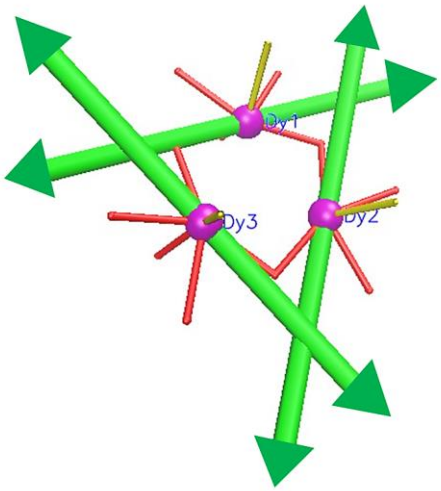

Figure 6.1 11: Toroidal magnetic moment of $Dy_3(L_3)(\mu 3\text{-}OH)_2(CH_3OH)(H_2O)_2Cl_3$ (structure 2)

Table 6.1 9: Main g-tensor values for individual Kramer's doublets and Zero field splitting parameter for structure 2

		KD1	KD2	KD3	KD4	KD5	KD6	KD7	KD8	ZFS parameter
Center 1	x	0.77	1.67	1.71	6.44	3.91	1.72	0.16	0.15	D = -5.50
	y	0.10	0.07	0.71	3.64	1.10	1.17	0.11	0.009	E = 0.88
	z	18.26	17.16	12.80	9.30	13.32	17.62	17.57	18.32	
Case 2	x	0.17	5.72	3.23	2.68	2.25	2.34	1.43	0.46	D = -6.84
	y	0.10	4.01	2.08	0.44	0.39	0.57	0.94	0.27	E = 0.90
	z	19.12	11.74	11.13	11.77	15.17	14.24	14.19	16.96	
Case 3	x	0.11	2.92	3.78	3.64	3.32	1.90	0.59	0.09	D = -6.81
	y	0.10	2.31	2.90	2.01	0.96	0.49	0.36	0.01	E = 2.20
	z	19.34	14.18	10.90	12.23	14.31	15.47	17.51	19.06	

(a)

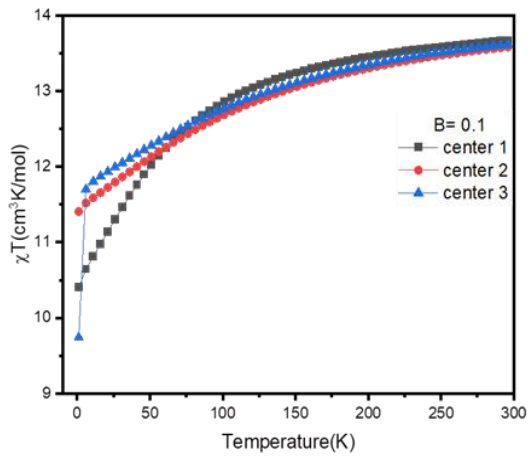

(b)

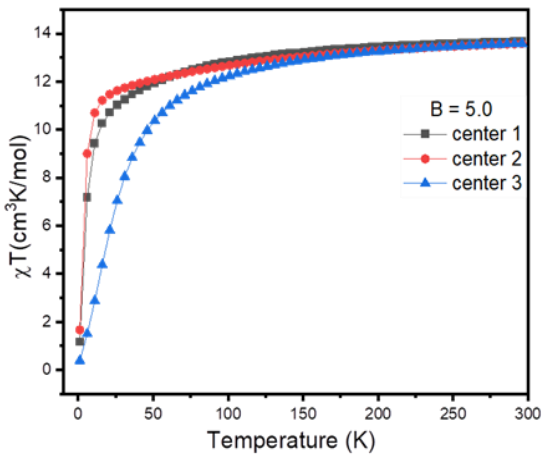

Figure 6.1 12: (a) Magnetic susceptibility of three Dy centers in Magnetic field B =0.1 T(b) Magnetic Susceptibility of three centers in Magnetic field B = 5.0 T in case of structure 2

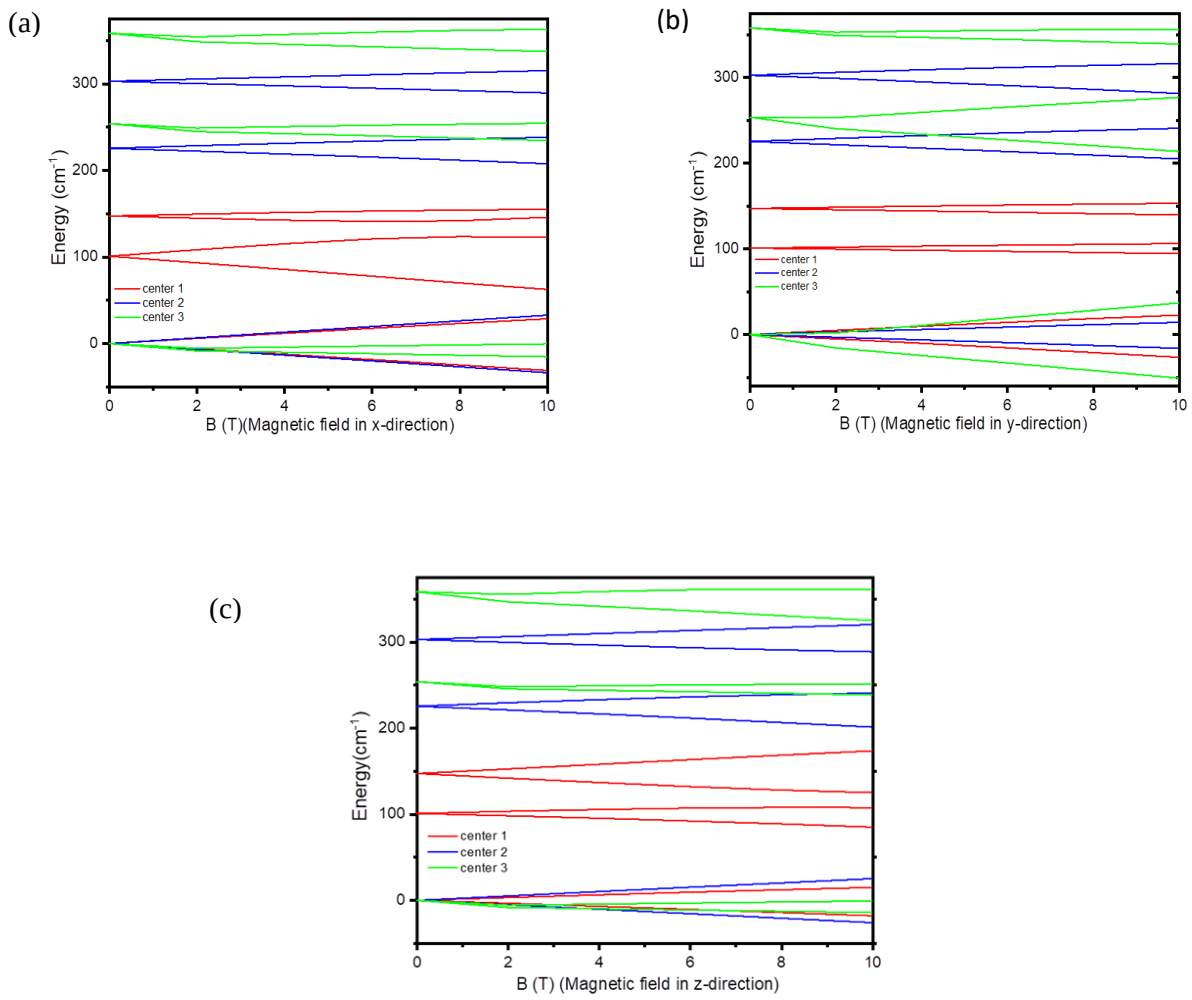

Figure 6.1 13: Zeeman plot of structure 2 including three lowest Kramer's doublets (a) magnetic field in x-direction (b) magnetic field in y-direction and (c) magnetic field in z-direction

Structure 1 and **2** haven't shown a major change because of change in ligand in both cases magnetic susceptibility is around 13.60 cm^3K/mol and both structures have toroidal magnetic moment which shows capability of attaining the maximal magnetization which can be expected from Dy center complexes.

6.1.3 Er(III)

Erbium has electrons configuration with $4f^{12}6s^2$ as outermost shell. As expected being in lanthanide group, Er(III) is the most stable oxidation state. According to Er(III), it has 11 electrons in 7 orbitals with the total spin of $S = 3/2$ and total orbital angular momentum, $L = 6$,.resulting in a quartet state as a ground state.

However, after spin-orbit coupling, ground state splits further into the multiplets of J, total angular momentum, leading to $^4I_{15/2}$ as ground state, with $^4I_{13/2}$, $^4I_{11/2}$, $^4I_{9/2}$ as next excited states. The lowest state leads to eight Kramer's doublets in the ligand field. Below calculations were performed with two complexes containing Er(III) as metal center.

6.1.3.1 Complex 1

In Table 6.1.11 energies for each center with Er(III) were calculated and compared. Without spin-orbit coupling, the lowest quartet states are split by the ligand field in the following way: ground state at 0.0 cm^{-1} and the next excited quartet states which belong to ^4I ranges to 344 cm^{-1},330cm^{-1}, 349 $cm^{-1}$for center a, center b and center c, respectively along with next excited doublet around 18011.31, 17968.87 & 18239.23 cm^{-1}, respectively. The large energy gap between the quartet and the excited doublet state suggests that the influence of the doublet states is low. After spin orbit coupling, the ground state produced eight Kramer's doublets and the next excited states are at 6650, 6621 and 6669 cm^{-1} in center 1, center 2, and center 3, respectively, for CASSCF and for ROHF, they are around 6545, 6532 and 6553 cm^{-1}, respectively, which is in agreement with the results for other Er complexes. [115,116,131–135] First excited KD of CASSCF is approximately 60 cm^{-1} higher in energy as compared to first excited KD of ROHF.

Table 6.1 10 Energies (cm^{-1}) of the lowest eight Kramer's doublets of Er(III) complexes obtained after Spin-Orbit coupling for **structure 1**

Structure 1(Spin orbit states)						
	center 1		center 2		center 3	
	CASSCF	ROHF	CASSCF	ROHF	CASSCF	ROHF
KD1	0.00	0.00	0.00	0.00	0.00	0.00
KD2	72.75	33.32	73.89	21.01	96.52	32.60
KD3	154.50	58.86	124.00	49.47	179.66	62.22
KD4	213.46	83.32	156.16	65.02	277.71	98.36
KD5	406.14	146.66	286.41	117.36	444.36	153.33
KD6	477.82	180.26	355.55	141.44	512.29	190.86
KD7	574.69	222.47	458.89	188.73	576.54	211.30
KD8	629.164	258.13	604.13	273.65	667.79	267.62

In complex 1, lowest eight Kramers doublets for all three Er(III) center are in the energy range of 650 cm^{-1} and 300 cm^{-1} for CASSCF and ROHF methods respectively. Through the computed g_{xx}, g_{yy} and g_{zz} of the lowest Kramer's doublets for each center it can be predicted that it is rather axial (as seen in Table 6.1.11). Although, the next excited Kramer's doublets have shown transverse anisotropic behavior. The g_{zz} axis of lowest KD for each center is plotted for each center as seen in Figure 6.1.14 and it can be clearly visible that for each center, orientation of g_{zz} axis point towards the ligand. Magnetic susceptibilities for Er(1), Er(2), Er(3) for magnetic field 0.1 T at 300K was 10.96, 11.10 and 10.92 $cm^3K\ mol^{-1}$, respectively, magnetic susceptibilities obtained here is bit lower than the values expected for free ion but plausible reason for this can be assumption of the diamagnetism [86,89]. For the magnetic field 5.0 T, magnetic susceptibilities gradually increase to 10.95, 11.10 and 10.92 cm^3Kmol^{-1} at 300 K, respectively. In the Figure 6.1.16 energy difference of lowest three KD is plotted with respect to magnetic field in particular direction is shown and it is observed that all center mainly has easy axis in x and y direction, while in z direction energy difference is comparatively less. According to Zero field splitting parameter, E/D ratio for Er(1) is 0.26 which is bit large vale from the expected value but Er(2) and Er(3) it is 0.16 and 0.09, respectively.

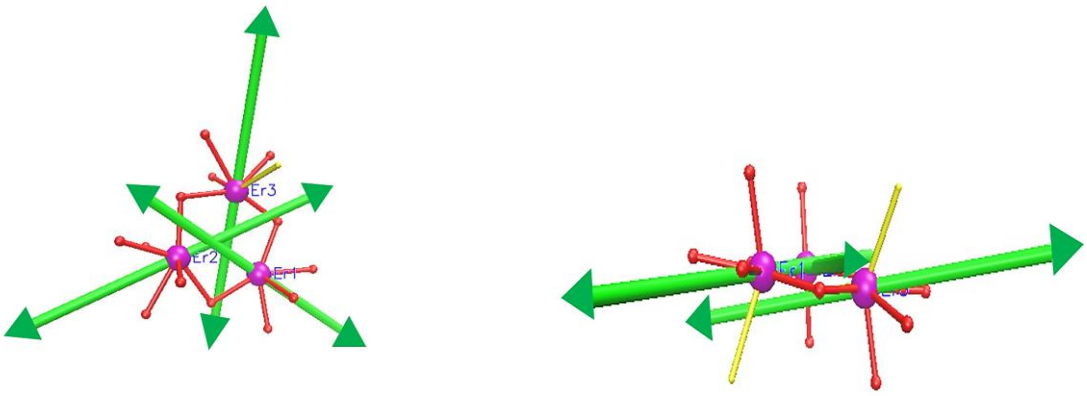

Figure 6.1 14: Direction of g-tensors of the ground state KD of Er3 center for **structure 1**: (color scheme purple, Er; red, O; yellow, Cl; all hydrogen and carbon and bridge O atom is removed for clarity

Table 6.1 11 Main g-tensor values for individual Kramer's doublets and Zero field splitting parameter for Er(III) for **structure 1**

		KD1	KD2	KD3	KD4	KD5	KD6	KD7	KD8	ZFS parameter
Center 1	x	2.09	5.74	5.60	4.22	4.12	4.98	4.43	1.07	D = -3.18
	y	1.69	7.48	7.61	7.50	2.64	1.65	1.41	0.77	E = 0.83
	z	13.46	2.16	2.92	0.20	7.93	9.40	11.81	15.03	
Center 2	x	4.99	0.88	4.82	1.46	4.64	2.42	6.09	0.53	D = 4.30
	y	2.09	0.23	2.04	0.58	3.41	0.63	7.57	0.39	E = 0.71
	z	12.03	13.15	7.86	10.32	7.55	11.48	4.17	16.23	
Center c	x	0.93	3.19	6.09	3.17	2.86	3.55	2.87	2.27	D = 3.53
	y	0.58	1.94	9.71	2.19	0.73	1.17	0.85	0.50	E = 0.35
	z	14.72	10.13	1.44	9.77	9.72	10.16	12.52	14.89	

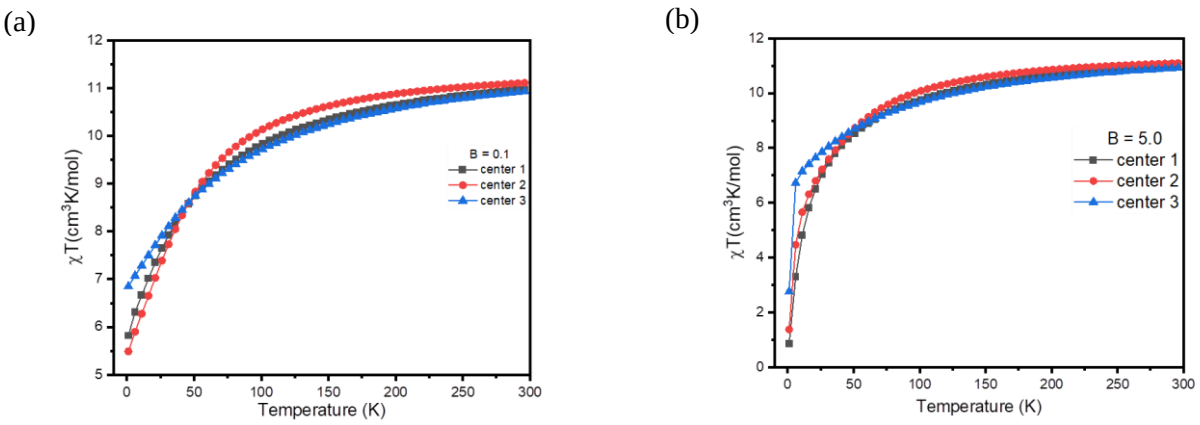

Figure 6.1 15:(a) Magnetic susceptibility of three Er centers in Magnetic field B =0.1 T(b) Magnetic Susceptibility of three centers in Magnetic field B = 5.0 T in case of structure 1

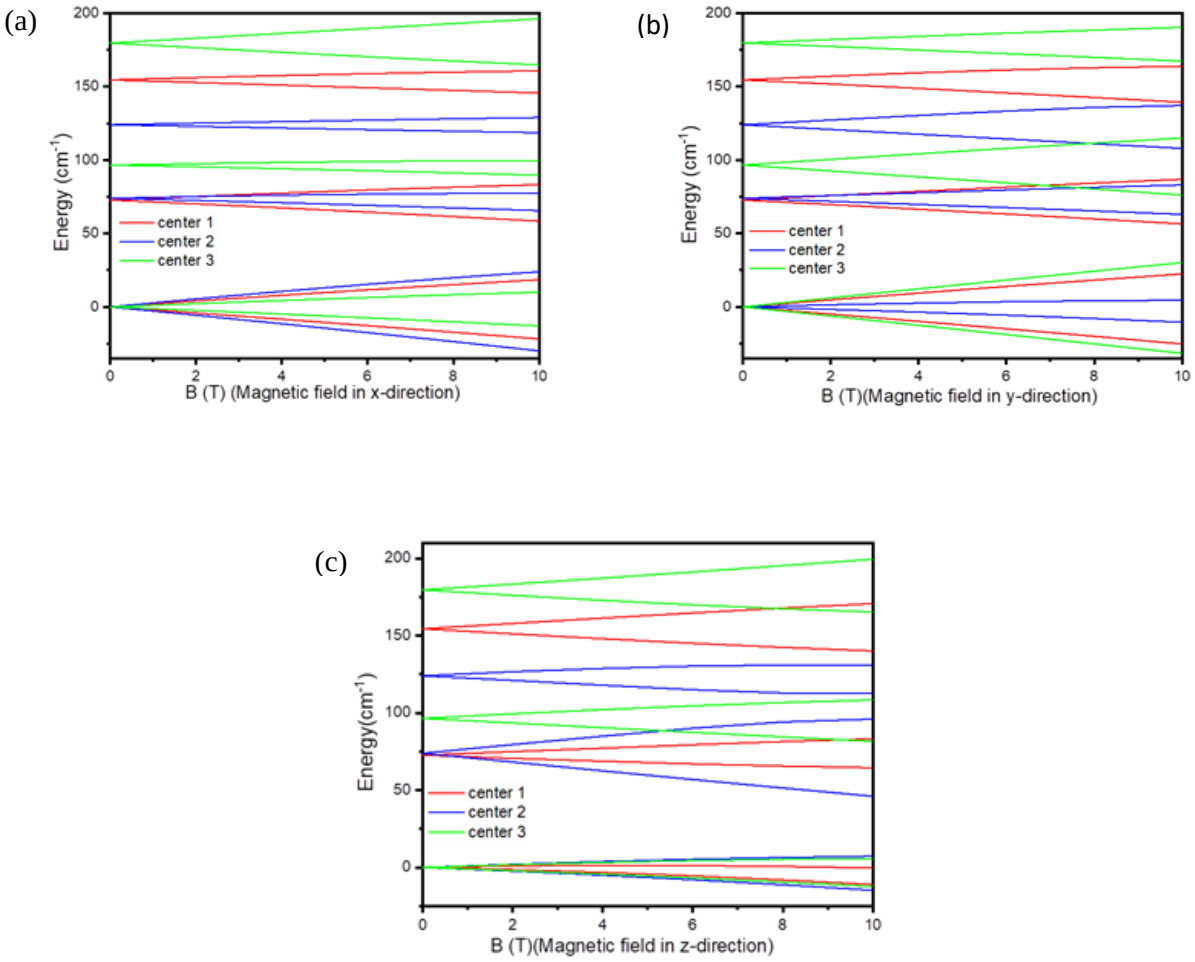

Figure 6.1 16: Zeeman plot of structure 1 including three lowest Kramer's doublets with (a) magnetic field in x-direction (b) magnetic field in y-direction and (c) magnetic field in z-direction

6.1.3.2 Complex 2

In this case, it is same as in complex 1 discussed above, without spin orbit coupling lowest state is as expected quartet state and the next excited quartet state is at 14.64, 15.84 and 17.23 cm^{-1} for center 1, center 2 and center 3, respectively, with a next excited doublet at higher energies. In case of complex 2, spin orbit coupling calculations followed by CASSCF method resulted in larger zero field splitting with the difference of 20 cm^{-1} relative to what is seen in complex 1 and spin orbit states in ROHF method showing smaller zero field splitting. The lowest eight Kramer's doublets are in the order of 750 cm^{-1} and 300 cm^{-1} in CASSCF and ROHF calculations, respectively. First excited KD is about 100 cm^{-1} higher in energy than the ground KD. The next excited multiplet of J is at 6600 cm^{-1} in each center.

Table 6.1 12 Energies of the lowest eight Kramer's doublets of Er(III) complexes obtained after Spin-Orbit coupling for structure 2

Structure 2(spin-orbit states cm^{-1})						
	center 1		center 2		center c	
	CASSCF	ROHF	CASSCF	ROHF	CASSCF	ROHF
KD1	0.000	0.00	0.000	0.00	0.000	0.00
KD2	90.010	15.82	97.698	28.50	117.891	38.90
KD3	170.569	49.41	176.571	63.44	210.866	68.99
KD4	294.314	99.96	250.633	97.83	327.447	111.59
KD5	462.300	149.84	448.375	161.09	538.318	179.23
KD6	535.788	183.48	541.192	208.70	592.532	206.25
KD7	602.147	212.24	609.121	230.10	656.149	231.84
KD8	689.354	261.09	698.503	276.60	743.664	280.86

The g-tensors computed are for the energies taken from the CASSCF orbitals (as seen in Table 6.1.13), first and last KD have shown an axial behavior while KD in between are exhibited transverse anisotropic nature. Orientation of the main magnetic axis that is g_{zz} taken from the ground KD predicts that

magnetic axis from each center is working opposite direction and pointing out of the plane (as seen in Figure 6.1.17). Rhombicity ratio (E/D), which is derived from zero field splitting parameter, for center 1 is bit close to 1/3 whereas it is small in case of center 2 and center 3. Calculated magnetic susceptibilities with B = 0.1 T was 10.75, 10.84 and 10.76 cm^3Kmol^{-1} at 300 K and with B = 5.0 T was 10.74, 10.83 and 10. 75 at 300 K for center 1, center 2 and center 3 respectively as can be seen in Figure 6.1.18. By observing the energy change with respect to the magnetic field, it can be seen that center 1 has an easy axis in x direction while center 2 and 3 have easy axis in y and z direction which is in contradiction with the complex 2.

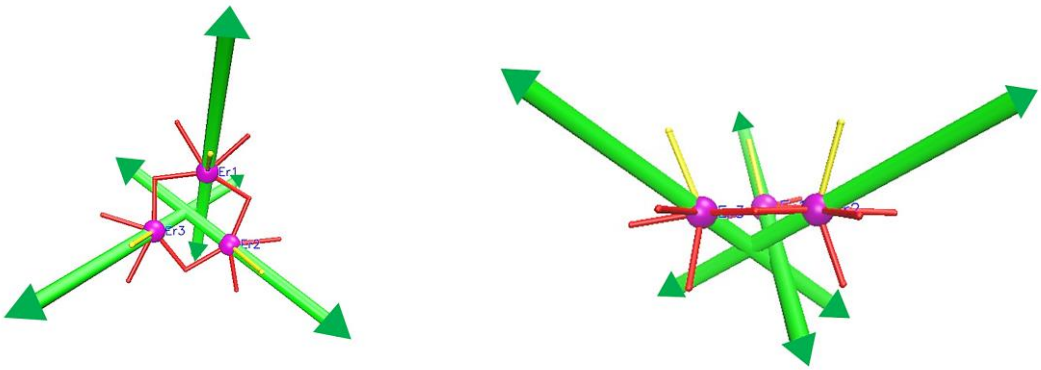

Figure 6.1 17: Direction of g-tensors of the ground state KD of Er3 center for **structure 2**: (color scheme purple, Er; red, O; yellow, Cl; all hydrogen and carbon and bridge O atom is removed for clarity

Table 6.1 13: Main g-tensor values for individual Kramer's doublets and Zero field splitting parameter for Er(III) for **structure 2**

		KD1	KD2	KD3	KD4	KD5	KD6	KD7	KD8	ZFS parameter
Center 1	x	0.64	2.67	3.80	4.05	3.76	3.79	5.36	3.13	D = 2.95
	y	0.13	1.88	0.63	0.75	0.31	0.77	3.08	0.87	E = 0.73
	z	14.82	12.76	9.17	8.76	9.88	9.26	9.01	13.71	
Center 2	x	1.69	4.39	3.71	3.44	5.38	4.96	4.56	0.88	D = 2.22
	y	0.91	3.25	2.54	0.43	8.58	1.78	3.06	0.35	E = 0.12
	z	14.53	9.16	9.85	8.45	0.15	10.03	9.49	14.23	
Center 3	x	0.53	3.54	3.52	5.60	2.90	4.58	2.65	2.97	D = 2.82
	y	0.23	2.24	0.78	7.78	0.67	0.67	0.77	0.52	E = 0.29
	z	15.16	11.59	10.74	1.60	8.65	9.85	12.44	13.67	

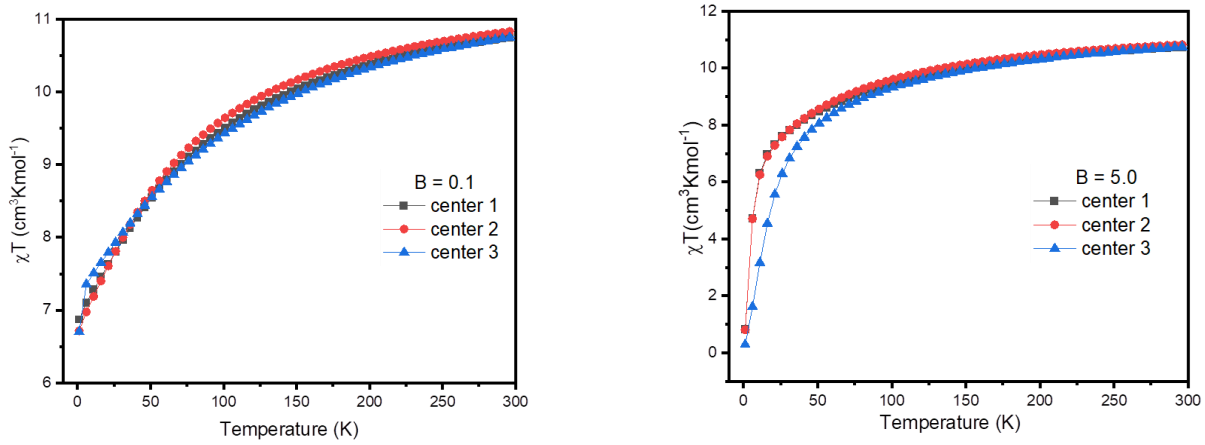

Figure 6.1 18: (a) Magnetic susceptibility of three Er centers in Magnetic field B =0.1 T(b) Magnetic Susceptibility of three centers in Magnetic field B = 5.0 T in case of **structure 1**

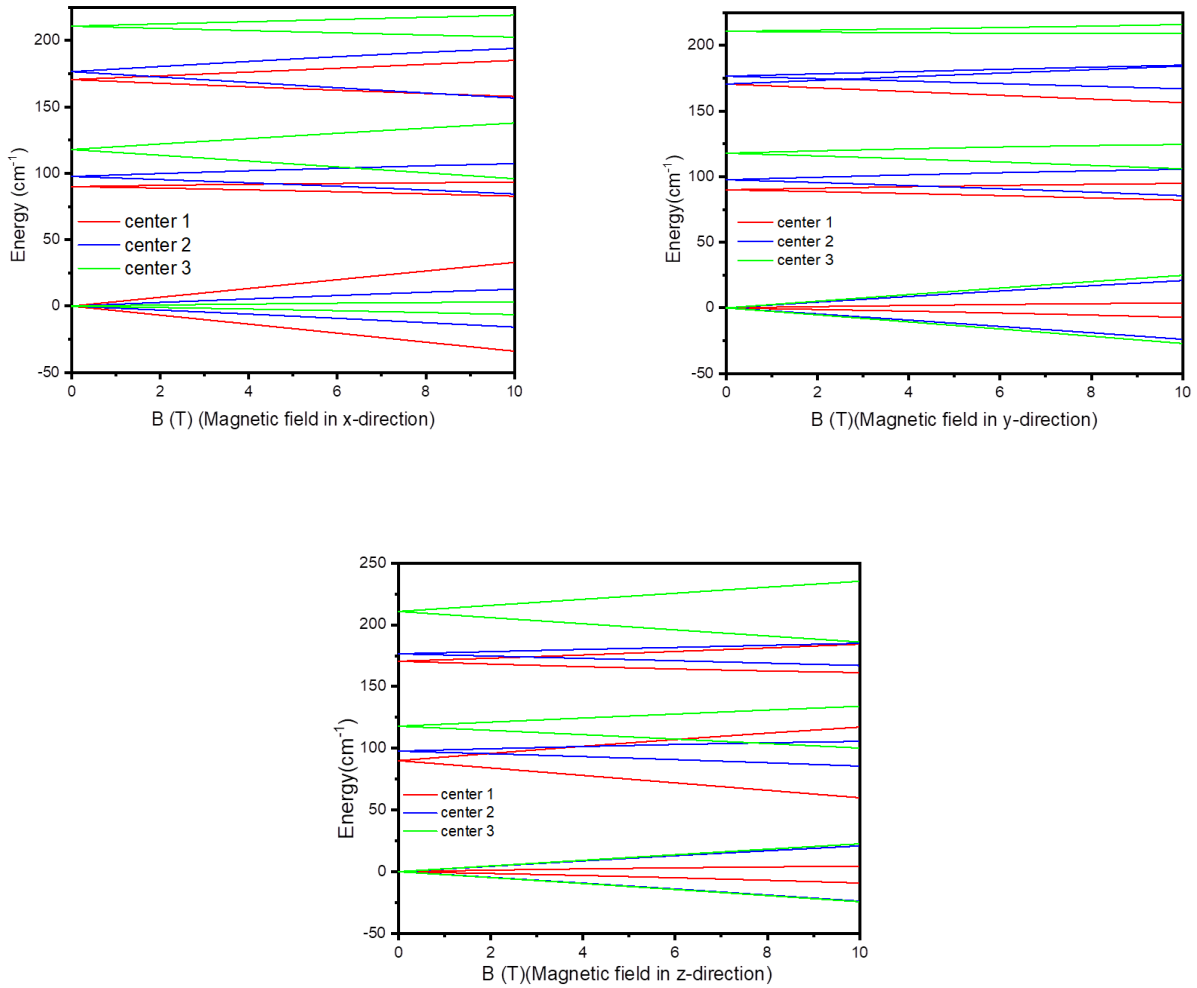

Figure 6.1 19: Zeeman plot of **structure 2** including three lowest Kramer's doublets (a) magnetic field in x-direction (b) magnetic field in y-direction and (c) magnetic field in z-direction

Important observations derived from the calculations with the Er(III) ion is that in this case, a toroidal magnetic moment was absent, reason for this could be the presence of prolate nature in Er(III)[136] ion in which electron density expand axially resulted in different orientation of g_{zz} axis to the magnetic center triangle as compared to Dy(III) ion.

6.1.4 Ho(III)

The Ho(III) ion in the complexes have $4f^{10}$ configuration resulting in quintet as a ground spin, triplet and singlet as excited spins. $4f^{10}$ electronic configuration creates 35 quintet, 210 triplet and 196 singlet spin states.[137] After spin orbit coupling in Ho(III) where $L = 6$, $S = 2$ and $J = |L + S| = 8$, the ground state term is $^5I_8$ which gives rise to 17 non-degenerate lowest states and the next excited states belongs to $^5I_7$.

6.1.4.1 Complex 1

For complex 1, in calculation for CASSCF method active space is taken as 10 electrons in 7 orbitals which are responsible for as discussed above quintet as a ground state and next excited quintet state is 26 cm^{-1} higher in energy for each center. Spin orbit coupling produced 17 low lying states by 591, 585 and 624 cm^{-1} for center 1, center 2 and center 3, respectively and the first excited state just above the ground state is not very far away but just at 5.12, 0.97 and 13.47 cm^{-1} for center 1, center 2 and center 3, respectively and the next excited state which belongs to term $^5I_7$ state is about 5200 cm^{-1} higher in energy. Magnetization comes through the second order Zeeman interaction as the lowest states are non-degenerate[138] In ROHF calculations, the spin orbit states obtained are lower in energy as compared to the CASSCF method (as seen in Table 6.1.14 below). In case of ROHF method, zero field splitting is 1.37, 0.03 and 2.93 cm^{-1} for center 1, center 2 and center 3, respectively and the next excited state is 5100 cm^{-1} higher in energy. Nevertheless, both methods provided energies well in the range of other reported values.[137,139–141]

Table 6.1.14 Energies (cm^{-1}) of the 17 states of Ho(III) complexes obtained after Spin-Orbit coupling for **structure 2**

Structure 1					
center 1		center 2		center 3	
CASSCF	ROHF	CASSCF	ROHF	CASSCF	ROHF
0.000	0.00	0.000	0.00	0.00	0.00
5.12	1.37	0.97	0.03	13.47	2.93
54.85	28.98	125.95	69.47	80.18	47.20

62.24	33.27	144.16	74.30	93.90	49.45
110.57	60.31	168.70	96.09	133.26	61.81
170.59	77.49	256.90	126.14	174.87	75.77
175.28	90.42	278.75	133.88	176.73	87.80
229.276	102.22	303.33	143.25	226.00	105.00
302.37	130.74	374.25	166.51	277.78	121.62
416.76	167.84	392.79	176.15	386.39	158.29
426.74	170.64	456.51	203.18	439.89	179.90
464.21	183.05	466.41	207.91	481.14	190.45
493.73	195.54	488.99	215.59	501.31	197.67
523.49	206.74	513.09	224.37	541.50	217.80
542.30	213.61	547.34	241.02	559.09	222.47
585.78	240.47	565.86	253.50	619.05	245.06
591.36	240.68	585.90	256.57	624.06	246.91

Magnetic properties are calculated from the lowest six states as three pseudo doublets, at low temperature. When g tensors were calculated for non-Kramers doublet, two g factors were zero except one, implying that magnetization was only in one direction and not in other two directions. Anisotropic axis i.e. g_{zz} =17.06, 18.03 and 17.38 for center 1, center 2 and center 3, respectively, taken from the lowest doublet and plotted to find out the directions of the local magnetic moment and as it can be seen in Figure 6.1.20 below that local magnetic moment of each center resulted in toroidal magnetic moment. The g factor calculated first for all the 17 non degenerate states which belong to the ground state $^5I_8$ is isotropic. Calculated zero field splitting parameter for center 1 and center 2 are bit large while for center 3 it is a different case. The calculated magnetic susceptibility (χ) for B = 0.1 T is 13.49, 13.55 and 13.49 cm^3K/mol at 300K for center 1, center 2 and center 3 respectively. At lower temperature around 5 K, there is a rapid increase in the population of the m_j states which can be explained as temperature dependence of χT. Also, the magnetic susceptibility calculated for B = 5.0 T have shown no change (as can be seen in Figure 6.1.21). The Zeeman diagram (as seen in Figure 6.1.22) is plotted for lowest four states or lowest two non-Kramer's doublets with magnetic field B = 2.0, 4.0. 6.0,8.0 and 10.0 T in x, y and z direction and it can be observed that center 1 and center 2 have easy axis in magnetic field applied

in y direction whereas center 3 has easy axis when magnetic field applied in x direction, however, magnetic field applied in z direction do not witness much change in energy

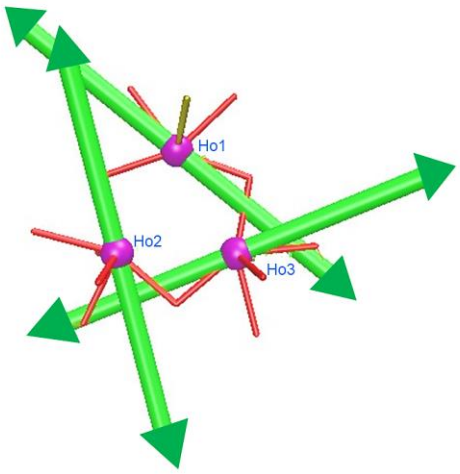

Figure 6.1 20: Direction of g_z-tensors of the ground pseudo doublet state of three Ho(III) centers for **structure 1**: (color scheme purple, Ho; red, O; yellow, Cl; all hydrogen and carbon and bridge O atom is removed for clarity

Table 6.1 15 g tensors of the pseudo doublets and the ZFS parameters

		Lowest pseudo doublet		1st pseudo doublet		g-tensor	ZFS parmater
		E (cm^{-1})	g-fac	E (cm^{-1})	g-fac		
Center 1	x	0.000	0.00	54.85	0.00	1.24	D = 2.63
	y	5.12	0.00	62.24	0.00	1.24	E = 0.71
	z		17.06		14.77	1.24	E/D = 0.26
Center 2	x	0.000	0.00	125.95	0.00	1.24	D = -3.60
	y	0.97	0.00	144.16	0.00	1.24	E = 0.78
	z		18.03		10.69	1.24	E/D = -0.21
Center 3	x	0.00	0.00	80.18	0.00	1.24	D = -2.81
	y	13.47	0.00	93.90	0.00	1.24	E = 0.28
	z		17.38		14.46	1.24	E/D = -0.09

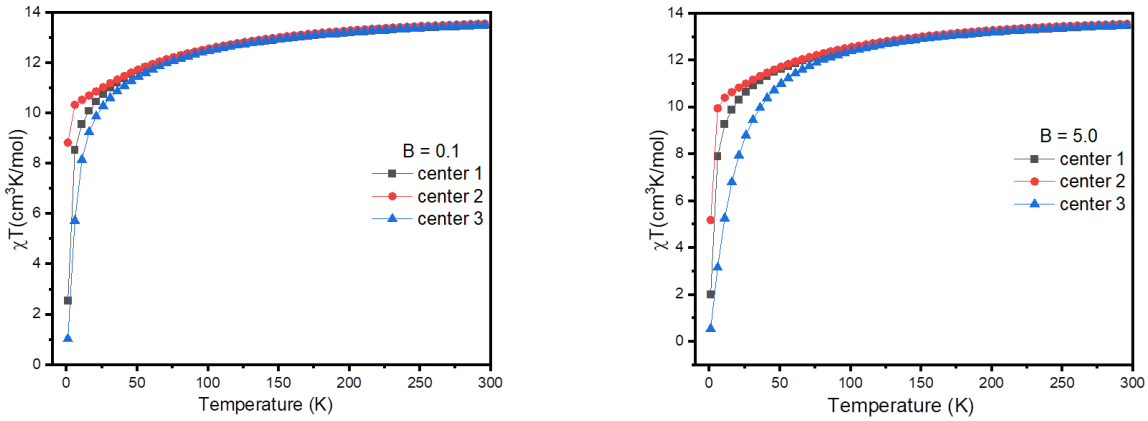

Figure 6.1 21: (a) Magnetic susceptibility of three Ho centers in Magnetic field B =0.1 T(b) Magnetic Susceptibility of three centers in Magnetic field B = 5.0 T in case of **structure 1**

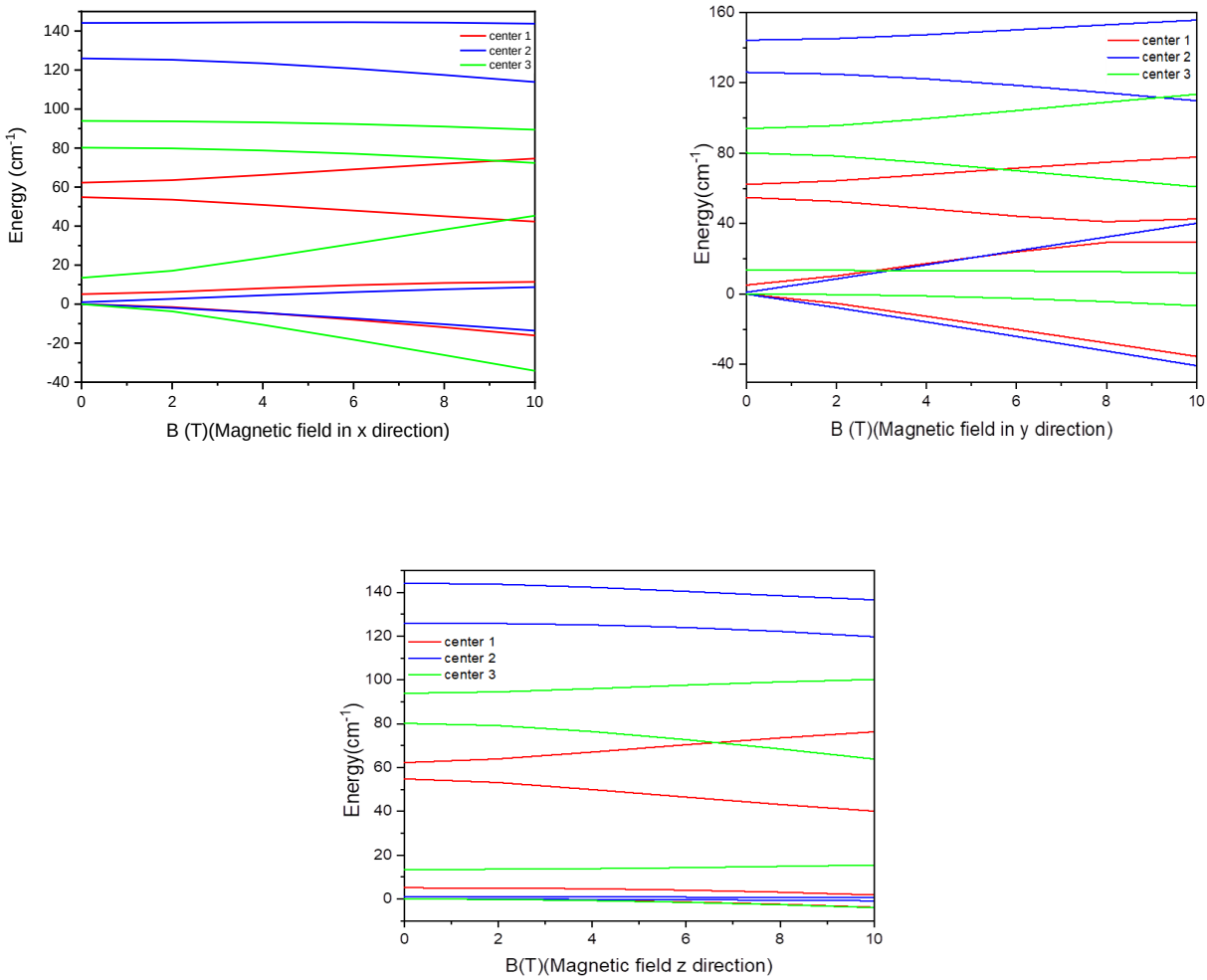

Figure 6.1 22: Zeeman plot of structure 1 including three lowest four states (a) magnetic field in x-direction (b) magnetic field in y-direction and (c) magnetic field in z-direction

6.1.4.2 Complex 2

In case of complex 2, active space is taken same as complex 1 ten electrons in 7 orbitals. After CASSCF calculations, next excited quintet state is 5 cm^{-1}, 41 cm^{-1}, 37 cm^{-1} higher in energy for center 1, center 2 and center 3, respectively. SOCI calculations gave 17 lowest states in the range of 260 cm^{-1} including few pseudo doublets and singlets for each center which belongs to ground multiplet and next excited multiplet is lying around 5100 cm^{-1} higher in energy for center 1 and center 2 whereas 5500 cm^{-1} for center 3. Results from ROHF calculations are in agreement with the SOCI calculations from CASSCF as can be seen in Table 6.1.16. In case of ROHF calculations also, next excited multiplet lies around 5100 cm^{-1} which is in agreement with the previously reported values.[142]

Table 6.1.16 Energies (cm^{-1}) of the 17 states of Ho(III) complexes obtained after Spin-Orbit coupling for **structure 2**

Structure 2					
center 1		center 2		center 3	
CASSCF	ROHF	CASSCF	ROHF	CASSCF	ROHF
0.000	0.00	0.000	0.00	0.00	0.00
0.70	0.70	4.94	5.04	4.91	4.38
32.61	31.67	40.74	38.97	31.37	45.45
35.73	34.80	50.77	48.42	39.56	55.86
59.60	58.66	55.00	53.12	44.41	58.15
62.41	61.41	73.86	71.66	73.10	86.99
82.48	80.91	81.21	78.88	80.39	93.03
104.91	103.38	96.85	94.21	95.67	114.23
125.50	123.92	118.19	115.79	108.92	123.08
162.20	160.44	153.62	151.21	134.71	160.35
182.90	181.15	169.62	167.30	157.49	177.83
190.68	188.92	183.92	181.10	165.17	195.81
205.72	203.77	208.79	205.47	177.14	205.43
214.47	212.09	229.05	225.61	190.92	222.54
219.91	217.47	246.72	242.81	197.26	228.80
234.28	231.74	256.199	251.99	211.44	247.75
235.51	233.11	261.84	257.64	216.00	249.91

The g-tensors were calculated for ground pseudo doublet for each center and it is found that g_z = 17.32, 17.07 and 17.26 which is typical for non-Kramer's ion to exhibit pure Ising nature. For each center, the magnetic main axes for the highest g-value, the g_z orientation for ground state, is plotted (as shown in Figure 6.1.23) and it is observed that the g_z-axes form a triangle giving toroidal moment which helps in maximal magnetization as discussed in the sections above. For center 1 and center 2, the E/D ratio is in a good range whereas for center 3 contribution of E is substantial. The calculated magnetic susceptibility (χT) at B = 0.1 T remains almost constant 13.80 cm^3K/mol at room temperature but decreases very fast at low temperature shown in Figure 6.1.24. Even at high magnetic field B= 5.0 T, χT remains 13.80 cm^3K/mol at room temperature and there is a sharp decrease at low temperature. The energies of the lowest four states are plotted with respect to the magnetic field and it is observed that center 1 shows a large energy difference when the magnetic field is applied in x direction and center 3 shows a large energy difference when applied in y direction (as shown in Figure 6.1.25). Also mixing of states is observed in center 1 and center 3.

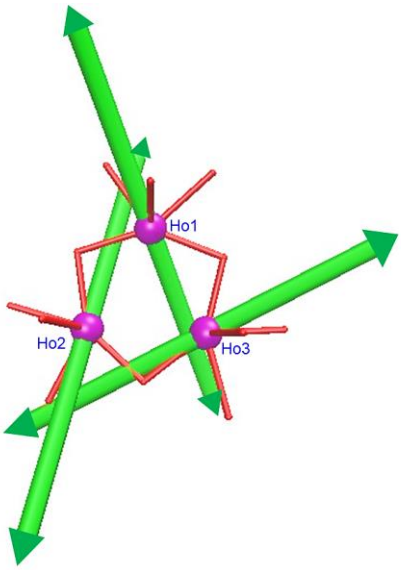

Figure 6.1 23: Direction of g_z-tensors of the ground pseudo doublet state of three Ho(III) centers for **structure 2**: (color scheme purple, Ho; red, O; yellow, Cl; all hydrogen and carbon and bridge O atom is removed for clarity

Table 6.1.17 g tensors of the pseudo doublets and the ZFS parameters for **structure 2**

		Lowest pseudo doublet		1st pseudo doublet		g-tensor	ZFS parameter
		E (cm^{-1})	g-fac	E (cm^{-1})	g-fac		
Center 1	x	0.00	0.00	32.61	0.00	1.24	D = -1.018
	y	0.70	0.00	35.73	0.00	1.24	E = 0.06
	z		17.32		16.91	1.24	E/D = -0.05
Center 2	x	0.00	0.00	40.74	0.00	1.24	D = -1.32
	y	4.94	0.00	50.77	0.00	1.24	E = 0.10
	z		17.07		12.24	1.24	E/D = -0.08
Center 3	x	0.00	0.00	31.37	0.00	1.24	D = -0.85
	y	4.91	0.00	39.56	0.00	1.24	E = 0.19
	z		17.26		11.66	1.24	E/D = -0.23

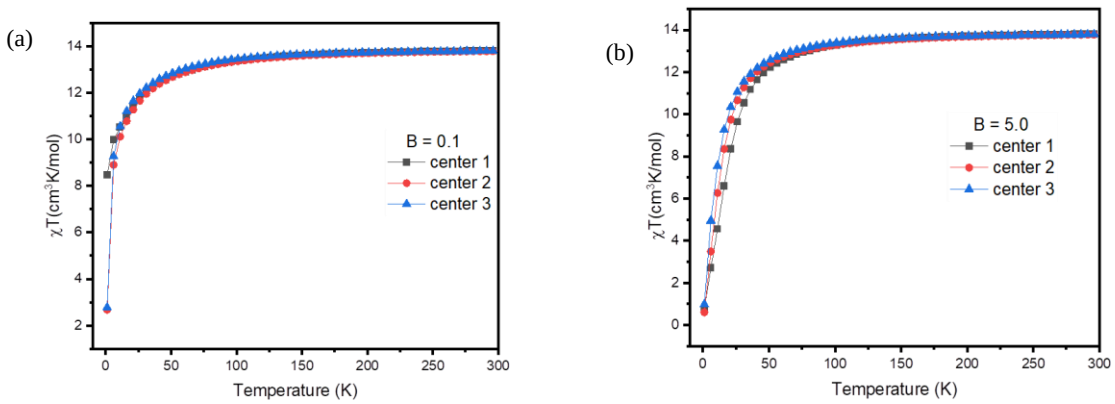

Figure 6.1 24: (a) Magnetic susceptibility of three Ho centers in Magnetic field B =0.1 T(b) Magnetic Susceptibility of three centers in Magnetic field B = 5.0 T in case of **structure 2**

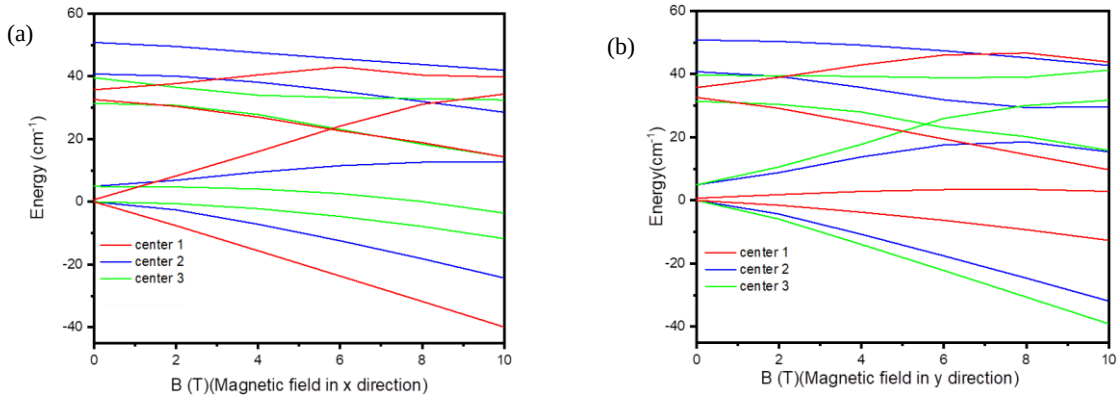

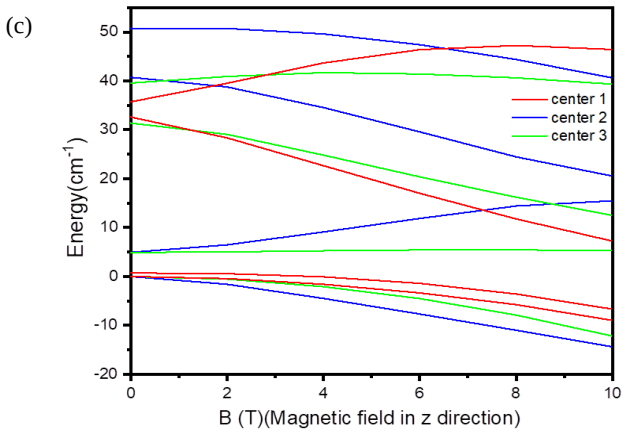

Figure 6.1 25: Zeeman plot of structure 2 including lowest four states (a) magnetic field in x-direction (b) magnetic field in y-direction and (c) magnetic field in z-direction

6.1.5 Tb(III)

Tb (III) is the ion which occurs naturally as one stable isotope which makes it a desirable choice for qubits.[143] Tb(III) ions also possess high anisotropic oblate electronic charge distribution and that's why it is expected to give higher anisotropy.[143] Tb(III) has a $4f^8$ valence configuration which results in 7 septets, 140 quintets and 195 triplets.[144] The ground state for the Tb(III) ion is $^7F_6$.

6.1.5.1 Complex 1

In complex 1, for CASSCF calculations, next excited state lies at 102 cm^{-1}, 86 cm^{-1} and 18cm^{-1} for center 1, center 2 and center 3, respectively. After CASSCF calculations, SOCI calculations were observed and as expected from Tb(III) ion $^7F_6$ is ground multiplet term which resulted in thirteen lowest energy states including pseudo-doublets and singlets in the range of 800 cm^{-1}. The next excited multiplet which belongs to $^7F_5$ is 2065 cm^{-1}, 2370 cm^{-1} and 2100 cm^{-1} higher in energy for center 1, center 2 and center 3 respectively which agree well with the reported values.[142,145] The energy spectrum of the lowest thirteen states obtained by ROHF calculation however is lower in energy than CASSCF method as can be seen in Table 6.1.18. While, the next excited state is around 2100 cm^{-1} higher in energy just like CASSCF results.

Table 6.1 18 Energies (cm^{-1}) of the 13 states of Tb(III) complexes obtained after Spin-Orbit coupling for **structure 1**

Structure 1					
center 1		center 2		center 3	
CASSCF	ROHF	CASSCF	ROHF	CASSCF	ROHF
0.00	0.00	0.000	0.00	0.00	0.00
1.38	0.56	0.26	0.06	1.69	0.40
92.15	44.86	132.73	81.67	117.25	83.56
101.42	48.47	133.69	82.21	128.76	87.47
197.13	104.27	213.12	131.45	233.85	145.89
227.53	121.63	216.40	134.69	267.66	155.54
280.83	147.56	319.06	184.31	363.19	216.14
331.03	189.12	332.51	204.89	413.07	235.77
354.73	195.37	408.09	233.57	444.27	257.30
458.30	260.33	514.53	315.08	499.49	292.64
466.14	262.37	541.49	322.45	522.79	298.22
676.89	390.72	784.42	466.55	694.73	390.90
677.79	390.779	788.19	467.31	698.73	391.72

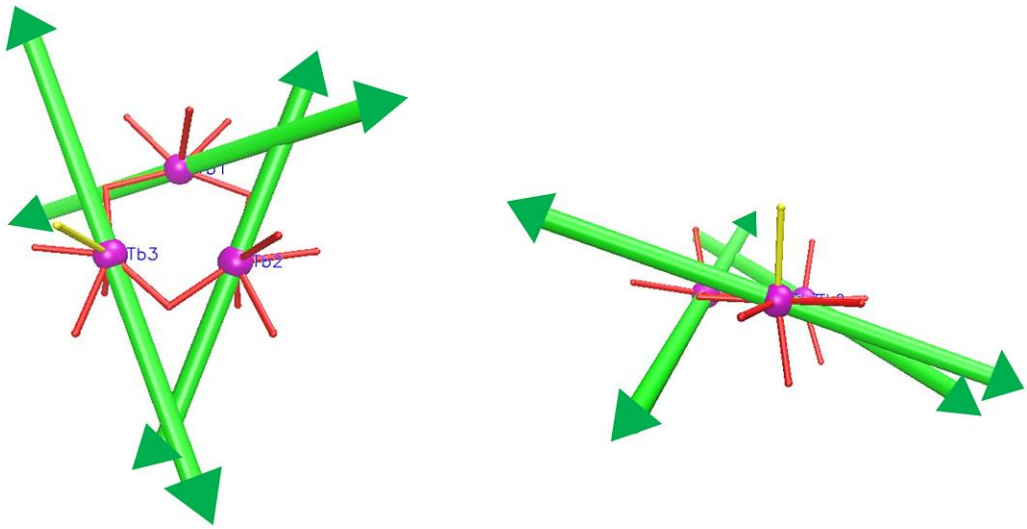

Figure 6.1 26: Direction of g_z-tensors of the ground pseudo doublet state of three Tb(III) centers for **structure 1**

The g-tensors were analyzed for ground non-Kramer's doublets and it exhibits pure Ising nature by giving g_z value of 17.07, 17.53 and 17.28 for center 1, center 2 and center 3 which is expected from Tb(III) ions. Then, calculated g_z tensors were used to determine the orientation of main magnetic axis which looks like toroidal manner which is expected from Tb(III) ion being oblate in nature. The calculated magnetic susceptibility (χT) for B = 0.1 T is 11.47 cm^3K/mol at 300 K which gradually decreases at low temperature as shown in Figure 6.1.27. The energies of the lowest four states with magnetic field as a function shows that that center 2 in y direction and center 3 in x direction has easy axis while center 1 has same response in each direction as shown in Figure 6.1.28

Table 6.1.19 g tensors of the pseudo doublets and the ZFS parameters for **structure 1**

		Lowest pseudo doublet		1st pseudo doublet		g-tensor	ZFS parmater
		E (cm^{-1})	g-fac	E (cm^{-1})	g-fac		
Center 1	x	0.00	0.00	92.15	0.00	1.48	D = 11.77
	y	1.38	0.00	101.42	0.00	1.48	E = 3.60
	z		17.07		16.91	1.49	E/D = 0.30
Center 2	x	0.00	0.00	132.73	0.00	1.48	D = -16.14
	y	0.26	0.00	133.69	0.00	1.49	E = 2.45
	z		17.53		16.30	1.47	E/D = -0.15
Center 3	x	0.00	0.00	117.25	0.00	1.48	D = -13.75
	y	1.69	0.00	128.76	0.00	1.49	E = 0.71
	z		17.28		14.96	1.47	E/D = -0.05

(a)

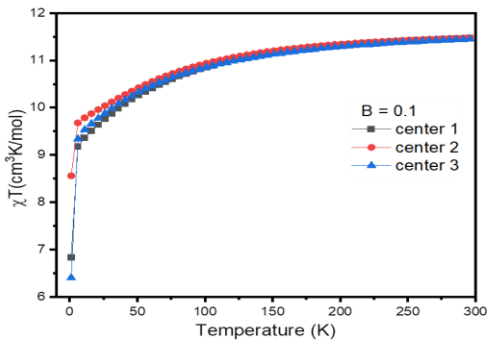

(b)

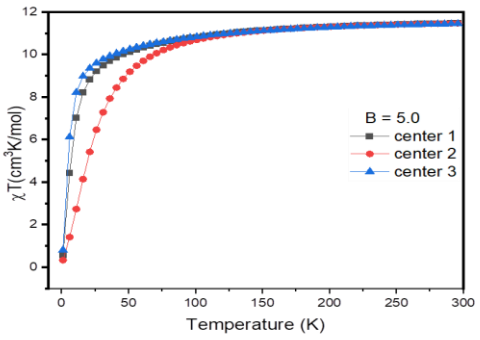

Figure 6.1 27: (a) Magnetic susceptibility of three Ho centers in Magnetic field B =0.1 T (b) Magnetic Susceptibility of three centers in Magnetic field B = 5.0 T in case of structure 1

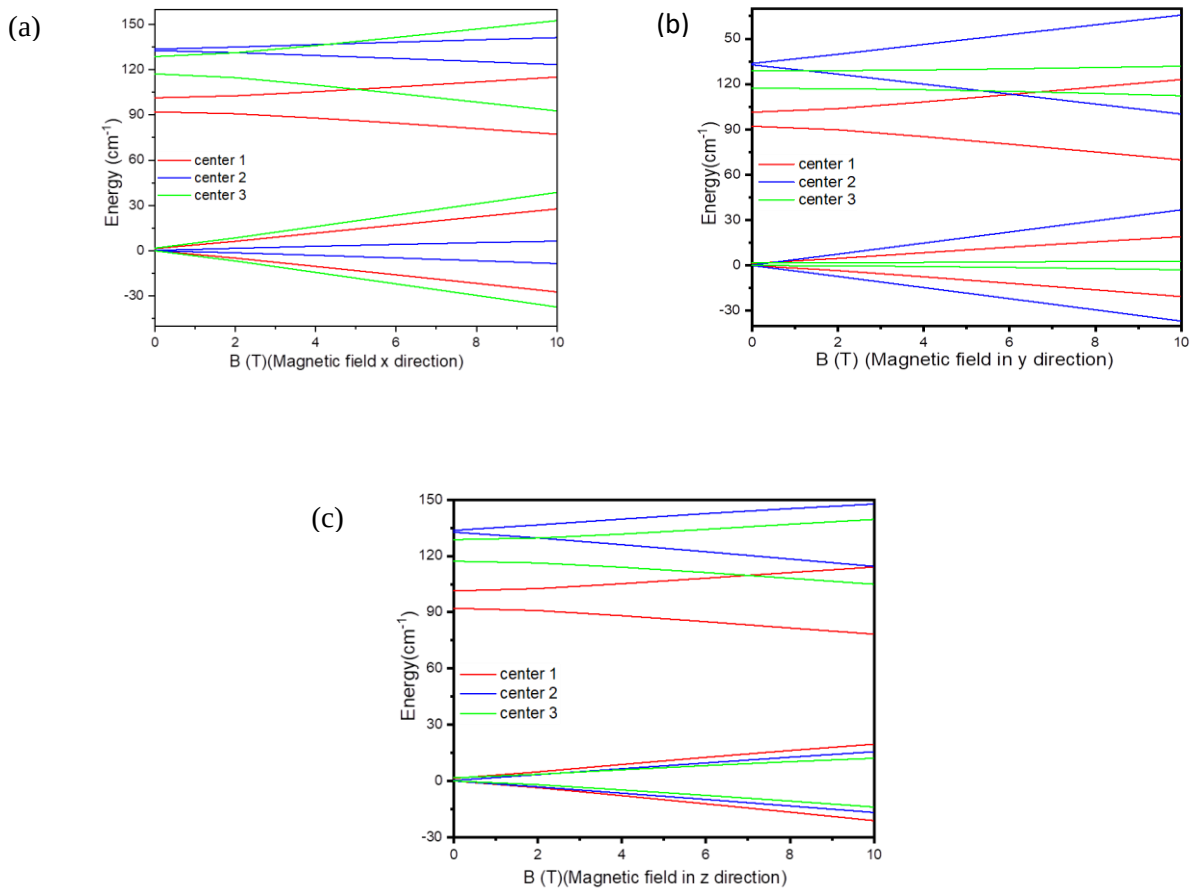

Figure 6.1 28: Zeeman plot of structure 1 including lowest four states (a) magnetic field in x-direction (b) magnetic field in y-direction and (c) magnetic field in z-direction

6.1.5.2 Complex 2

In case of complex 2, For CASSCF calculations, next excited state lies at 72 cm^{-1}, 83 cm^{-1} and 67 cm^{-1} for center 1, center 2 and center 3, respectively. After CASSCF calculations, SOCI calculations were performed and ground multiplet resulted in thirteen lowest energy states including pseudo-doublets and singlets in the range of 500 cm^{-1} which is lower than complex 1. The next excited multiplet is over 2000 cm^{-1} higher in energy for each center which agrees well with the reported values.[144,145] Energy spectrum of lowest thirteen states obtained by ROHF calculation however is lower in energy than CASSCF method as can be seen in Table 6.1.20. The next excited state is around 2100 cm^{-1} higher in energy for center 1 and 3 but for center energy difference increases 4000 cm^{-1}. The g-tensors were analyzed for ground non-Kramer's doublets just like complex 1 and g_z values are 16.33, 16.35 and 17.02 for center 1,

center 2 and center 3, respectively. Then, calculated g_z tensors were used to determine the orientation of main magnetic axis as shown in

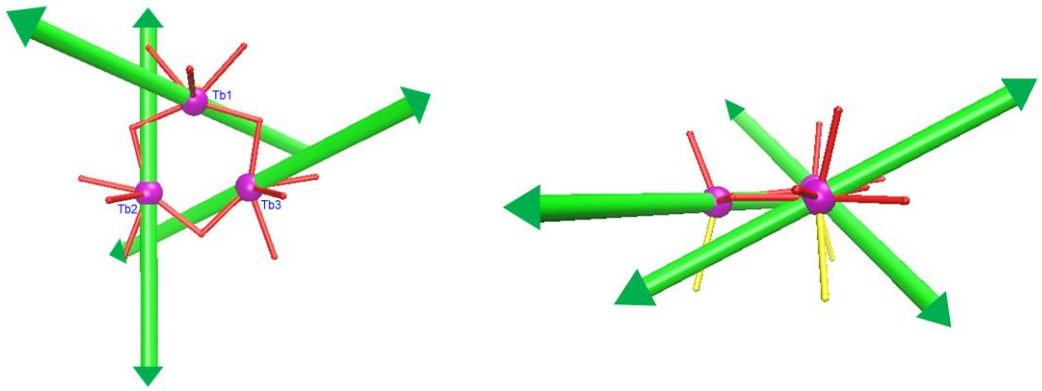

Figure 6.1 29: Direction of g_z-tensors of the ground pseudo doublet state of three Tb(III) centers for **structure 2**

Figure 6.1.29 for each center is in toroidal manner. The calculated magnetic susceptibility (χT) for B = 0.1 T is 11.50, 11.69, 11.72 cm^3K/mol at 300 K for center 1, center 2 and center 3 respectively, which gradually decreases at low temperature as shown in Figure 6.1.30. The energies of the lowest four states with respect to the magnetic field shows that that center 1 exhibits large energy difference in x direction while center 2 in both x, y direction and center in 3 in y and z direction shown in Figure 6.1.31. Mixing of excited states is also observed at high magnetic field for center 2 and center 3.

Table 6.1. 20 Energies (cm^{-1}) of the 13 states of Tb(III) complexes obtained after Spin-Orbit coupling for **structure 2**

Structure 2					
center 1		center 2		center 3	
CASSCF	ROHF	CASSCF	ROHF	CASSCF	ROHF
0.00	0.00	0.00	0.00	0.00	0.00
0.66	1.54	1.22	1.20	0.26	0.28
50.91	33.26	30.71	31.03	65.19	64.88
55.90	41.58	34.22	34.52	73.81	73.63
93.68	56.15	101.01	101.38	96.97	96.52
120.31	64.96	108.68	109.05	117.47	117.20

145.45	92.39	151.44	152.11	120.76	120.42
272.27	140.38	178.49	179.08	161.89	161.53
297.52	156.38	200.37	201.01	168.42	168.07
390.18	216.28	215.05	215.90	226.74	226.40
402.07	222.75	227.26	228.00	228.88	228.52
507.09	245.17	299.01	300.02	345.45	345.19
507.66	247.26	300.28	301.29	345.51	345.25

Table 6.1.21 g tensors of the pseudo doublets and the ZFS parameters for **structure 2**

		Lowest pseudo doublet		1st pseudo doublet		g-tensor	ZFS parameter
		E (cm^{-1})	g-fac	E (cm^{-1})	g-fac		
Center 1	x	0.00	0.00	50.91	0.00	1.48	D = 4.74
	y	0.66	0.00	55.90	0.00	1.48	E = 1.56
	z		16.33		15.55	1.48	E/D = 0.32
Center 2	x	0.00	0.00	30.71	0.00	1.49	D = -5.97
	y	1.22	0.00	34.22	0.00	1.49	E = 0.48
	z		16.35		13.63	1.48	E/D = -0.08
Center 3	x	0.00	0.00	65.19	0.00	1.48	D = 6.07
	y	0.26	0.00	73.81	0.00	1.49	E = 1.48
	z		17.02		11.73	1.49	E/D = 0.24

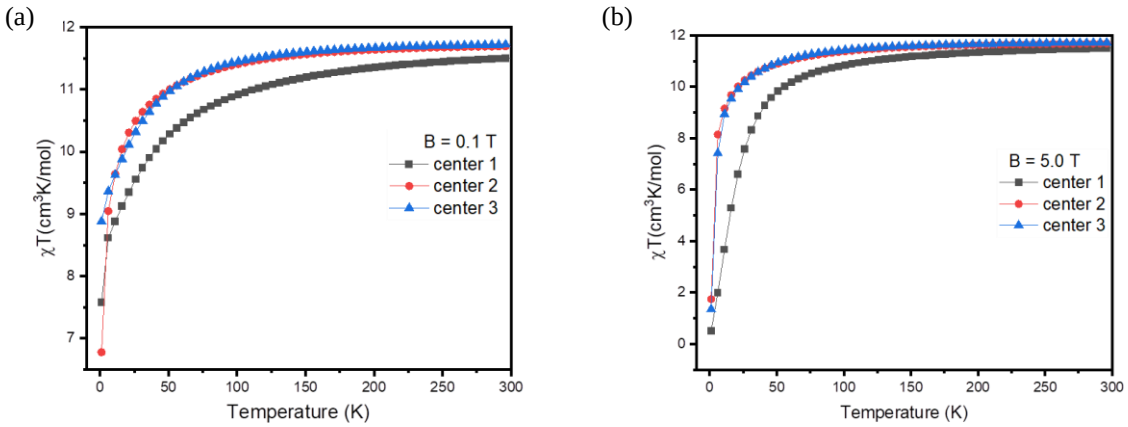

Figure 6.1 30: (a) Magnetic susceptibility of three Ho centers in Magnetic field B = 0.1 T(b) Magnetic Susceptibility of three centers in Magnetic field B = 5.0 T in case of **structure 2**

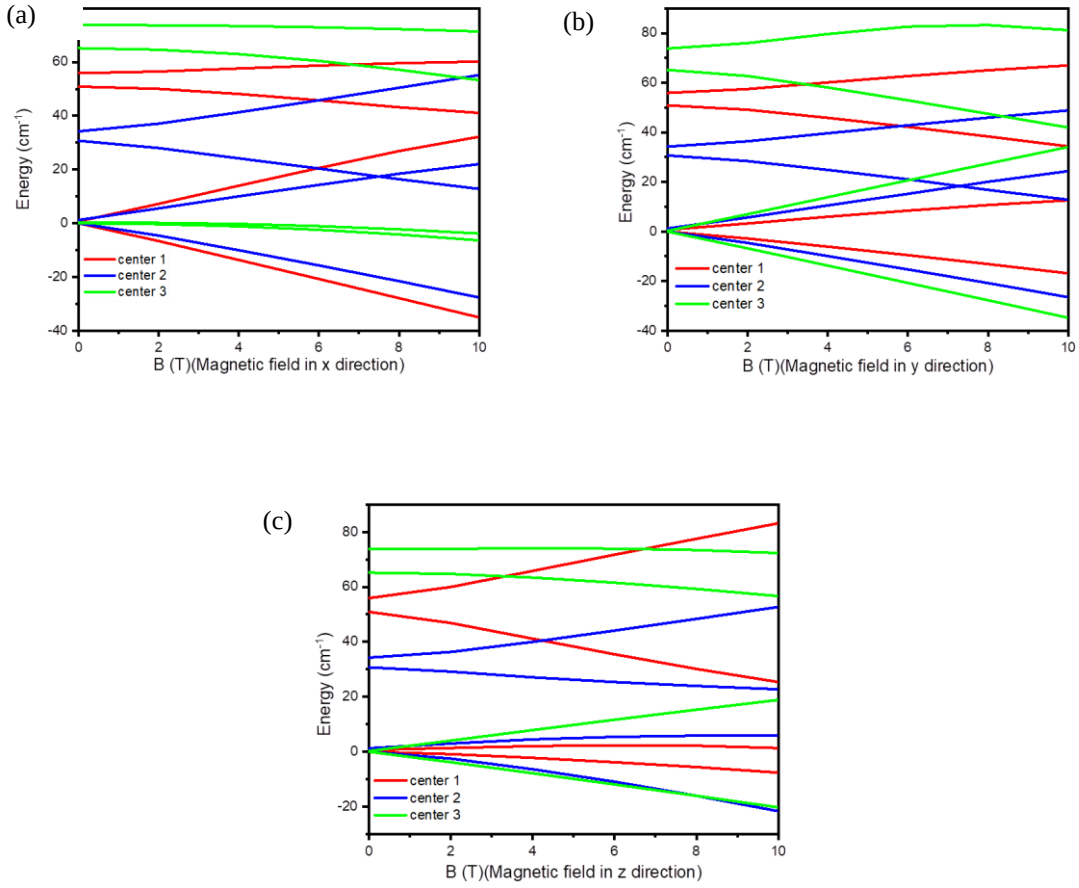

Figure 6.1 31: Zeeman plot of structure 2 including lowest four states (a) magnetic field in x-direction (b) magnetic field in y-direction and (c) magnetic field in z-direction

6.2 Poly-nuclear- Ln(III)-Ln(III)

6.2.1 Gd(III)-Gd(III)

In this case study, two lanthanides are studied together. For the calculation purposes, one Ln(III) ion is replaced with an Y(III) ion to make a given complex binuclear and each as seen in Figure 6.2.1. Computational details are the same as mentioned in the section above. For Gd(III)-Gd(III) complex, the ground state spin this case is derived from $S_{Gd1} = 7/2$ and $S_{Gd2} = 7/2$ which results in total spin S = 7.

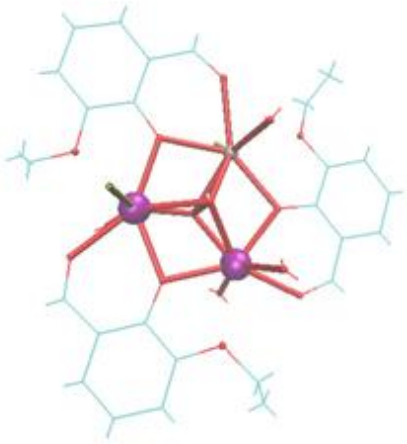

Figure 6.2 1: Ln(III)-Ln(III) complex

Ground multiplet state for each Gd(III) center gives four Kramer's doublets i.e 8 states states resulted in 64 states, SOCI calculations were performed to calculate lowest four state or pseudo quartet state shown in Table 6.2.1. Energies of the obtained four states shows that two Gd(III) centers are in the range of 1.50 cm^{-1}. g-tensors were calculated for first including all four states and it exhibits transverse anisotropic behavior with $g_x = 3.42$, $g_y = 0.26$ and $g_z = 7.31$. The calculated magnetic susceptibility (χT) for the system is 10.19 cm^3K/mol at room temperature which is lower to the theoretically expected values based on two non-interacting Gd(III) centers[146,147] and as it gradually reaches to the low temperature, 30 K , χT value sharply decreases to 5.31 cm^3K/mol as can be seen in Figure 6.2.2.

Table 6.2 1: Energies (cm^{-1}) of the four states obtained after Spin-Orbit coupling of Gd(III)-Gd(III) and main magnetic axes (g-tensor) and ZFS parameter

Energy (cm^{-1})	ZFS Parameter	Main magnetic axes	
0.00	D =0.59	x	3.42
0.06	E = 0.06	y	0.26
1.30	E/D = 0.11	z	7.31
1.45			

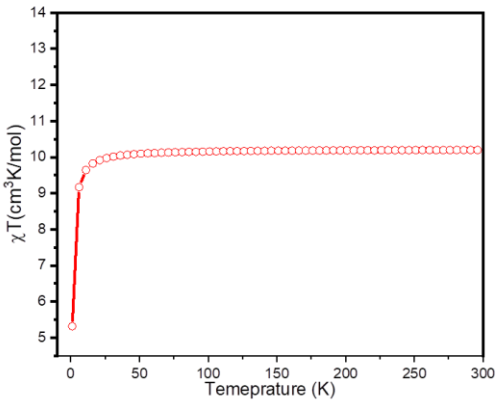

Figure 6.2 2 : Magnetic susceptibility of Gd(III)-Gd(III) with B = 0.1 T

6.2.2 Dy(III)-Dy(III)

In this case study, two lanthanides are studied together. As in the above case we found that ROHF method is in agreement with the CASSCF method and previously reported values. With Dy(III)-Dy(III) calculations, main issue with CASSCF is large number of state. So ROHF approach is used instead. For the calculation purposes, one Ln(III) ion are replaced with Y(III) ions to make a given complex binuclear and each as seen in Figure 5.2.1. Ground state spin in this case is derived from S_{Dy1} = 5/2 and S_{Dy2} = 5/2 which results in total spin S = 10.

Ground multiplet state for each Dy(III) center gives eight Kramer's doublets i.e. 16 states resulted in 256 states (16 x16) which is a large number of states and unfortunately, it's not possible to calculate these much states and hence Subciexpert program is used in SOCI calculations to calculate only lowest KD doublet from each Dy center which resulted in lowest four state or two non-Kramer's doublets shown in Table 6.2.2. Energies of the obtained four states shows that two Dy(III) centers are non-interacting as energy spectrum is less than 0.3 cm^{-1}. The g-tensors were calculated for first including all four states and it exhibits transverse anisotropic behavior with g_x = 5.22, g_y = 0.71 and g_z = 10.44. G_z –tensors were also calculated for pseudo doublets and it is observed that first pseudo doublet has highly axial g_z value of 30.80. The calculated magnetic susceptibility (χT) for the system is 21.40 cm^3K/mol at room temperature which is near to the theoretically expected values based on two non-interacting Dy(III) centers [146,148] but as the at low temperature, 30 K , χT value increases to 22.2 cm^3K/mol as can be seen in Figure 6.2.3.

Table 6.2 2: Energies (cm^{-1}) of the four states obtained after Spin-Orbit coupling of Dy(III)-Dy(III) and main magnetic axes (g-tensor) and ZFS parameter

Energy (cm^{-1})	ZFS Paremeter	Main magnetic axes	
0.00	D = -0.073	x	5.22
0.04	E = 0.0008	y	0.71
0.17	E/D = -0.011	z	10.44
0.204			

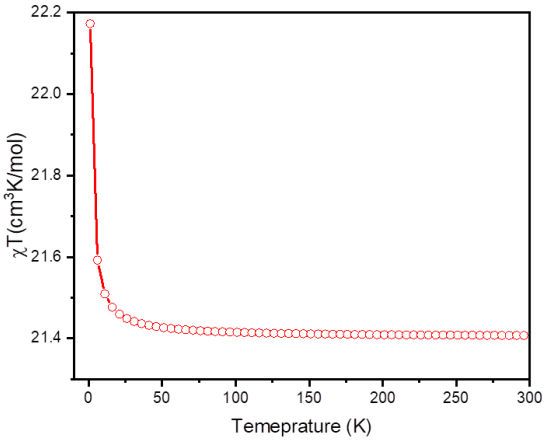

Figure 6.2 3 : Magnetic susceptibility of Dy(III)-Dy(III) with B = 0.1 T

6.2.3 Er(III)-Er(III)

In the dinuclear Er(III)-Er(III) complex, Ground state spin in this case is derived from S_{Er1} = 3/2 and S_{Er2} = 3/2 which results in total spin S = 7. The ground state multiplet for each Er(III) center gives eight Kramer's doublets i.e 16 states resulted in 256 states (16 x 16) which is large number of states. As in the case of Dy, it is not possible to calculate so many states at the same time, hence only the lowest states obtained in the SUBCI were used in the SOCI calculations. Only the lowest KD doublet from each Er center was included which resulted in the lowest four states shown in Table 6.2.3. Energies of the obtained four states shows that the two Er(III) centers are non-interacting as the energy spectrum is in the range of 0.02 cm^{-1}. The g-tensors were calculated for first including all four states and it exhibits transverse anisotropic behavior with g_x = 2.07, g_y = 1.73 and g_z = 9.00. The calculated magnetic susceptibility (χT) for the system is 13.86 cm^3K/mol at room temperature which is lower than the

theoretically expected values based on two non-interacting Er(III) centers[146] and at low temperature, χT value decreases to 12.99 cm^3K/mol as can be seen in Figure 6.2.4

Table 6.2 3 : Energies (cm^{-1}) of the four states obtained after Spin-Orbit coupling of Er(III)-Er(III) and main magnetic axes (g-tensor) and ZFS parameter

Energy (cm^{-1})	ZFS Paremeter	Main magnetic axes	
0.00	D =0.004	x	2.07
0.005	E = 0.0007	y	1.73
0.018	E/D = 0.18	z	9.00
0.021			

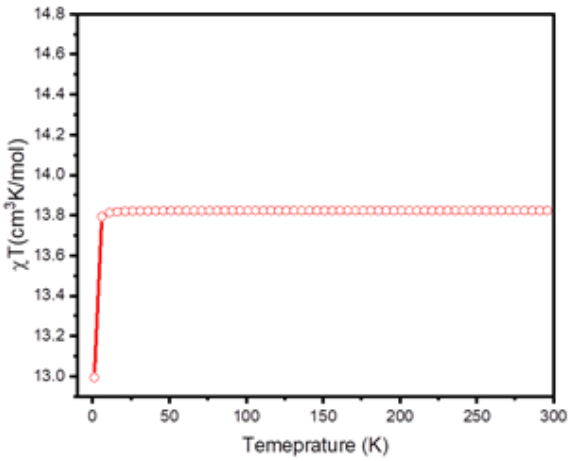

Figure 6.2 4 : Magnetic susceptibility of Er(III)-Er(III) with B = 0.1 T

6.2.4 Dy(III)-Tb(III)

In this case, we studied a hetero-nuclear complex with Dy(III) at one center and Tb(III) at second center. This combination is preferred because of the low number of states. Here, CASSCF calculations were employed with 11 states of Dy(III) that belonged to ground state ^6H and 7 states of Tb(III) that belonged to ^7F resulted in 77 state which manageable by the CASSCF approach. With a total spin of Dy(III) S= 5/2 and Tb(III) S=3 the total spin of the complex is S = 11/2. After the CASSCF calculation, the next

excited state is 28 cm^{-1} higher in energy compared to the ground state. SOCI calculations resulted in pseudo-quartet states. The magnetic susceptibility (χT) for the system is 21.40 cm^3K/mol at room temperature which is lower than the theoretically expected values based on two non-interacting Dy(III) centers[146] and at low temperature, χT value decreases to 17.67 cm^3K/mol as can be seen in Figure 6.2.5

Table 6.2 4 : Energies (cm^{-1}) of the four states obtained after Spin-Orbit coupling of Dy(III)-Tb(III) and main magnetic axes (g-tensor) and ZFS parameter

Energy (cm^{-1})	ZFS Paremeter	Main magnetic axes	
0.00	D =-0.32	x	6.41
	E = 0.07	y	9.79
0.70	E/D = -0.23	z	0.04

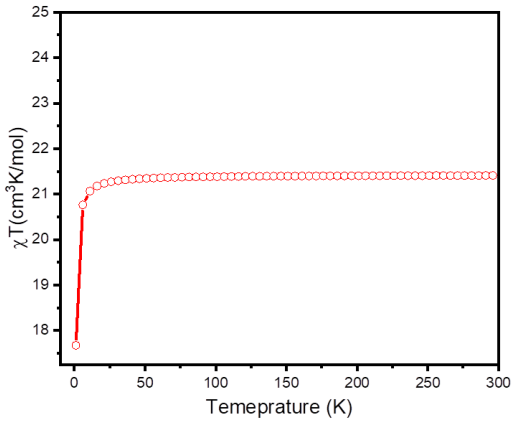

Figure 6.2 5: Magnetic susceptibility of Dy(III)-Tb(III) with B = 0.1 T

6.3 $GdBr_3$-Complex

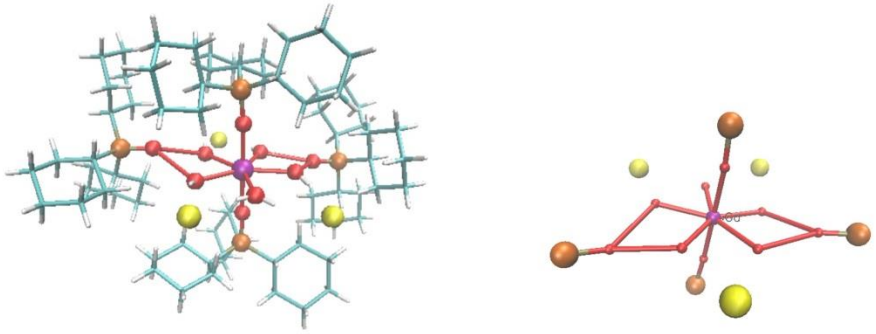

Figure 6.3 1: Structure of Gd(III) complex (purple– Gd(III) ion; red – Oxygen, yellow - Bromide)

The complex shown above in Figure 6.3.1 has a Gd(III) ion in the center. The Gd(III) ion is coordinated by six oxygen atoms of the ligands and one water molecule. All the bond distances of Gd-O are the range of 2.18 – 2.36Å. For all calculations, density functional theory (DFT) is used using TURBOMOLE[94] package. BP86 functional and the x2c-TZVPall basis set[118] for Gd, and def-SV(P) basis set for rest of the atoms were applied. Bond distances of Gd-O were calculated which agrees with the reported literature.[117,119,147] The optimized structures were used for the (CASSCF) calculations and spin orbit coupling calculations. The fourth order Douglas-Kroll-Hess hamiltonian was included, where scalar relativistic contributions were taken into account. Furthermore, spin orbit coupling is calculated based on ROHF orbitals and all the calculations are compared.

As discussed in sections 6.1.1, the Gd(III) ion is f^7 i.e. it has exactly half filled f orbitals. In CASSCF calculations, active space is considered to be CAS(7,7) i.e. 7 electrons in 7 orbitals which resulted in spin S= $^7/_2$. The f^7 system has ^8S as a ground state same as explained in above sections. The orbitals were obtained for the octet ground state.The lowest 4 Kramers doublets obtained in the SOCI are shown in table 1. The g-tensors were calculated (as shown in Table 6.3.1). For the ground state, g is rather isotropic in the order of 1.99 and the magnetic susceptibilities χT increases to 7.48 $cm^3K\ mol^{-1}$

Table 6.3 1 : Energies (cm^{-1}) of the lowest four Kramer's doublets of Gd(III) complexes obtained after Spin-Orbit coupling

	Spin-orbit states (cm-1)	
	CASSCF	ROHF
KD1	0.00	0.00
KD2	0.32	0.30
KD3	0.58	0.56
KD4	0.96	0.97

KD	1	2	3	4	Main magnetic axes(g-tensors)	
Energy	0.00	0.87	1.45	2.07		
x	0.07	1.84	5.20	0.07	1.99	D = -0.15
y	0.05	1.50	3.98	0.05	1.99	E = 0.03
z	13.88	9.37	6.88	13.88	1.99	E/D = -0.22

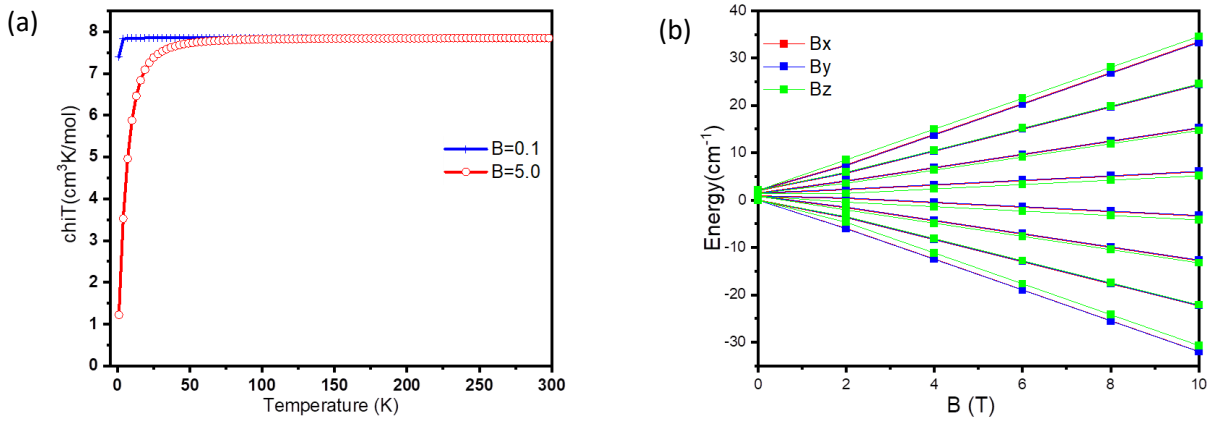

Figure 6.3 2 : (a) Magnetic susceptibilities calculated for lowest quartet state with B = 0.1; (b) 5.0 T and Energies of the Kramer's doublet in a magnetic field

6.4 Gd(III) Complex 2

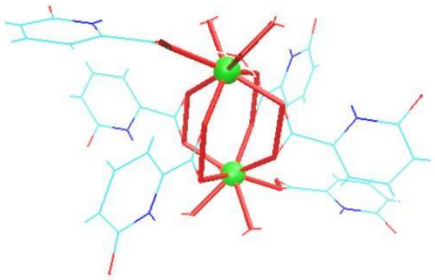

Figure 6.4 1: (a) Structure of Gd(III) complex (green – Gd(III) ions; red – Oxygen)

In this case study, we have a complex with two Gd(III)-Gd(III) centers, each center is coordinated with eight oxygen atoms. The bond distance of Gd-O in the complex is in the range of 2.30-2.40 Å.[146] As before, one center is replaced with a diamagnetic Y(III) to make the other a mononuclear center and each center is calculated one at a time. Computational details are the same as mentioned for the Gd - complex in section 6.3. As mentioned above the ground state for Gd(III) is ^{8}S . Four Kramer's doublets are in the range of 1 cm^{-1} for both CASSCF calculations and ROHF calculation as shown in Table 6.4.1. g-tensors including all eight states are calculated and it is found highly isotropic in order of 1.99 which agrees well with the expected value. The g-tensor including all eight states is calculated and it is found to be highly isotropic in order of 1.99. The simulated Magnetic susceptibility (χT) at B= 0.1 T is 7.84 $cm^{3}K/mol$ (as seen in Figure 6.4.2) for both centers which remains constant at room temperature but suddenly decreases at low temperature. The energies of 4 KD s with respect to the magnetic field B =10 T shows that at high magnetic field, splitting of four KDs is around 30 cm^{-1}.

Table 6.4 1: Energies (cm^{-1}) of the lowest four Kramer's doublets of Gd(III) complex obtained after Spin-Orbit coupling.

Spin orbit states				
	center a		center b	
	CASSCF	ROHF	CASSCF	ROHF
KD1	0.00	0.00	0.00	0.00
KD2	0.32	0.31	0.30	0.23
KD3	0.58	0.51	0.55	0.42
KD4	0.96	0.78	0.91	0.72

		KD1	KD2	KD3	KD4	ZFS parameter
Center 1	x	0.55	4.74	2.55	1.21	D = 0.06
	y	0.35	3.53	2.01	0.09	E = 0.01
	z	13.60	7.54	9.03	13.83	
Center 2	x	0.55	4.70	2.56	0.12	D = 0.06
	y	0.35	3.53	2.02	0.09	E = 0.07
	z	13.60	7.55	9.03	13.83	

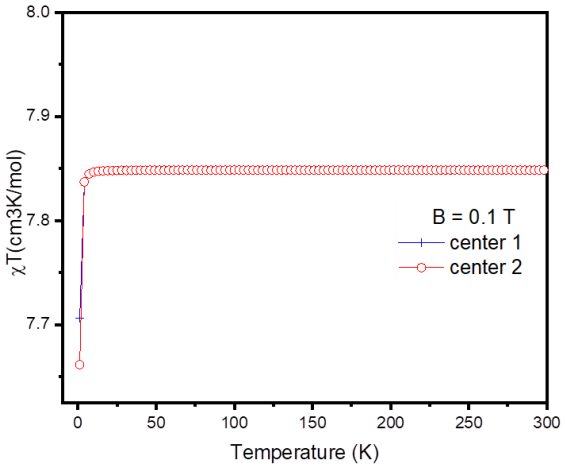

Figure 6.4 2: Magnetic susceptibility of Gd centers in a magnetic field B =0.1 T

6.5 Conclusions

In summary, ab initio calculations were performed on a series of lanthanide complexes with different ligands for a better understanding of the underlying physics responsible for magnetic properties and to shed light on the SMM behavior. For all the systems, along with the spin orbit configuration interaction calculations (SOCI) based on orbitals from complete active space self-consistent field calculations, new ROHF method developed in Kaiserslautern was also tested and the results were compared for all the centers. In the SOCI Slater determinants belonging only to the lowest ground state in an active space of the 4f-orbitals are considered to obtain the low lying electronic states, their zero-field splittings, g-tensors and magnetic susceptibilities.

Among the complexes studied, the ground state Kramers Doublet of, Ho(III) and Tb(III) is Ising in nature. For Dy(III) and Er(III), the ground state KD is axially anisotropic but excited state KDs shows a transverse anisotropy. In case of complexes with Dy(III) and Er(III), mirror symmetry in the g tensors implies that direction of the anisotropy axes rotate when moving to higher doublets. Dy(III), Ho(III) and Tb(III) possess toroidal moment. The second order spin orbit coupling is observed in Gd(III) complexes as $L = 0$. Presence of ligand results in slight distortion in spherical symmetry of Gd(III) which give rise to very small D (axial parameter) The E/D ratio is in the range of 1/3 for each Ln(III) centers which is considered as a condition for SMM. Results obtained from two Ln(III) ions calculation show that there is negligible interaction between them. Magnetic susceptibilities obtained in the polynuclear cases are lower than the reported data.

SOCI-calculations based on ROHF and CASSCF orbitals, respectively, show differences in the relative energies of the lowest states. The origin of the differences should be further analyzed in the future.

7 Summary

The goal of the present thesis is to theoretically investigate the magnetic properties of $3d^n$ and $4f^n$ elements with different surrounding and geometries. Because of the complex electronic structures of the partly filled d- and f-shells and the importance of spin orbit coupling for the magnetic properties, CASSCF and CAS-SO-CI calculations were performed. In the Chapter 5, the results for Ni(II) and Co(II) based 3d compounds are shown. First, a Ni(II) with azopyridine ligand was studied not only as mononuclear complex but as well as directly related radical complex by hosting a radical electron on the azopyridine ligand and the parameter calculated with our calculation is in the agreement with the previously reported values. In this case, a positive axial zero field parameter D was found for the triplet ground state of $[\mathrm{Ni(II)L}]^{2+}$ which is in agreement with the magnetostructural correlation seen for similar Ni complexes. The Zeeman plots and magnetic susceptibilities (χT) are comparable with the experimentally obtained values and the anisotropy axis is found to be along the axial ligands. In case of $[\mathrm{Ni(II)L^{-}}]^{1+}$, the additional unpaired electron is coupled ferromagnetically to the Ni(II) spin. The calculated magnetic susceptibility shows a decrease at higher temperature because of the influence of the higher electronic states. Most of the calculated parameters are in agreement with the experimental values except for the sign of the D which is positive in case of the quantum chemical calculations while the experimental results obtained from EPR suggest a negative sign. In the related complex with three spin center, two Ni(II) centers with S=1 and one unpaired ligand electron both Ni(II) centers are coupled ferromagnetically to the ligand spin. D in this case is positive which suggest anisotropy axis lying axial. The magnetic susceptibility shows a dip at high temperature after higher states start to contribute.

Furthermore a series of Co(II) complexes with different ligands and geometries was investigated to see how the ligand field effects the magnetic properties of Co(II). All three complexes exhibit strong easy axial anisotropy with significant transversal contibution[149] One of the complexes has a distorted tetrahedral symmetry. For this complex, it is observed that the ground state quartet is well separated from the higher states. Therefore, second order spin –orbit coupling is observed and ground quartet state contributed with 94 % and 98 % to the lowest two Kramer' doublet in the CAS-SO-CI. D obtained in this case is negative which confirms the easy axis magnetic anisotropy and this also matches well with the experimental values. The other two Co(II) complexes have distorted octahedral geometry and both

complexes show that the axial bonds are shorter than the equatorial bonds (compressed octahedron). In this case, first order spin-orbit effects are observed and hence the first three quartet states exhibit contribution to the lowest KDs. In this case, the g values point towards an easy axis type of magnetic anisotropy. These calculations show that the above mentioned complexes have the potential to behave as SMMs.

In chapter 6, I investigated different complexes of 4f elements. First, the anisotropy axes of the 4f ions in two complexes with three Ln(III) ions in one plane but slightly different ligands were investigated. **Structure 1** (as shown in Figure 2a) is $Ln_3(L)_3(\mu 3\text{-}OH)_2(H_2O)_4Cl_2$ and **structure 2** (as shown in Figure (2b) is $Ln_3(L_3)(\mu 3\text{-}OH)_2(CH_3OH)(H_2O)_2Cl_3$ where L is 3-ethoxysalicylaldehyde. In the calculations, one center is Ln(III)- Gd, Dy, Er, Ho and Tb and the other two centers were replaced by Y(III) to analyze the properties of the individual centers in a mononuclear complex. In all these calculations, the orbitals were obtained by restricted open shell Hartree-Fock and compared to CASSCF calculations from literature[64,121,129,131,134]. The energies obtained from the less time consuming ROHF method are in the good agreement with the previously reported values. As expected, Dy(III) and Ho(III) exhibit toroidal moments which is caused by the oblate electron density. For Er(III), the toroidal magnetic moment was absent. The reason for this could be the prolate nature of the electron density in Er(III) with a different orientation of the g_{zz} axis with respect to the triangle compared to the Dy(III) ion. However, in case of the non-Kramer's ions Ho(III) and Tb(III), a few pseudo doublets and singlets were obtained and the ground pseudo-doublet shows pure Ising nature and gave axial g_z values.

After calculation for mononuclear case, only one Ln center is replaced with the diamagnetic Y(III) to make the complex dinuclear. Here, **structure 1** is studied with two Ln(III)-Ln(III) (Ln= Dy, Er, Gd,) together. ROHF was used to study Dy(III)-Dy(III) and Er(III)-Er(III). CASSCF is used to calculate Gd(III)-Gd(III) and Dy(III)-Tb(III) because here the number of states is manageable. The magnetic susceptibilities obtained here are a bit smaller than the expected values.

In summary, spin orbit CI calculations can contribute to the understanding of the magnetic properties of 3d and 4f complexes. The calculations allow for a systematic variation of the 3d or 4f elements, the combination of different spin centers, and the influence of ligand variations.

8 Bibliography

1. Bogani, L. & Wernsdorfer, W. Molecular spintronics using single-molecule magnets. *Nat. Mater.* **7**, 179–186 (2008).

2. Nisticò, R., Cesano, F. & Garello, F. Magnetic Materials and Systems: Domain Structure Visualization and Other Characterization Techniques for the Application in the Materials Science and Biomedicine. *Inorganics* **8**, 6 (2020).

3. Cosquer, G., Shen, Y., Almeida, M. & Yamashita, M. Conducting single-molecule magnet materials. *Dalt. Trans.* **47**, 7616–7627 (2018).

4. Alcácer, L., Novais, H., Pedroso, F., Coulon, C., Chasseau, D., Gaultier, J. Synthesis, structure and preliminary results on electrical and magnetic properties of $(Perylene)_2$ $[Pt(mnt)_2]$. *Solid State Commun.* **35**, 945–949 (1980).

5. Pereira, L. C. J., Gulamhussen, A. M., Dias, J. C., Santos, I. C. & Almeida, M. Searching for switchable molecular conductors: Salts of $[M(dcbdt)_2]$ (M=Ni, Au) anions with $[Fe(sal_2\text{-trien})]^+$ and $[Fe(phen)_3]^{2+}$. *Inorganica Chim. Acta* **360**, 3887–3895 (2007).

6. Takahashi, K. *et al.* Electrical Conductivity Modulation Coupled to a High-Spin−Low-Spin Conversion in the Molecular System $[Fe^{III}(qsal)_2][Ni(dmit)_2]_3CH_3CNH_2O$. *Inorg. Chem.* **45**, 5739–5741 (2006).

7. Dorbes, S., Valade, L., Real, J. A. & Faulmann, C. $[Fe(sal_2\text{-trien})][Ni(dmit)_2]$: towards switchable spin crossover molecular conductors. *Chem. Commun.* 69 (2005) doi:10.1039/b412182a.

8. Sessoli, R., Gatteschi, D., Caneschi, A. & Novak, M. A. Magnetic bistability in a metal-ion cluster. *Nature* **365**, 141–143 (1993).

9. Shao, D. & Wang, X. Y. Development of Single-Molecule Magnets. *Chinese J. Chem.* **38**, 1005–1018 (2020).

10. Concas, G., Congiu, F., Muscas, G. & Peddis, D. Determination of Blocking Temperature in Magnetization and Mössbauer Time Scale: A Functional Form Approach. *J. Phys. Chem. C* **121**, 16541–16548 (2017).

11. Maniaki, D., Pilichos, E. & Perlepes, S. P. Coordination Clusters of 3d-Metals That Behave as Single-Molecule Magnets (SMMs): Synthetic Routes and Strategies. *Front. Chem.* **6**, (2018).

12. Perlepe, P. S., Maniaki, D., Pilichos, E., Katsoulakou, E. & Perlepes, S. P. Smart Ligands for Efficient 3d-, 4d- and 5d-Metal Single-Molecule Magnets and Single-Ion Magnets. *Inorganics* **8**, 39 (2020).

13. McAdams, S. G., Ariciu, A.-M., Kostopoulos, A. K., Walsh, J. P. S. & Tuna, F. Molecular single-ion magnets based on lanthanides and actinides: Design considerations and new advances in the context of quantum technologies. *Coord. Chem. Rev.* **346**, 216–239 (2017).

14. Ungur, L., Le Roy, J. J., Korobkov, I., Murugesu, M. & Chibotaru, L. F. Fine-tuning the Local Symmetry to Attain Record Blocking Temperature and Magnetic Remanence in a Single-Ion Magnet. *Angew. Chemie Int. Ed.* **53**, 4413–4417 (2014).

15. Swain, A., Sarkar, A. & Rajaraman, G. Role of Ab Initio Calculations in the Design and Development of Organometallic Lanthanide-Based Single-Molecule Magnets. *Chem. – An Asian J.* **14**, 4056–4073 (2019).

16. Jiles, D. *Introduction to Magnetism and Magnetic Materials*. (Springer US, 1991).

17. Poritsky, H. A generalization of biot-savart's law. *Phys. Rev.* **21**, 360–364 (1923).

18. Stadelmaier, H. . Magnetic properties of materials. *Mater. Sci. Eng. A* **287**, 138–145 (2000).

19. Spain, E. & Venkatanarayanan, A. Review of Physical Principles of Sensing and Types of Sensing Materials. in *Comprehensive Materials Processing* vol. 13 5–46 (Elsevier, 2014).

20. McGrayne, Sharon Bertsch , Bleaney, Brebis , Kashy, Edwin , Robinson, Frank Neville H. and Suckling, E. E. 'Magnetism'. Encyclopedia Britannica, 29 Aug. 2019.

21. Wills, B. A. & Finch, J. A. Magnetic and Electrical Separation. in *Wills' Mineral Processing Technology* 381–407 (Elsevier, 2016).

22. Cullity, B. D. & Graham, C. D. *Introduction to Magnetic Materials*. *Chemical Reviews* vol. 111 (John Wiley & Sons, Inc., 2008).

23. Fagan, M. A. Fundamental Studies of Heap Leaching Hydrology Using Magnetic Resonance Imaging. (2013)

24. Ida, N. *Engineering Electromagnetics*. *Engineering Electromagnetics* (Springer International Publishing, 2015).

25. Della Torre, E. *Magnetic Hysteresis*. *Magnetic Hysteresis* (IEEE, 2000).

26. Kirchmayr, H. Magnetic Anisotropy. in *Encyclopedia of Materials: Science and Technology* 4754–4757 (Elsevier, 2001).

27. Bjørnholt, C., Mercebach, P., Rudner, M. S. & Nathan, F. S. The Hartree-Fock Method. (2019).

28. Dunn, K. M. Introduction to Quantum Mechanics: In Chemistry, Material Science, and Biology (S. M. Blinder). *J. Chem. Educ.* **82**, 383 (2005).

29. Spaldin, N. A. *Magnetic Materials Fundamentals and Applications*. (2010).

30. Heisenberg, W. Mehrkörperproblem und Resonanz in der Quantenmechanik. *Zeitschrift für Phys.* **38**, 411–426 (1926).

31. Majlis, N. Magnetic anisotropy. *Quantum Theory Magn.* 101–116 (2007)

32. Kaplan, I. G. Pauli exclusion principle and its theoretical foundation. *arXiv* 1–24 (2019)

33. Kutzelnigg, W. & Morgan, J. D. Hund's rules. *Zeitschrift für Phys. D Atoms, Mol. Clust.* **36**, 197–214 (1996).

34. Yamauchi, J. *1 Fundamentals of Magnetism*. (1822).

35. Li, W.-K. & Blinder, S. M. Atomic electronic states: the L-S and j-j coupling schemes and their correlation. 1–11 http://arxiv.org/abs/1409.2032 (2014).

36. Atomic spectral lines. in *IUPAC Compendium of Chemical Terminology* (IUPAC, 2008). doi:10.1351/goldbook.A00502.

37. Zeeman effect. *Phys. Today* **18**, 108–110 (1965).

38. Eppley, H. J., Aubin, S. M. J.,Wemple, M., Hendrickson, D., Christou, G. Single-Molecule Magnets: Characterization of Complexes Exhibiting Out-of-Phase AC Susceptibility Signals. *Mol. Cryst. Liq. Cryst. Sci. Technol. Sect. A. Mol. Cryst. Liq. Cryst.* **305**, 167–179 (1997).

39. Aubin, S. M. J., Spagna, S., Eppley, H.J., Sager, R.E., Folting, K., Christou, G., Hendrickson, D. Single-Molecule Magnets: Magnetization Relaxation and Quantum Tunneling in Dodecanuclear Manganese Complexes. *Mol. Cryst. Liq. Cryst. Sci. Technol. Sect. A. Mol. Cryst. Liq. Cryst.* **305**, 181–192 (1997).

40. Christou, G., Gatteschi, D., Hendrickson, D. N. & Sessoli, R. Single-molecule magnets. *MRS Bull.* **25**, 66–71 (2000).

41. Gatteschi, D., Sessoli, R. & Villain, J. *Molecular Nanomagnets*. *Etica e Politica* vol. 15 (Oxford University Press, 2006).

42. Lis, T. Preparation, structure, and magnetic properties of a dodecanuclear mixed-valence manganese carboxylate. *Acta Crystallogr. Sect. B Struct. Crystallogr. Cryst. Chem.* **36**, 2042–2046 (1980).

43. Yoo, J. *et al.* Magnetization tunneling in Mn-12 and Mn-4 single-molecule magnets. *J. Appl. Phys.* **91**, 7155 (2002).

44. Zheng, L.-M., Tang, J., Sun, H.-L. & Ren, M. Low Dimensional Molecular Magnets and Spintronics. in *Handbook of Spintronics* 617–680 (Springer Netherlands, 2016). doi:10.1007/978-94-007-6892-5_26.

45. Ruiz-Molina, D., Christou, G. & Hendrickson, D. N. Single-Molecule Magnets. *Mol. Cryst. Liq. Cryst. Sci. Technol. Sect. A. Mol. Cryst. Liq. Cryst.* **343**, 17–27 (2000).

46. Paulsen, C., Park, J.-G., Barbara, B., Sessoli, R. & Caneschi, A. Studies of hysteresis in $Mn_{12}Ac$. *J. Magn. Magn. Mater.* **140**–**144**, 1891–1892 (1995).

47. Mishra, A., Wernsdorfer, W., Abboud, K. A. & Christou, G. Initial Observation of Magnetization Hysteresis and Quantum Tunneling in Mixed Manganese−Lanthanide Single-Molecule Magnets.

J. Am. Chem. Soc. **126**, 15648–15649 (2004).

48. Zaleski, C. M., Depperman, E. C., Kampf, J. W., Kirk, M. L. & Pecoraro, V. L. Synthesis, Structure, and Magnetic Properties of a Large Lanthanide–Transition-Metal Single-Molecule Magnet. *Angew. Chemie Int. Ed.* **43**, 3912–3914 (2004).

49. Costes, J.-P., Shova, S. & Wernsdorfer, W. Tetranuclear [Cu–Ln]2 single molecule magnets: synthesis, structural and magnetic studies. *Dalt. Trans.* 1843 (2008)

50. Craig, G. A. & Murrie, M. 3d single-ion magnets. *Chem. Soc. Rev.* **44**, 2135–2147 (2015).

51. Frost, J. M., Harriman, K. L. M. & Murugesu, M. The rise of 3-d single-ion magnets in molecular magnetism: Towards materials from molecules? *Chem. Sci.* **7**, 2470–2491 (2016).

52. Coutinho, J. T., Monteiro, B. & Pereira, L. C. J. Ln(III)-based SIMs. in *Lanthanide-Based Multifunctional Materials* 195–231 (Elsevier, 2018).

53. Malrieu, J. P., Caballol, R., Calzado, C. J., de Graaf, C. & Guihéry, N. Magnetic Interactions in Molecules and Highly Correlated Materials: Physical Content, Analytical Derivation, and Rigorous Extraction of Magnetic Hamiltonians. *Chem. Rev.* **114**, 429–492 (2014).

54. Fink, K. & Staemmler, V. A modified CAS-CI approach for an efficient calculation of magnetic exchange coupling constants. *Mol. Phys.* **111**, 2594–2605 (2013).

55. Burns, R. G. Outline of crystal field theory. *Mineral. Appl. Cryst. F. Theory* 7–43 (2009)

56. Fernández, F. M. Simple model for Crystal Field Theory. **2020**, 1–22 (2016).

57. Housecroft, C. & Sharpe, A. *Inorganic Chemistry (Catherine E. Housecroft and Alan G. Sharpe)*. *Pearson* (2012).

58. Lancashire John Robert. Calculations using Tanabe-Sugano diagrams. *The Department of Chemistry, University of the West Indies,* http://wwwchem.uwimona.edu.jm/courses/Tanabe-Sugano/TScalcs.html (2015).

59. Benelli, C. & Gatteschi, D. Magnetism of lanthanides in molecular materials with transition-metal ions and organic radicals. *Chem. Rev.* **102**, 2369–2387 (2002).

60. Jiang, S.-D., Wang, B.-W. & Gao, S. Advances in Lanthanide Single-Ion Magnets. in *Structure and Bonding* vol. 164 111–141 (2014).

61. Lueken, H. Course of lectures on magnetism of lanthanide ions under varying ligand and magnetic fields. *Review* 1–91 (2008).

62. Electronic Configuration and Periodic Table.

63. Zhu, Z. & Tang, J. Geometry and Magnetism of Lanthanide Compounds. in *Coordination Chemistry Reviews* vols 206–207 191–226 (2018).

64. Sorace, L. & Gatteschi, D. Electronic Structure and Magnetic Properties of Lanthanide Molecular Complexes. in *Lanthanides and Actinides in Molecular Magnetism* vol. 2 1–26 (Wiley-VCH Verlag GmbH & Co. KGaA, 2015).

65. Bloch, F. über die Quantenmechanik der Elektronen in Kristallgittern. *Zeitschrift für Phys.* **52**, 555–600 (1929).

66. Fink, R. & Staemmler, V. A multi-configuration reference CEPA method based on pair natural orbitals. *Theor. Chim. Acta* **87**, 129–145 (1993).

67. Meier, U. & Staemmler, V. An efficient first-order CASSCF method based on the renormalized Fock-operator technique. *Theor. Chim. Acta* **76**, 95–111 (1989).

68. Bodenstein, T. Entwicklung und Anwendung von Multireferenzverfahren zur Beschreibung magnetischer Eigenschaften von Metallkomplexen. (2015).

69. Knowles, P. J. & Handy, N. C. A new determinant-based full configuration interaction method. *Chem. Phys. Lett.* **111**, 315–321 (1984).

70. Sjøvoll, M., Gropen, O. & Olsen, J. A determinantal approach to spin-orbit configuration interaction. *Theor. Chem. Accounts Theory, Comput. Model. (Theoretica Chim. Acta)* **97**, 301–312 (1997).

71. Davidson, E. R. The iterative calculation of a few of the lowest eigenvalues and corresponding eigenvectors of large real-symmetric matrices. *J. Comput. Phys.* **17**, 87–94 (1975).

72. Leininger, M. L., Sherrill, C. D., Allen, W. D. & Schaefer, H. F. Systematic Study of Selected Diagonalization Methods for Configuration Interaction Matrices. *J. Comput. Chem.* **22**, 1574–1589 (2001).

73. Heß, B. A., Marian, C. M., Wahlgren, U. & Gropen, O. A mean-field spin-orbit method applicable to correlated wavefunctions. *Chem. Phys. Lett.* **251**, 365–371 (1996).

74. Boča, R. Zero-field splitting in metal complexes. *Coord. Chem. Rev.* **248**, 757–815 (2004).

75. de Graaf, C. & Broer, R. *Magnetic Interactions in Molecules and Solids*. *Magnetic Interactions in Molecules and Solids* (Springer International Publishing, 2016). doi:10.1007/978-3-319-22951-5.

76. Maurice, R. *et al*. Universal Theoretical Approach to Extract Anisotropic Spin Hamiltonians. *J. Chem. Theory Comput.* **5**, 2977–2984 (2009).

77. Rudowicz, C. & Chung, C. Y. The generalization of the extended Stevens operators to higher ranks and spins, and a systematic review of the tables of the tensor operators and their matrix elements. *J. Phys. Condens. Matter* **16**, 5825–5847 (2004).

78. Löwdin, P. On the Non-Orthogonality Problem Connected with the Use of Atomic Wave Functions in the Theory of Molecules and Crystals. *J. Chem. Phys.* **18**, 365–375 (1950).

79. Fink, K., Wang, C. & Staemmler, V. Superexchange and spin-orbit coupling in chlorine-bridged binuclear cobalt(II) complexes. *Inorg. Chem.* **38**, 3847–3856 (1999).

80. Odom, B., Hanneke, D., D'Urso, B. & Gabrielse, G. New Measurement of the Electron Magnetic Moment Using a One-Electron Quantum Cyclotron. *Phys. Rev. Lett.* **97**, 030801 (2006).

81. Gabrielse, G., Hanneke, D., Kinoshita, T., Nio, M. & Odom, B. Erratum: New Determination of the Fine Structure Constant from the Electron g Value and QED [Phys. Rev. Lett. **97** , 030802 (2006)]. *Phys. Rev. Lett.* **99**, 039902 (2007).

82. Bolvin, H. An Alternative Approach to the g-Matrix: Theory and Applications. *ChemPhysChem* **7**, 1575–1589 (2006).

83. Putz, M. V., Cimpoesu, F. & Ferbinteanu, M. *Structural Chemistry*. *Journal of Chemical Education* vol. 25 (Springer International Publishing, 2018).

84. Atanasov, M., Comba, P., Helmle, S., Müller, D. & Neese, F. Zero-Field Splitting in a Series of Structurally Related Mononuclear Ni^{II} –Bispidine Complexes. *Inorg. Chem.* **51**, 12324–12335 (2012).

85. Nemec, I., Herchel, R., Machata, M. & Trávníček, Z. Tetranuclear Ni(II) and Co(II) Schiff-base complexes with an M_4O_6 defective dicubane-like core: zero-field SMM behavior in the cobalt analogue. *New J. Chem.* **41**, 11258–11267 (2017).

86. Marriott, K. E. R. *et al.* Pushing the limits of magnetic anisotropy in trigonal bipyramidal Ni(II). *Chem. Sci.* **6**, 6823–6828 (2015).

87. Goodenough, J. B. An interpretation of the magnetic properties of the perovskite-type mixed crystals La1−xSrxCoO3−λ. *J. Phys. Chem. Solids* **6**, 287–297 (1958).

88. Kanamori, J. Superexchange interaction and symmetry properties of electron orbitals. *J. Phys. Chem. Solids* **10**, 87–98 (1959).

89. Nasani, R. *et al.* Probing through-space and through-bond magnetic exchange couplings in a new benzotriazinyl radical and its metal complexes. *Dalt. Trans.* **48**, 14189–14200 (2019).

90. Woods, T. J. *et al.* Strong Ferromagnetic Exchange Coupling Mediated by a Bridging Tetrazine Radical in a Dinuclear Nickel Complex. *Inorg. Chem.* **56**, 12094–12097 (2017).

91. Demir, S., Jeon, I.-R., Long, J. R. & Harris, T. D. Radical ligand-containing single-molecule magnets. *Coord. Chem. Rev.* **289**–**290**, 149–176 (2015).

92. Caneschi, A., Gatteschi, D., Rey, P. & Sessoli, R. Structure and magnetic properties of ferrimagnetic chains formed by manganese(II) and nitronyl nitroxides. *Inorg. Chem.* **27**, 1756–1761 (1988).

93. Chakarawet, K., Harris, T. D. & Long, J. R. Semiquinone radical-bridged M 2 (M = Fe, Co, Ni) complexes with strong magnetic exchange giving rise to slow magnetic relaxation. *Chem. Sci.* **11**, 8196–8203 (2020).

94. Furche, F. *et al.* Turbomole. *WIREs Comput. Mol. Sci.* **4**, 91–100 (2014).

95. Lu, T. & Panneerselvam, K. Structural Statistics For the Nickel(II) and Copper(II) complexes

with Tetraazacyclotetradecane ligands. *Mater. Struct.* **6**, 170–180 (1999).

96. Balamurugan, M., Mayilmurugan, R., Suresh, E. & Palaniandavar, M. Nickel(II) complexes of tripodal 4N ligands as catalysts for alkane oxidation using m-CPBA as oxidant: ligand stereoelectronic effects on catalysis. *Dalt. Trans.* **40**, 9413 (2011).

97. Walther, B. Structure and Bonding 68 Theoretical Approaches: Von R. L. Johnston, O. Kahn, O. S. Mortensen, D. M. P. Mingos, Springer-Verlag, 1987; V, 176. *Zeitschrift für Chemie* **29**, 303–304 (2010).

98. Chibotaru, L. F. Ab Initio Methodology for Pseudospin Hamiltonians of Anisotropic Magnetic Complexes. in *Journal of Molecular Structure* vol. 10 397–519 (2013).

99. Mehlich, C. & van Wüllen, C. Broken Symmetry Approach to Magnetic Properties of Oligonuclear Transition-Metal Complexes: Application to Hyperfine Tensors of Mixed-Valence Manganese Compounds. *J. Phys. Chem. C* **123**, 7717–7730 (2019).

100. Kubica, A., Kowalewski, J., Kruk, D. & Odelius, M. Zero-field splitting in nickel(II) complexes: A comparison of DFT and multi-configurational wavefunction calculations. *J. Chem. Phys.* **138**, 064304 (2013).

101. Piwowarska, D., Gnutek, P. & Rudowicz, C. Origin of the Ground Kramers Doublets for $Co2^{+}(3d^{7})$ Ions with the Effective Spin 3/2 Versus the Fictitious 'Spin' ½. *Appl. Magn. Reson.* **50**, 797–808 (2019).

102. Romanenko, G. V., Fursova, E. Y. & Ovcharenko, V. I. Crystal structure of cobalt(II) complexes with imidazoline nitroxide. *J. Struct. Chem.* **40**, 580–588 (1999).

103. Neese, F. Efficient and accurate approximations to the molecular spin-orbit coupling operator and their use in molecular g-tensor calculations. *J. Chem. Phys.* **122**, 034107 (2005).

104. Helmich-Paris, B., Hättig, C. & van Wüllen, C. Spin-Free CC2 Implementation of Induced Transitions between Singlet Ground and Triplet Excited States. *J. Chem. Theory Comput.* **12**, 1892–1904 (2016).

105. Gerloch, M. & McMeeking, R. F. Paramagnetic properties of unsymmetrical transition-metal

complexes. *J. Chem. Soc. Dalt. Trans.* 2443 (1975).

106. Smolko, L. *et al.* Three tetracoordinate Co(II) complexes [Co(biq)X_2] (X = Cl, Br, I) with easy-plane magnetic anisotropy as field-induced single-molecule magnets. *Dalt. Trans.* **44**, 17565–17571 (2015).

107. Barnet, M. T., Craven, B. M., Freeman, H. C., Kime, N. E. & Ibers, J. A. The Co–N bond lengths in Co II and Co III hexammines. *Chem. Commun. (London)* 307–308 (1966)

108. Woodruff, D. N., Winpenny, R. E. P. & Layfield, R. A. Lanthanide single-molecule magnets. *Chemical Reviews* vol. 113 5110–5148 (2013).

109. Rinehart, J. D. & Long, J. R. Exploiting single-ion anisotropy in the design of f-element single-molecule magnets. *Chem. Sci.* **2**, 2078 (2011).

110. Tang, J. *et al.* Dysprosium Triangles Showing Single-Molecule Magnet Behavior of Thermally Excited Spin States. *Angew. Chemie* **118**, 1761–1765 (2006).

111. Chibotaru, L. F., Ungur, L. & Soncini, A. The Origin of Nonmagnetic Kramers Doublets in the Ground State of Dysprosium Triangles: Evidence for a Toroidal Magnetic Moment. *Angew. Chemie Int. Ed.* **47**, 4126–4129 (2008).

112. Aronica, C. *et al.* A Nonanuclear Dysprosium(III)–Copper(II) Complex Exhibiting Single-Molecule Magnet Behavior with Very Slow Zero-Field Relaxation. *Angew. Chemie* **118**, 4775–4778 (2006).

113. Zhang, Z. *et al.* Di- and tetranuclear heterometallic Cu^{II}-Ln^{III} complexes (Ln = Gd and Dy): Synthesis, structure and magnetic properties. *Sci. China Chem.* **55**, 934–941 (2012).

114. Rudolph, W. W. & Irmer, G. On the Hydration of the Rare Earth Ions in Aqueous Solution. *J. Solution Chem.* **49**, 316–331 (2020).

115. Yu, W. *et al.* Single-molecule magnet behavior in 2,2'-bipyrimidine-bridged dilanthanide complexes. *Beilstein J. Nanotechnol.* **7**, 126–137 (2016).

116. Li, J. *et al.* Photochemically Tuned Magnetic Properties in an Erbium(III)-Based Easy-Plane Single-Molecule Magnet. *Inorg. Chem.* **58**, 14440–14448 (2019).

117. Girichev, G. V. *et al.* Molecular Structures of Tris(dipivaloylmethanato) Complexes of the Lanthanide Metals, $Ln(dpm)_3$, Studied by Gas Electron Diffraction and Density Functional Theory Calculations: A Comparison of the Ln−O Bond Distances and Enthalpies in $Ln(dpm)_3$ Complexes.and the Cubic Sesquioxides, Ln_2O_3 *Inorg. Chem.* **45**, 5179–5186 (2006).

118. Franzke, Y. J., Spiske, L., Pollak, P. & Weigend, F. Segmented Contracted Error-Consistent Basis Sets of Quadruple-ζ Valence Quality for One-and Two-Component Relativistic All-Electron Calculations. *J. Chem. Theory Comput.* **16**, 5658–5674 (2020).

119. Silva, G. S., Dutra, J. D. L., da Costa, N. B., Alves, S. & Freire, R. O. Lanthanide Contraction in Lanthanide Organic Frameworks: A Theoretical and Experimental Study. *J. Phys. Chem. A* **124**, 7678–7684 (2020).

120. Khan, S., Kubica-Misztal, A., Kruk, D., Kowalewski, J. & Odelius, M. Systematic theoretical investigation of the zero-field splitting in Gd(III) complexes: Wave function and density functional approaches. *J. Chem. Phys.* **142**, 034304 (2015).

121. Gupta, T., Rajeshkumar, T. & Rajaraman, G. Magnetic exchange in {Gd III – radical} complexes: method assessment, mechanism of coupling and magneto-structural correlations. *Phys. Chem. Chem. Phys.* **16**, 14568–14577 (2014).

122. Handzlik, G. *et al.* Magnetization Dynamics and Coherent Spin Manipulation of a Propeller Gd(III) Complex with the Smallest Helicene Ligand. *J. Phys. Chem. Lett.* **11**, 1508–1515 (2020).

123. Yoshida, T. *et al.* Field-Induced Slow Magnetic Relaxation of Gd III Complex with a Pt−Gd Heterometallic Bond. *Chem. - A Eur. J.* **23**, 4551–4556 (2017).

124. Bleaney, B. The paramagnetic resonance spectra of gadolinium and neodymium ethyl sulphates. *Proc. R. Soc. London. Ser. A. Math. Phys. Sci.* **223**, 15–29 (1954).

125. Martínez-Pérez, M. J. *et al.* Gd-Based Single-Ion Magnets with Tunable Magnetic Anisotropy: Molecular Design of Spin Qubits. *Phys. Rev. Lett.* **108**, 247213 (2012).

126. Holmberg, R. J. *et al.* Observation of unusual slow-relaxation of the magnetisation in a Gd-EDTA chelate. *Dalt. Trans.* **44**, 20321–20325 (2015).

127. Ungur, L. & Chibotaru, L. F. Magnetic anisotropy in the excited states of low symmetry lanthanide complexes. *Phys. Chem. Chem. Phys.* **13**, 20086 (2011).

128. Durrant, J. P., Tang, J., Mansikkamäki, A. & Layfield, R. A. Enhanced single-molecule magnetism in dysprosium complexes of a pristine cyclobutadienyl ligand. *Chem. Commun.* **56**, 4708–4711 (2020).

129. Kripal, R., Yadav, D., Gnutek, P. & Rudowicz, C. Alternative zero-field splitting (ZFS) parameter sets and standardization for Mn^{2+} ions in various hosts exhibiting orthorhombic site symmetry. *J. Phys. Chem. Solids* **70**, 827–833 (2009).

130. Rudowicz, C. & Bramley, R. On standardization of the spin Hamiltonian and the ligand field Hamiltonian for orthorhombic symmetry. *J. Chem. Phys.* **83**, 5192–5197 (1985).

131. Singh, S. K., Gupta, T. & Rajaraman, G. Magnetic Anisotropy and Mechanism of Magnetic Relaxation in Er(III) Single-Ion Magnets. *Inorg. Chem.* **53**, 10835–10845 (2014).

132. Sarkar, A. & Rajaraman, G. Modulating magnetic anisotropy in Ln(III) single-ion magnets using an external electric field. *Chem. Sci.* **11**, 10324–10330 (2020).

133. Feng, M. *et al.* Chiral Erbium(III) Complexes: Single-Molecule Magnet Behavior, Chirality, and Nuclearity Control. *Inorg. Chem.* **58**, 10694–10703 (2019).

134. Zhang, H. *et al.* Low coordinated mononuclear erbium(III) single-molecule magnets with C_{3v} symmetry: a method for altering single-molecule magnet properties by incorporating hard and soft donors. *Dalt. Trans.* **47**, 302–305 (2018).

135. Vignesh, K. R. *et al.* Slow Magnetic Relaxation and Single-Molecule Toroidal Behaviour in a Family of Heptanuclear $\{Cr^{III}\ Ln^{III}_6\}$ (Ln=Tb, Ho, Er) Complexes . *Angew. Chemie* **130**, 787–792 (2018).

136. Langley, S. K., Vignesh, K. R., Moubaraki, B., Rajaraman, G. & Murray, K. S. Oblate versus Prolate Electron Density of Lanthanide Ions: A Design Criterion for Engineering Toroidal Moments? A Case Study on $\{Ln^{III}_6\}$ (Ln=Tb, Dy, Ho and Er) Wheels. *Chem. – A Eur. J.* **25**, 4156–4165 (2019).

137. Langley, S. K. *et al.* New examples of triangular terbium(III) and holmium(III) and hexagonal dysprosium(III) single molecule toroics. *Dalt. Trans.* **48**, 15657–15667 (2019).

138. Viciano-Chumillas, M. *et al.* Hysteresis in a bimetallic holmium complex: A synergy between electronic and nuclear magnetic interactions. *Phys. Rev. B* **96**, 214427 (2017).

139. Ishikawa, N. *et al.* Determination of Ligand-Field Parameters and f-Electronic Structures of Double-Decker Bis(phthalocyaninato)lanthanide Complexes. *Inorg. Chem.* **42**, 2440–2446 (2003).

140. Ghosh, S. *et al.* Multi-frequency EPR studies of a mononuclear holmium single-molecule magnet based on the polyoxometalate $[Ho^{III}(W_5O_{18})_2]^{9-}$. *Dalt. Trans.* **41**, 13697 (2012).

141. Chen, Y.-C. *et al.* Hyperfine-Interaction-Driven Suppression of Quantum Tunneling at Zero Field in a Holmium(III) Single-Ion Magnet. *Angew. Chemie Int. Ed.* **56**, 4996–5000 (2017).

142. Gupta. T., Velmurugan, G., Rajeshkumar, T., Rajaraman, G. Role of Lanthanide-Ligand bonding in the magnetization relaxation of mononuclear single-ion magnets: A case study on Pyrazole and Carbene ligated Ln III(Ln=Tb, Dy, Ho, Er) complexes. *J. Chem. Sci.* **128**, 1615–1630 (2016).

143. Gupta, S. K., Rajeshkumar, T., Rajaraman, G. & Murugavel, R. Is a strong axial crystal-field the only essential condition for a large magnetic anisotropy barrier? The case of non-Kramers Ho(III) *versus* Tb(III). *Dalt. Trans.* **47**, 357–366 (2018).

144. Kharwar, A. K., Mondal, A. & Konar, S. Field Induced Slow Magnetic Relaxation in a Non Kramers Tb(III) Based Single Chain Magnet. *Magnetochemistry* **4**, 59 (2018).

145. Vignesh, K. R., Langley, S. K., Murray, K. S. & Rajaraman, G. Exploring the Influence of Diamagnetic Ions on the Mechanism of Magnetization Relaxation in $\{Co^{III}_2\ Ln^{III}_2\}$ (Ln = Dy, Tb, Ho) "Butterfly" Complexes. *Inorg. Chem.* **56**, 2518–2532 (2017).

146. Casanovas, B., Font-Bardía, M., Speed, S., El Fallah, M. S. & Vicente, R. Field-Induced SMM and Visible/NIR-Luminescence Behaviour of Dinuclear Ln^{III} Complexes with 2-Fluorobenzoate. *Eur. J. Inorg. Chem.* **2018**, 1928–1937 (2018).

147. Ullmann, S., Hahn, P., Blömer, L., Mehnert, A., Laube, C., Abel, B., Kersting, B. Dinuclear

lanthanide complexes supported by a hybrid salicylaldiminato/calix[4]arene-ligand: synthesis, structure, and magnetic and luminescence properties of $(HNEt_3)[Ln_2(HL)(L)]$ (Ln = Sm^{III} , Eu^{III} , Gd^{III} , Tb^{III}). *Dalt. Trans.* **48**, 3893–3905 (2019).

148. Shui, Y., Zhaobo, H., Zilu, C., Bo, L., Yi-Quan Z., Yuning, L., Dongcheng, L., Di, Y., Fupei, L. Two Dy(III) Single-Molecule Magnets with Their Performance Tuned by Schiff Base Ligands. *Inorg. Chem.* **58**, 1191–1200 (2019).

149. Guo, P., Yu-Feng, Q., Zhi-Wen W., Yue, C., Yadav, T., Fink, K., Xiao-Ming, R. Tuning the Coordination Geometry and Magnetic Relaxation of Co(II) Single-Ion Magnets by Varying the Ligand Substitutions. *Cryst. Growth Des.* **21**, 1035–1044 (2021).

❖ Publication

- Guo, P., Yu-Feng, Q., Zhi-Wen W., Yue, C., Yadav.T, Fink.K Tuning the Coordination Geometry and Magnetic Relaxation of Co(II) Single-Ion Magnets by Varying the Ligand Substitutions" *Cryst. Growth Des,***21**, 1035-1044(2021)